

**EXTREME EVENTS:
MAINTENANCE MECHANISMS AND ENERGETICS**

**DISSERTATION
WITH THE AIM OF ACHIEVING A DOCTORAL DEGREE
AT THE FACULTY OF MATHEMATICS,
INFORMATICS AND NATURAL SCIENCES
DEPARTMENT OF EARTH SCIENCES
AT UNIVERSITÄT HAMBURG**

**SUBMITTED BY
QIYUN MA
FROM INNER MONGOLIA, CHINA**

HAMBURG, 2021

ACCEPTED AS DISSERTATION AT THE DEPARTMENT OF EARTH SCIENCES

DAY OF ORAL DEFENSE:

31.08.2021

REVIEWERS:

Prof. Dr. Christian Franzke

Prof. Dr. Johanna Baehr

MEMBERS OF THE EXAMINATION COMMISSION:

Chair Prof. Dr. Johanna Baehr

Prof. Dr. Christian Franzke

Prof. Dr. Stefan Bühler

Prof. Dr. Jürgen Böhner

Prof. Dr. Uwe A. Schneider

CHAIR OF THE SUBJECT DOCTORAL COMMITTEE

EARTH SYSTEM SCIENCES:

Prof. Dr. Dirk Gajewski

DEAN OF FACULTY OF MIN:

Prof. Dr. Heinrich Graener

ABSTRACT

Mid-latitude extreme weather events are becoming increasingly frequent due to anthropogenic global warming, causing catastrophic impacts on human health and society. Such extremes are generally governed by large-scale circulation anomalies in the mid-latitudes. However, the physical and dynamical processes that maintain these extremes through anomalous circulations are not well understood. This thesis focuses on a better understanding of the maintenance mechanisms of the devastating summer heat waves associated with large-scale circulations. We also investigate the effect of concurrent global warming on the maintenance mechanisms during heat waves. The investigation requires us to fully examine the variations in global circulation under climate change.

Using a nonlinear stationary wave model (NSWM), we first investigate large-scale circulation anomalies associated with European heat waves. The heat waves are identified using the Japanese Reanalysis (JRA-55) dataset for the period 1958 - 2017. We conduct numerical experiments based on the NSWM during heat waves. Results show the NSWM can faithfully reproduce the main features of the observed anomalous stationary waves in the upper troposphere when all forcings are included. The forcings include realistic orography, diabatic heating, and transient momentum fluxes (including transient divergence and vorticity flux). Decomposition of the total response of NSWM to the forcings indicates that transient momentum fluxes are the primary drivers of the observed anomalous stationary waves. The orography and diabatic heating contribute to the total response mainly through their nonlinear interactions. Further separation of the transients elucidates that the high-frequency transient vorticity fluxes dominate the contributions in transients. Numerical results show heating anomalies located in the tropical Indian Ocean and the west Pacific region are primarily responsible for maintaining the observed anomalous stationary waves linked to European heat waves, and the heating in the mid-latitude and tropical Atlantic region plays a secondary role.

Changes in atmospheric circulation patterns have been connected to the increase in heat extremes over some regions in the Northern Hemisphere. We then focus on heat waves over inner East Asia, where intensified high-pressure anomalies have been observed. Based on the JRA-55 data from 1958 to 2019, the temperatures for the period of 1989 – 2019 are confirmed to be significantly warmer than those for the period 1958 – 1988. Then, we identify heat waves for each period. The NSWM is used to investigate the maintenance mechanisms of the large-scale circulation anomalies associated with heat waves. By comparing the mechanisms in these two periods, this

research explores whether recent climate change has altered the maintenance processes of heat waves. The transient vorticity flux is still the dominant driver of the observed anomalous stationary waves during heat waves for both periods. However, model results suggest that recent warming might have altered the maintenance mechanisms mainly through the nonlinear interactions between different forcing components. In particular, diabatic heating becomes more dominant via its nonlinear interactions with orography and transient momentum fluxes over the last 3 decades. Further decomposition of diabatic heating indicates that the enhanced heating anomalies in the mid-latitude Northern Pacific, the tropical Indian Ocean, and the tropical western Pacific region contribute to changes in circulation under a warmer climate.

We then investigate the variations of atmospheric dynamics and circulation from an atmospheric energetics perspective. Based on the Lorenz energy cycle formalism and JRA-55 data, we show that the atmospheric circulation is overall becoming increasingly energetic and efficient. Results reveal significant trends in the conversion rates between zonal available potential and kinetic energy, which is consistent with an expansion of the Hadley cell. The significant trends also appear in the conversion rates between eddy available potential and kinetic energy, suggesting an increase in mid-latitude baroclinic instability. Moreover, results indicate that planetary-scale waves dominate the stationary eddy energy, while synoptic-scale waves dominate the transient eddy energy with a significantly increasing trend. We then explore the relationships between atmospheric energy components and modes of climate variability. Results show that significant global and hemispheric energy fluctuations are caused by the El Niño-Southern Oscillation, the Arctic Oscillation, the Southern Annular Mode, and the meridional temperature gradient over the Southern Hemisphere.

Finally, this thesis demonstrates a potential linkage between atmospheric energetics and summer heat extremes over the Northern Hemisphere in the mid-latitudes. The preliminary evidence shows that the transient eddy kinetic energy is responsible for the overall decreasing trend in the eddy kinetic energy, while the stationary eddy kinetic energy accounts largely for the correlations between the eddy kinetic energy and persistent summer heat waves. Further decomposition illustrates that the stationary eddy kinetic energies embedded in synoptic-scale waves contribute the most to the persistent positive summer temperature anomalies over the mid-latitudes, especially over Europe. This potential linkage offers a promising way to better understand changing circulations and persistent summer heat waves.

ZUSAMMENFASSUNG

Extremwetterereignisse in den mittleren Breiten werden aufgrund der anthropogenen globalen Erwärmung immer häufiger und können katastrophale Auswirkungen auf die menschliche Gesundheit und Gesellschaft haben. Diese Wetterextreme werden im Allgemeinen durch großräumige Zirkulationsanomalien in den mittleren Breiten bestimmt, allerdings sind die physikalischen und dynamischen Prozesse zur Aufrechterhaltung dieser Extreme durch die anomalen Zirkulationen bislang nicht gut verstanden. Diese Arbeit konzentriert sich auf ein besseres Verständnis der Mechanismen zur Aufrechterhaltung der mit den großräumigen Zirkulationen verbundenen verheerenden sommerlichen Hitzewellen. Zugleich untersuchen wir die Auswirkungen der gleichzeitigen globalen Erwärmung auf die Erhaltungsmechanismen während der Hitzewellen. Die Untersuchung dieser Auswirkungen erfordert eine vollständige Untersuchung der Variationen der globalen Zirkulation unter dem Klimawandel.

Unter Verwendung eines nichtlinearen, stationären Wellenmodells (NSWM) untersuchen wir zunächst die großräumigen Zirkulationsanomalien im Zusammenhang mit den europäischen Hitzewellen. Die Hitzewellen werden anhand des japanischen Reanalysedatensatzes (JRA-55) für den Zeitraum 1958 - 2017 identifiziert. Basierend auf dem NSWM führen wir numerische Experimente während dieser Hitzewellen durch. Die Ergebnisse zeigen, dass das NSWM die Hauptmerkmale der beobachteten anomalen stationären Wellen in der oberen Troposphäre originalgetreu reproduzieren kann, wenn alle Forcings einbezogen werden. Diese Forcings umfassen die realistische Orographie, diabatische Erwärmung sowie transiente Impulsflüsse (einschließlich der transienten Divergenz- und Vorticity-Flüsse). Die Zerlegung der Gesamtantwort von NSWM auf die Forcings zeigt, dass die transienten Impulsflüsse der Hauptantreiber der beobachteten anomalen stationären Wellen sind. Die Orographie und die diabatische Erwärmung tragen hauptsächlich durch ihre nichtlinearen Wechselwirkungen zur Gesamtantwort bei. Des Weiteren zeigt die Zerlegung der Transienten, dass die hochfrequenten Anteile der Vorticity-Flüsse die Hauptbeiträge in den Transienten dominieren. Die numerischen Ergebnisse zeigen, dass Heizungsanomalien in den tropischen Bereichen des Indischen Ozeans sowie im Westpazifik für die Aufrechterhaltung der beobachteten anomalen stationären Wellen im Zusammenhang mit den europäischen Hitzewellen hauptverantwortlich sind; die Erwärmung in den Regionen der mittleren Breiten sowie des tropischen Atlantiks spielt dagegen eine sekundäre Rolle.

Veränderungen in den atmosphärischen Zirkulationsmustern wurden mit der Zunahme von Hitzeextremen in einigen Regionen der Nordhemisphäre in Verbindung gebracht. Wir legen unseren Fokus dann auf Hitzewellen in Inner-Ostasien, wo verstärkte Hochdruckanomalien beobachtet wurden. Basierend auf den JRA-55-Reanalysedaten von 1958 bis 2019 wird bestätigt, dass die Temperaturen für den Zeitraum von 1989 bis 2019 deutlich höher waren als für den Zeitraum von 1958 bis 1988. Für beide Zeiträume identifizieren wir anschließend die Hitzewellen und verwenden das NSWMM, um die Mechanismen zur Aufrechterhaltung der mit den Hitzewellen einhergehenden großräumigen Zirkulationsanomalien zu untersuchen. Durch Vergleichen der Mechanismen in beiden Zeiträumen können wir untersuchen, ob der jüngste Klimawandel die Prozesse zur Aufrechterhaltung der Hitzewellen verändert hat. Der transiente Vorticity-Fluss bleibt der dominante Hauptantreiber der beobachteten anomalen stationären Wellen während der Hitzewellen in beiden Zeiträumen. Die Modellergebnisse deuten jedoch darauf hin, dass die jüngste Erwärmung die Erhaltungsmechanismen vor allem durch die nichtlinearen Wechselwirkungen zwischen den verschiedenen Komponenten des Forcings verändert haben. Insbesondere wurde die diabatische Erwärmung durch ihre nichtlinearen Wechselwirkungen mit der Orographie und den transienten Impulsflüssen in den letzten 3 Jahrzehnten immer dominanter. Die Zerlegung der diabatischen Erwärmung deutet darauf hin, dass die verstärkten Heizungsanomalien in den mittleren Breiten des Nordpazifiks sowie in den tropischen Bereichen des Indischen Ozeans und im Westpazifik zu den Veränderungen der Zirkulation unter einem wärmeren Klima beitragen.

Anschließend untersuchen wir die Variationen der atmosphärischen Dynamik und der Zirkulation aus einer atmosphärischen-energetischen Perspektive. Basierend auf dem Lorenz-Energiezyklus-Formalismus und den JRA-55-Reanalysedaten zeigen wir, dass die atmosphärische Zirkulation insgesamt immer energiereicher und effizienter wird. Die Ergebnisse zeigen signifikante Trends in den Umwandlungsraten zwischen der zonalen „available potential energy“ und der kinetischer Energie, welche mit einer Ausdehnung der Hadley-Zelle konsistent sind. Diese signifikanten Trends zeigen sich auch in den Konversionsraten zwischen der „eddy available potential energy“ und der kinetischer Energie, welche auf eine Zunahme der baroklinen Instabilität in den mittleren Breiten hindeuten. Darüber hinaus zeigen die Ergebnisse, dass planetare Wellen die stationäre „eddy energy“ dominieren, während synoptische Wellen die transiente „eddy energy“ mit einem signifikant zunehmenden Trend dominieren. Anschließend untersuchen wir die Beziehungen zwischen den atmosphärischen Energiekomponenten und den Modi der Klimavariabilität. Die Ergebnisse zeigen, dass signifikante globale und hemisphärische Energieschwankungen durch das El Niño/Southern Oscillation-Phänomen, durch die Arktische Oszillation sowie durch den „Southern Annular Mode“ und den meridionalen Temperaturgradienten in der Südhemisphäre verursacht werden.

Diese Arbeit zeigt einen potentiellen Zusammenhang zwischen der atmosphärischen Energetik und den sommerlichen Hitzeextremen in den mittleren Breiten der nördlichen Hemisphäre auf. Die vorläufigen Erkenntnisse zeigen, dass die transiente „eddy kinetic energy“ für den insgesamt abnehmenden Trend in der „eddy kinetic energy“ verantwortlich ist, während die stationäre „eddy kinetic energy“ weitgehend für die Korrelationen zwischen der „eddy kinetic energy“ und den anhaltenden sommerlichen Hitzewellen verantwortlich ist. Eine weitere Zerlegung zeigt, dass die stationäre „eddy kinetic energy“, eingebettet in den synoptischen Wellen, am meisten zu den andauernden, positiven sommerlichen Temperaturanomalien in den mittleren Breiten insbesondere in Europa beiträgt. Dieser potentielle Zusammenhang bietet einen vielversprechenden Weg, um die veränderten Zirkulationen und die anhaltenden sommerlichen Hitzewellen besser zu verstehen.

PUBLICATIONS RELATED TO THIS DISSERTATION

APPENDIX A

Ma, Q., Franzke, C.L.E. (2021), "The role of transient eddies and diabatic heating in the maintenance of European heat waves: a nonlinear quasi-stationary wave perspective", *Climate Dynamics* 56, 2983–3002. doi: <https://doi.org/10.1007/s00382-021-05628-9> (last accessed on 30th of May 2021).

APPENDIX B

Ma, Q., Franzke, C.L.E. (2021), "Changes in the maintenance mechanisms of heat waves over Inner East Asia over the last few decades", *Journal of Climate* (to be submitted)

APPENDIX C

Ma, Q., Lembo, V. & Franzke, C.L.E. (2021), "The Lorenz energy cycle: trends and the impact of modes of climate variability", *Tellus A: Dynamic Meteorology and Oceanography* 73:1, 1-15. doi: <https://doi.org/10.1080/16000870.2021.1900033> (last accessed on 30th of May 2021).

CONTENTS

1	EXTREME EVENTS: MAINTENANCE MECHANISMS AND ENERGETICS	1
1.1	Status of the physical understanding of heat waves	4
1.1.1	Definition of heat waves	4
1.1.2	Physical and dynamical mechanisms of heat waves . . .	5
1.1.3	Summary	12
1.2	Scientific understanding of the Lorenz energy cycle	13
1.2.1	Conceptual model of the Lorenz energy cycle	14
1.2.2	Estimate of the Lorenz energy cycles and its applications	16
1.2.3	Summary	17
1.3	Contributions of this dissertation	18
1.3.1	Maintenance mechanisms of heat waves	18
1.3.2	Changes in the maintenance mechanisms	21
1.3.3	Trends in atmospheric energy cycles	23
1.3.4	Atmospheric energy cycles and heat waves	26
1.4	Concluding remarks and paths forward	31
1.4.1	Concluding remarks	31
1.4.2	Paths forward	32

APPENDICES

A	THE ROLE OF TRANSIENT EDDIES AND DIABATIC HEATING IN THE MAINTENANCE OF EUROPEAN HEAT WAVES: A NONLINEAR STATIONARY WAVE PERSPECTIVE	1
A.1	Introduction	4
A.2	Data, methods, and model experiments	6
A.2.1	Data source	6
A.2.2	Definition of heat waves	7
A.2.3	Model and experimental design	8
A.2.4	Decomposition of the forcing terms in the NSWM	11

A.3	Results and discussion	13
A.3.1	Identification of heat waves	13
A.3.2	NSWM responses to heat waves	17
A.3.3	Decomposing the processes in NSWM	20
A.3.4	Interrelationship between various nonlinear effects	25
A.3.5	The role of transient momentum fluxes	26
A.3.6	The role of diabatic heating	30
A.4	Conclusions	33
B	CHANGES IN THE MAINTENANCE MECHANISMS OF HEAT WAVES OVER INNER EAST ASIA OVER THE LAST FEW DECADES	1
B.1	Introduction	4
B.2	Data and methods	5
B.2.1	Data and study domain	5
B.2.2	Identification of heat waves	6
B.2.3	Trends analysis of heat wave magnitude	9
B.2.4	Model Simulations	9
B.3	Identification of heat waves and observed stationary waves	10
B.3.1	Identification of heat waves	10
B.3.2	Observed anomalous stationary waves	13
B.4	Numerical experiments and diagnostic results from NSWM	15
B.4.1	Selections of Experiment	15
B.4.2	NSWM responses to total forcing	17
B.5	Decomposing various forcing mechanisms in NSWM	19
B.5.1	Direct nonlinear effects	19
B.5.2	Individual total nonlinear effects	19
B.5.3	Nonlinear interactions	21
B.6	Decomposition of transients	23
B.7	Decomposition of contributions from diabatic heating	25
B.7.1	Spatial distribution of diabatic heating	25
B.7.2	Contributions from regional diabatic heating	27

B.8	Role of modes of climate variability	29
B.9	Summary	32
C	THE LORENZ ENERGY CYCLE: TRENDS AND THE IMPACT OF MODES OF CLIMATE VARIABILITY	1
C.1	Introduction	4
C.2	Data and methodology	6
C.3	Results	7
C.3.1	How reliable is the pre-satellite period for atmospheric energetics?	7
C.3.2	Climatology of the Lorenz energy cycle	8
C.3.3	Trends in global energies	9
C.3.4	Decomposition of global generation, dissipation, and conversion rates	10
C.3.5	Hemispheric differences in eddy potential and kinetic energies	14
C.3.6	Wave number decomposition of the global eddy energies	15
C.3.7	The impact of modes of climate variability on the Lorenz Energy Cycle	17
C.4	Conclusion	21

BIBLIOGRAPHY

EXTREME EVENTS: MAINTENANCE MECHANISMS AND ENERGETICS

Weather and climate extreme events are inherent phenomena of the climate system (Zhang et al., 2014). Accurate prediction of these extreme events can reduce their catastrophic impacts on society including economic loss and health risks (Franzke and Sentelles, 2020; Ma et al., 2018b; Vose et al., 2014). For example, heat waves are a major cause of weather-related deaths in northern mid-latitude regions (Robinson, 2001), especially when they are persistent for a long period. The need to mitigate the impact of weather and climate extreme events and understand their variations incurred by anthropogenic climate change facilitates the research on the extreme events, such as the attribution of their formation, the assessment of their consequences, and the projection of their further trends under the ongoing climate change. Peterson et al. (2013) summarized the progress of the research status of the shift of various extreme events in a changing climate in Figure 1 with two dimensions: the detection of the causes of changes in extremes, and the physical understanding of these changes. Even though heat waves are among the most well-studied extreme events in the climate thanks to the abundance of observations, the physical mechanisms that maintain heat waves are still unclear, and this hinders accurate heat wave forecasts.

This dissertation aims at a better physical understanding of heat waves in a changing climate. Recent studies show that heat waves are affected by variations in global circulation. For example, changes in circulation can strongly affect the frequency, intensity, and duration of heat waves in the northern mid-latitudes (Lehmann and Coumou, 2015). Several recent heat waves, such as the European heat wave in 2003 and the Russian heat wave in 2010, were associated with persistent hemispheric circulation patterns (Petoukhov et al., 2016). In general, the dynamics of the large-scale circulation in the mid-latitude are controlled by Rossby waves, which are related to synoptic-scale cyclones and anticyclones. These waves cause weather variations on time scales of less than a week (Coumou et al., 2015) and this may be prolonged under climate change. The role of the summertime Rossby waves in the maintenance of heat waves (Schubert et al., 2014; Ting, 1994) leads to the first question addressed by the thesis:

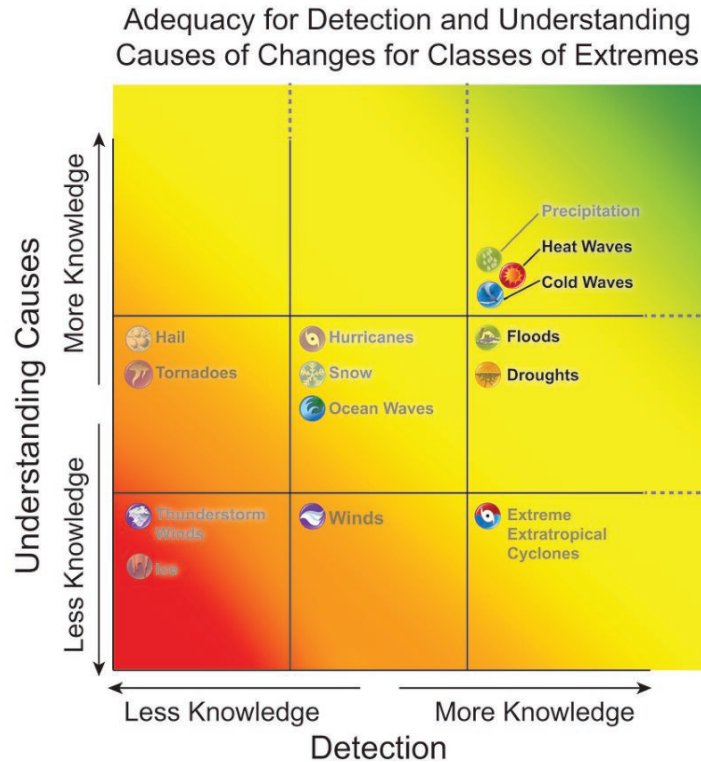


Figure 1: Scientists' physical understanding of detection and attribution of changes in different weather extremes. The x axis denotes the adequacy of data to detect trends of extremes, while the y axis represents the scientific understanding on the attribution of those trends. The dashed lines on the right side and top of the graph implies that the knowledge about the phenomena is not complete. Figure taken from Peterson et al. (2013).

- What are the physical and dynamic mechanisms that maintain the persistent large-scale stationary waves during heat waves?

Observations have shown a significant trend in the occurrence of anticyclonic circulations during boreal summer (Barnes et al., 2014; Horton et al., 2015; Screen and Simmonds, 2013), which generally explains the increase of surface hot extremes. For instance, Lee et al. (2017) reported that a circum-global teleconnection pattern occurrence increased remarkably since the late 1990s. This pattern is closely linked to boreal summer extreme temperatures over several land areas, such as Europe and northeastern Asia. Although the linkage between the frequent heat waves and the increasing trend of anticyclonic circulations are well studied, the maintenance mechanisms behind the changes of circulations remain largely equivocal. In a changing climate, the changes of stationary waves have been studied in Wills et al. (2019). However, it is unknown whether climate warming has altered the maintenance mechanisms of large-scale circulation anomalies during heat extremes. Thus, this dissertation focuses on the second question:

- How does climate warming affect the maintenance mechanisms of stationary waves during heat waves?

The intrinsic link between heat waves and large-scale dynamics also indicates the need for investigation of the changes in the global circulation under climate change. One particular perspective which can be used to examine the changing of large-scale circulation is the Lorenz atmospheric energy cycle (Lorenz, 1955; Pan et al., 2017). The Lorenz atmospheric energy cycle focuses on energy transfer in the atmosphere – how the incoming solar radiation generates available potential energy, which is then transferred to kinetic energy and finally dissipated by friction (Li et al., 2007). From the perspective of energy transformation, the air motion is mainly driven by the unevenly distributed energy inside the Earth's atmosphere. Weather variations occur with the zonal mean atmospheric energy cascades into smaller eddies (Kim and Choi, 2017). Thus, an accurate estimate of atmospheric energy structure can inform the variation of the large-scale dynamics in a changing climate.

In particular, an accurate evaluation of the atmospheric energy structure could provide insights into the changes of mid-latitude baroclinic instability and improve the prediction of long-term extremes limited by current earth system models (Kim and Choi, 2017; Li et al., 2007). Mid-latitude baroclinic instability, driven by the horizontal temperature gradient, is responsible for generating the dominant weather systems in the mid-latitude. The baroclinic instability can be understood as a result of the mean-to-eddy energy conversion. Hence, this dissertation addresses the third question:

- How does the atmospheric energy cycle vary with the variability of climate modes?

Overall, this cumulative dissertation is based on two peer-reviewed papers and one manuscript (to be submitted), addressing partly the aforementioned research questions in the study of heat waves and atmospheric energetics. Moreover, the potential link between temperature extremes and atmospheric energetics is also preliminarily evidence-based examined.

The structure of the thesis is described as follows. I first provide a brief review of the main research questions mentioned above: heat waves and atmospheric energy cycle. Next, I elaborate on the background of these three research articles and summarize their conclusions. In a broader perspective, I then discuss the potential linkage between extreme temperatures and the changes of general circulation under the lens of atmospheric energetics. In the concluding remarks, a summary of the research findings and the prospect of future research are given. Finally, the full texts of the three articles are presented as three appendices.

1.1 STATUS OF THE PHYSICAL UNDERSTANDING OF HEAT WAVES

The recent incentive to the active research on heat waves arises from the increase in intensity, frequency, and duration of heat waves in observational records due to the anthropogenic climate change (Campbell et al., 2018; Perkins-Kirkpatrick and Lewis, 2020). The trend of the increasing heat wave occurrence will continue as the global average temperature is projected to escalate by 1.8 °C to 4.0 °C relative to 1961–1990 by the end of this century (Change, 2007). These heat wave events pose an imminent threat to our society, the ecosystems, and human beings (Cogato et al., 2019; Xu et al., 2014). To address these concerns, recent decades have seen substantial advances in the understanding of heat waves (Horton et al., 2016; Perkins, 2015). This section presents a brief introduction of the research on the definitions and physical mechanisms of heat waves.

1.1.1 *Definition of heat waves*

There is no universal definition of heat waves. Heat waves are generally viewed as prolonged periods of heat exceeding an absolute or a relative threshold. Based on the non-exhaustive list of definitions of heat waves used in the literature in Table 1, three factors are crucial to the definition of a heat wave event: a meteorological variable that measures the amount of heat, a threshold that evaluates the extremity, and a quantity that characterizes the event. The daily temperature, including daily minimum, maximum, and mean temperatures, is commonly used as the meteorological variable. Also, the humidity amplifies the thermal stress in humans and other large mammals in extreme heat events (Davis et al., 2016; Robinson, 2001; Russo et al., 2017). Many heat wave indices, such as apparent temperature, combine the humidity and temperature information to measure the impact of heat waves on human beings (Perkins, 2015).

The threshold for a heat wave can be divided into two categories. The first category relies on a fixed absolute threshold to identify high temperatures (Wang et al., 2018). The absolute thresholds are defined based on the impact of heat waves on society and the environment, e.g. the biophysical heat tolerance of mammals, the resilience of infrastructure, and the production of crops (Luo, 2011; Perkins, 2015). However, the absolute thresholds can be dependent on the dominant species and climate of a particular region leading to difficulties in the comparison across the globe. The other category defines a relative threshold based on the percentiles of the local climatology of the selected meteorological variable. This allows for comparison across various locations, time, and results from different models and observations. The possibility of comparison outweighs the disadvantage that the percentile-based definitions lose the physical intuition of actual temperature. For example, (Wang et al.,

2018) demonstrated that the relative threshold is a better metric to identify regional extreme temperature events over China.

The definition of heat waves should also indicate their characteristics such as frequency, duration, and intensity. The duration of extreme heat events is widely used (Robinson, 2001). Every definition in Table 1 includes duration as a component of the definition of a heat wave - number of consecutive days of an extreme heat event. The duration criterion is motivated by the influence of persistent high temperatures on human health, crop production systems, and terrestrial ecosystems (Anderson and Bell, 2011). Guo et al. (2017) suggested that intermittent short periods of extreme temperature may reduce the stress of human health, and the increased mortality and hospitalizations rate is only related to extreme heat events that lasted for more than 3 days. Hence, at least 3 days of extreme heat events are part of a definition of the heat wave in this dissertation.

Even though definitions in Table 1 include the three common factors, each definition is different based on the context of the research problem (Holton and Hakim, 2012a). The differences in these definitions lead to difficulties in comparing heat waves in different regions, particularly when a specific characteristic is of interest. To unify the framework for heat wave studies, the widely used 17 climate indices in climate models were proposed by the Expert Team on Climate Change Detection (ETCCDI, Alexander et al. (2006)) under the aegis of the World Climate Research Programme (WCRP), which can measure extreme temperatures to compare the characteristics of heat waves across the globe. Perkins and Alexander (2013) and Perkins et al. (2012) further established a general framework with the purpose of reducing the plethora of metrics employed for measuring heat waves. According to this framework, some heat wave characteristics can be easily deduced, like the frequency, magnitude, and duration, the timing of onset timing of termination. This dissertation adopts the recently proposed daily Heat Wave Magnitude Index (HWMID, see Table 1) by Russo et al. (2014) to measure the intensity of our identified heat waves.

Existing definitions of heat waves reflect the various physical mechanisms underlying the drivers of extreme events (Horton et al., 2016). However, due to the impact of heat waves on a broad spectrum of systems, a universal definition of heat wave is hard to achieve. A sensible approach is to balance different metrics in heat wave research based on the research goal and reduce the diversity of the metrics (Perkins, 2015).

1.1.2 *Physical and dynamical mechanisms of heat waves*

The moderate increase of global mean temperature can induce significant changes in the characteristics of regional extreme heat events (Coumou and Robinson, 2013; Horton et al., 2016). The requirement of tackling the increasing risk of heat waves drives the emerging research field for a better

Table 1: Selected heat wave indices proposed in recent climate science literature (after 2010). Some of indices are summarized from Perkins (2015) and other summaries are from recent literatures.

Study	Index description	Heat wave characteristics measured
Fischer and Schär (2010)	The number of days when apparent temperature (computed from relative humidity and temperature) exceeds 40.6 °C	Frequency and intensity
Fischer and Schär (2010)	Consisted of hot days (maximum temperatures exceeding 35 °C) and tropical nights (minimum temperatures exceeding 20 °C)	Frequency and intensity
Anderson and Bell (2011)	More than 2 consecutive days the daily temperatures exceeding the 95th percentile	Intensity, duration, and timing in season
Stefanon et al. (2012)	Exceeding the 95th percentile (centered on a 21-day time window) of the local probability density function	Spatial extent, duration
Vautard et al. (2013)	Daily mean temperature exceeding the 90th percentile for various consecutive days	Frequency, intensity, duration and persistence
Russo et al. (2014, 2015)	HWMId - daily heat wave magnitude index, at least 3 days exceeding the 90th percentile (centered on a 31-day time window) of maximum temperature	Cumulative intensity (sum of daily magnitude)
Schoetter et al. (2015)	At least 3 days the maximum temperature exceeding the 98th percentile	Intensity, duration, and spatial extent
Perkins-Kirkpatrick and Gibson (2017)	At least 3 days the maximum temperature exceeding the 90th percentile (a smoothed 15-day moving average)	Frequency, duration, and peak intensity
Wang et al. (2018)	Regional heat wave - absolute (exceeding 35 °C) and relative (daily maximum temperatures exceeding the 90th percentile of a centered on a 15-day time window) thresholds, with considering the temporal and spatial extension	Duration, intensity, and spatial extent
Baldwin et al. (2019)	Compound heat wave - adding different temporal structure requirements to account for compounding heat waves, i.e., the maximum break length between two heat waves or hot days	Frequency and spatial extent

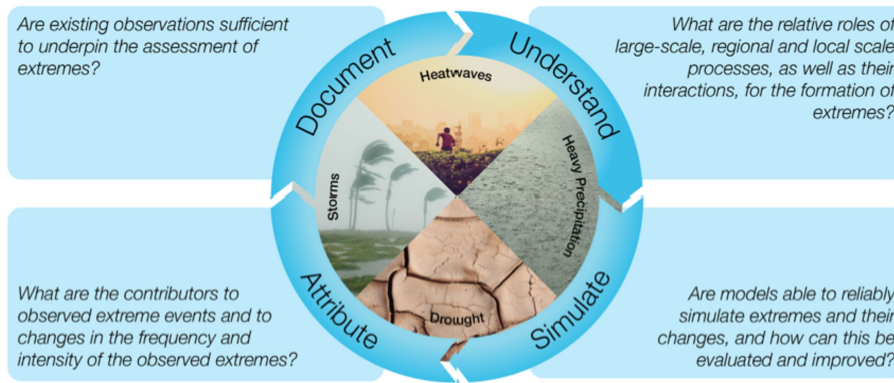


Figure 2: The grand challenges described in WCRP on weather and climate extremes. Figure taken from the website: <https://www.wcrp-climate.org/grand-challenges/gc-extreme-events>.

physical understanding of heat waves (Horton et al., 2016; Walsh et al., 2020). As stated in the WCRP Grand Challenges (Fig. 2), there is an urgent need for improvements in observations, reliable simulation, understanding of the driving mechanisms, and the attribution of contributing factors to extreme events (Zhang et al., 2014). In this section, some recent advances in the understanding of the drivers of heat waves will be presented with a focus on the mid-latitudes in the Northern Hemisphere. This region has suffered the most from recent heat waves (Miralles et al., 2014), motivating much in-depth analysis of those events (Campbell et al., 2018).

Atmospheric Rossby waves and local land-atmosphere feedbacks are two main mechanisms that are responsible for temperature extremes during the summertime. On the one hand, the large-scale quasi-stationary Rossby waves, induced by a myriad of forcings (Teng and Branstator, 2019), can form persistent high-pressure systems that lead to regional high-temperature anomalies (Fragkoulidis et al., 2018; Schubert et al., 2011). On the other hand, reduced soil moisture prevents latent cooling, which intensifies heat waves through the land-atmosphere feedback (Alexander, 2011; Fischer et al., 2007; Schär et al., 2004). These two mechanisms are intertwined closely pointing to a causative relationship given the non-linear dynamics (Horton et al., 2016).

BLOCKING AND ROSSBY WAVES Boreal summer heat waves usually last for several days or a week. In some exceptional cases, the heat waves can last for more than a month, like the Russian heat wave in 2010 (Dole et al., 2011). Persistent heat waves are connected with a synoptic-scale long-standing anticyclonic system (also known as a high-pressure system) in the affected region. As these high-pressure systems alter the climatological path of the jet stream and impede the propagation of synoptic weather systems (Pfahl et al., 2015), they are usually referred to as “blocking highs”, “persistent highs”, or

simply “blockings” (Charney and DeVore, 1979; Marshall et al., 2014; Stefanon et al., 2012).

The anticyclonic circulations are usually associated with subsiding air, which favors heat wave occurrence via three processes: 1) the subsidence of air masses causes warm and dry air by adiabatic compression; 2) the subsidence of air masses reduces precipitation by suppressing the local convection, which subsequently reduces the cloud cover and increases shortwave solar radiation inducing increased diabatic heating at the surface. Furthermore, anticyclonic circulations advect hot and dry air from southern desert areas to the heat wave inflicted regions over the northern hemisphere (Black et al., 2004; Della-Marta et al., 2007). Thus, if a region is under the control of a persistent anticyclone and high surface temperature, heat waves are expected. Analysis of the relationship between heat waves and persistent anticyclones can be found, for example, in Stefanon et al. (2012) and Zschenderlein et al. (2019). Therefore, to investigate the heat waves in the mid-latitudes, it seems necessary to look into the status of atmospheric blocking research.

Atmospheric blocking, in general, is a part of slow-moving planetary waves or quasi-stationary (or standing) Rossby waves in the jet streams (Kornhuber et al., 2017; Ma et al., 2018a). Rossby waves meander in the north-south direction and embed in the jet stream, manifested by pressure ridges (characterized by warm poleward winds) and troughs (characterized by cold equatorward winds) across the hemisphere (Horton et al., 2016). These quasi-stationary Rossby waves principally arise due to factors like topography, transient momentum fluxes, heating, and the distribution of the continents and oceans (Held et al., 2002; Simpson et al., 2016; Wills et al., 2019). The linkage between summertime quasi-stationary waves with temperature extremes is clear and well-studied (Schubert et al., 2011; Ting, 1994). However, the role of different forcings in the maintenance mechanisms of the quasi-stationary waves during heat waves is still unclear. This will be the main focus of the first part of this thesis.

The complex interaction of quasi-stationary Rossby waves and mean background flows such as the jet stream play an important role in forcing persistent anticyclonic anomalies related to mid-latitude heat extremes as well (Hannachi et al., 2017; Teng and Branstator, 2019). Studies propose that quasi-resonant amplification (QRA) and Arctic amplification (AA) are two main hypothetical mechanisms affecting the changes of quasi-stationary waves under the background of climate change (Coumou et al., 2014, 2018; Hoskins and Woollings, 2015; Petoukhov et al., 2013). The QRA theory indicates the increased wave amplitude of standing and short-wavelength Rossby waves (Coumou et al., 2014; Petoukhov et al., 2013), while the AA theory supports the weakening of fast-moving Rossby waves (Coumou et al., 2018; Hoskins and Woollings, 2015). These two theories are still ripe for research not only from the observational perspective but also under climate change (Horton et al., 2016). Both

hypotheses account for the reduction in boreal summer weather variability at synoptic time scales (Coumou et al., 2014).

The QRA theory is a result of wave interference of the quasi-stationary Rossby waves and fast-moving (free) Rossby waves of similar wavenumber (among wavenumber 6–8) (Kornhuber et al., 2019; Petoukhov et al., 2013, 2016). The resonance amplifies the circumglobal waveguide teleconnections (Teng and Branstator, 2019) and creates persistent summertime weather patterns in the Northern Hemisphere with decreased weather variability during the period of resonance (Horton et al., 2016). The amplified quasi-stationary waves lead to large-scale atmospheric blocking events that stay in place for days or even weeks, favoring the occurrence of extreme heat events. Evidence of the effect of the QRA has been found in the 2003 European, 2010 Russian, and 2011 North American heat waves (Horton et al., 2016), and in several record-breaking and persistent heat extremes in 2018 across the globe (Kornhuber et al., 2019). These summertime quasi-resonance phenomena and associated heat waves have become more likely in the last decades, which could be related to global warming (Coumou et al., 2014). The QRA theory infers that, with the forcing from global warming, the frequency of wave-resonance related heat waves will increase. However, due to the complexity of the climate dynamics, several alternative explanations of amplified quasi-stationary waves exist leading to the need for further rigorous tests of the causal effect of the QRA (Teng and Branstator, 2019).

The AA theory is another crucial effect under consideration for the mid-latitude heat waves under climate change. Observations show a dramatic rise in temperatures and declines of ice and snow cover in the Arctic leading to a reduced pole-to-mid-latitude temperature gradient (Notz and Stroeve, 2016). A commonly hypothesized consequence of AA is a weaker and wavier westerly flow that stimulates persistent extreme weather events over the mid-latitudes (Vavrus, 2018). Initially proposed in the 1970s (Newson, 1973; Warshaw and Rapp, 1973), the hypothesis was corroborated by the evidence of the relation between the AA and extreme weather events (Coumou et al., 2015; Vavrus, 2018). The Arctic warming affects the position and the strength of the mid-latitude jet stream, which influences the position of persistent anticyclones that give rise to heat waves (Barnes and Screen, 2015). Coumou et al. (2014) pointed out that the observed significant weakening of summer circulation connected with Arctic warming can contribute to more persistent heat waves in recent summers. However, controversy still exists for the impact of the AA on the mid-latitude atmospheric circulations Dai and Song (2020). Under global warming, the eddy-driven jet stream may shift equatorward based on the temperature gradient in the lower troposphere while the system should shift poleward based on the upper tropospheric temperature gradient causing a “tug-of-war” (Horton et al., 2016; Vavrus, 2018).

The intertwined effects of QRA and AA require continued investigations. The jet stream influences the amplified planetary waves in the QRA theory

while AA can affect the variations of the mid-latitude jet stream. Hence, the extreme heat waves related to the QRA require a clearer understanding of the relationship between the mid-latitude circulation and the AA (Mann et al., 2017; Vavrus, 2018). The nonlinear response of the mid-latitude extreme events to these intertwined effects of the AA and the QRA is an interesting topic ripe for future research (Horton et al., 2016; Vavrus, 2018).

Another contentious factor that affects mid-latitude extreme weather events is tropical forcing (Barnes et al., 2014; Francis and Vavrus, 2012). Recent studies show that tropical sea surface temperature anomalies may warm the Arctic and impact the mid-latitude circulations (Ding et al., 2014), which challenges the view that the mid-latitude circulations are generally insensitive to tropical forcing during summer. Moreover, tropical forcing is a major source of Rossby waves in connection with the mid-latitude wave trains (Cassou et al., 2005). These Rossby waves also influence planetary wave anomalies via the waveguide teleconnections (Teng and Branstator, 2019). However, the location of the heating for Rossby wave excitement is not certain (Teng and Branstator, 2019) because a short-lived tropical forcing is rather hard to detect compared to steady forcing, which is often connected with remote sea surface temperature anomalies (Branstator, 2014).

Furthermore, the quantification and the prediction of changes of atmospheric blockings is another active research topic. Some mid-latitude regions witnessed more frequent anticyclones in recent decades (Horton et al., 2015; Pfahl et al., 2015), but no clear hemispheric trend is identified in atmospheric blocking events during summer (Barnes et al., 2014). The effect of global warming on atmospheric blocking events is still under debate (Horton et al., 2016; Pfahl et al., 2015). For example, even though models from CMIP5 project a general declining trend of blocking events, Hoskins and Woollings (2015) argue that mid-latitude blocking events could change their characteristics influenced by a feature not captured by general circulation models (GCMs). In the light of the frequent occurrence of anticyclonic circulations, it is intriguing to investigate whether the maintenance mechanisms of the blockings have altered under a warmer climate during heat waves. This will be discussed in the second part of this thesis.

LAND-ATMOSPHERE FEEDBACKS Although persistent high-pressure systems are a necessary condition for the formation of heat waves, the land surface is a more important factor (Perkins, 2015). Quesada et al. (2012) reported that, without the low soil moisture content, heat waves cannot occur even if persistent high-pressure systems exist. The effect of land-atmosphere interactions on the heat waves has drawn increasing attention in recent years. The land interacts with the atmosphere through evapotranspiration (taking into account plant transpiration and soil evaporation) and energy fluxes (including latent and sensible heat fluxes) (Seneviratne et al., 2010). Due to the sensitivity of land-atmosphere interactions to soil moisture content, the soil

moisture content is a common indicator of these interactions. Under persistent high-pressure systems, the deficit of soil moisture and the subsequent decrease of evaporative cooling may further increase the air temperatures. The dry soil moisture conditions in the winter and spring can also amplify the intensity of summer heat waves (Deng et al., 2018b; Perkins, 2015). This amplification effect was crucial in the formation of several recent record-breaking heat waves (Fischer et al., 2007; Miralles et al., 2014).

The energy transfer between the land and atmosphere is dominated by the latent and sensible heat fluxes. The latent heat flux is released from the evaporation of liquid water while the sensible heat flux transfers heats directly to the air or the land (Alexander, 2011). Both fluxes are associated with the interaction between temperature and soil moisture. The latent heat flux dominates the energy transfer process if the soil moisture content is high. Evapotranspiration is active in moist soil, which cool the land surface, and release water vapor into the atmosphere, promoting cloud formation in the low-level atmosphere (Alexander, 2011). This land-atmosphere interaction cools the air temperature. In contrast, the sensible heat flux dominates the energy transfer process in a dry soil condition. The dry soil inhibits evapotranspiration, increases the sensible heat fluxes leading to a deeper, warmer, and drier atmospheric boundary layer suppressing cloud formation (Alexander, 2011; Perkins, 2015). The warm and dry atmosphere further dries the surface generating a positive soil moisture-temperature feedback, which intensifies the air temperature and extends the length of heat waves.

The land-atmosphere coupling during heat waves from Miralles et al. (2014) is outlined in Figure 3. The positive soil moisture–temperature feedback accumulates heat progressively leading to a higher boundary layer, and the higher boundary layer intensifies the entrainment of the warm air near the surface. If the land-atmosphere coupling coincides with heat advection, the positive feedback is strengthened due to the increased evaporation.

The deficit of soil moisture can also excite quasi-stationary Rossby wave anomalies (Teng and Branstator, 2019). Idealized experiments with prescribed soil moisture in GCMs indicate that the soil moisture deficit could generate a planetary wave response, which supports the cause-effect relationship between the soil moisture deficit and a strengthening large-scale wave response. Modeling research confirms that the inclusion of the soil moisture information improves the simulation of observed heat waves, such as the heat waves in Western Europe in 2003 and Russia in 2010 (Schumacher et al., 2019).

Anthropogenic climate change will likely modify global and regional soil moisture, and impact heat waves through the land-atmosphere interaction (Horton et al., 2016). Climate projections show that the mid-latitudes and subtropics will get drier in the future, which increases the responses of the surface temperature to the transient circulation anomalies leading to heat waves (Dirmeyer et al., 2012; Seneviratne et al., 2010). The dry lower boundary condition in the subtropics and the mid-latitudes is confirmed by the observed

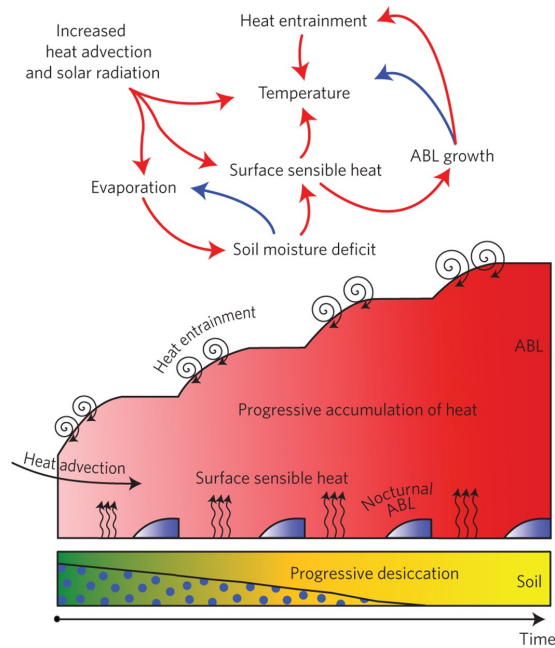


Figure 3: Schematic of the main soil moisture — air temperature interactions during heat waves. The ABL represents the atmospheric boundary layer. Red and blue arrows represent positive and negative correlations, respectively. Figure adopted from Miralles et al. (2014)

expansion of the Hadley cell (Davis and Davis, 2018) and the increase of aridity (Dai, 2013). This could potentially increase the frequency and duration of heat waves through land-atmosphere interactions. The energy transfer between the atmosphere and the land can be viewed as a type of heating forcing for the atmosphere. The complexity of the land-atmosphere feedback and the uncertainty of climate change indicates the need for even more observations to characterize the relevant processes (Seneviratne et al., 2010).

1.1.3 Summary

Great progress has been made for the identification of heat waves with both the absolute threshold and the definition considering heat wave characteristics. Despite being attractive, the unified metric or framework for heat waves is likely too laborious and difficult due to the extensive impact of heat waves ranging from human health and infrastructure to agriculture and terrestrial ecosystems. Moreover, the complex nature of the dynamics behind heat waves also makes the common framework difficult. Perkins (2015) suggested all communities affected by heat waves should work together as heat waves become more frequent and intense. Thus, we require a better physical understanding of heat waves (Horton et al., 2016).

The physical understanding of heat waves is also showing significant advances (Perkins-Kirkpatrick and Lewis, 2020). The theory of atmospheric

blocking and the land-atmosphere interactions lay the groundwork for future research. In this thesis, the response of quasi-stationary waves to various forcings is investigated during heat waves. These forcings can be viewed as a result of land-atmosphere interactions and other dynamical processes. Moreover, this thesis also discusses whether the maintenance mechanisms of the quasi-stationary waves during heat waves have altered under a warmer climate. Overall, the research findings of this thesis could benefit our society to better scientifically understand and forecast heat waves.

Climate variability and large-scale teleconnections also play an important role in heat waves as they influence the spatial distribution of temperature (Kenyon and Hegerl, 2008; Perkins, 2015). Multiple studies have investigated the relationship between climate variability and the heat waves at the global or regional scale (Arblaster and Alexander, 2012; Kenyon and Hegerl, 2008; Wang et al., 2017b; Zampieri et al., 2017). For example, the El Niño-Southern Oscillation (ENSO) has a strong impact on global mean temperatures depending on its phase, i.e., El Niño and La Niña (Arblaster and Alexander, 2012; Trenberth and Fasullo, 2012). Over Eurasia, the North Atlantic Oscillation (NAO) has strong impacts on temperature extremes (Folland et al., 2009; Li et al., 2020). Although these modes of climate variability are in close relation to blocking and land-atmosphere coupling (Perkins, 2015), the relationship often varies from region to region. Hence, modes of climate variability are also an important factor in research on heat waves and climate dynamics in general.

1.2 SCIENTIFIC UNDERSTANDING OF THE LORENZ ENERGY CYCLE

The inhomogeneous absorption of solar insolation is the principal fuel of atmospheric and oceanic dynamics (Ma et al., 2021). The absorbed energy is transformed with the motion within the climate system, controlling the mean state and variability of the atmosphere and the ocean (Clément et al., 2017; Hu et al., 2004; Ma et al., 2021). Hence, the study of atmospheric energetics offers an essential approach to understanding the physical behavior and maintenance mechanisms of the general circulation of the atmosphere and ocean (Hernández-Deckers and Storch, 2010).

The pioneering work of Lorenz (1955) presents the general circulation from an atmospheric energy cycle perspective – the unevenly distributed incoming solar radiation produces available potential energy which is then transferred to kinetic energy, and finally the kinetic energy is dissipated due to the frictional effect (Li et al., 2007). The process is referred to as the Lorenz energy cycle. This section presents a brief review of the recent advances in atmospheric energetics.

1.2.1 *Conceptual model of the Lorenz energy cycle*

The Earth's climate near the surface and in the upper atmosphere is determined by the incoming solar energy (Peixóto and Oort, 1974). However, only a tiny fraction (around 1 %) of the incoming solar energy can induce air motion, which is called available potential energy (Lorenz, 1955). The conversion between available potential and kinetic energy motivates the introduction of the global energy cycle, the Lorenz energy cycle (LEC) (Lorenz, 1955). The LEC is a concise thermodynamical description of the atmosphere (Marques et al., 2009).

After the introduction of the LEC, the ensuing investigation expands the theory of the energetics of the atmospheric circulation. For example, Saltsman (1957) reformulated atmospheric energetics in the zonal wavenumber domain using a Fourier analysis within latitude circles, allowing for the investigation of the rate of energy conversion in eddies for a given wavenumber and the interactions among different eddies. Ulbrich and Speth (1991) extended the LEC formulation using the Mixed Space-Time decomposition, which separates the eddy energies into stationary (departure from the zonal mean) and transient (departure from the time mean) components, and provided further information on the energy cycle related to different dynamical processes. The extension of LEC formulation by Ulbrich and Speth (1991) is of great importance to the study of global circulation.

In the Mixed Space-Time decomposition, the kinetic energy can be decomposed in space into the zonal mean kinetic energy (K_M) and the eddy kinetic energy (K_E) as the atmospheric motion can be understood as a zonally averaged field with superposed eddies (Holton and Hakim, 2012a; Lorenz, 1955). Eddy kinetic energy is essentially the variance of the wind field. Likewise, the available potential energy can be divided into the zonal mean available potential energy (P_M) and the eddy available potential energy (P_E). The latter is related to the variance of the temperature field. These energies can be further decomposed in time into stationary and transient energies. For example, the eddy energies can be decomposed into the energy related to the potential stationary eddy (P_{SE}) and the potential transient eddy (P_{TE}), or the kinetic stationary eddy (K_{SE}) and kinetic transient eddy (K_{TE}) energies. The maintenance of each type of energy within the atmosphere, such as the processes of generation, transformation, and dissipation, characterizes the atmospheric energy cycle (Marques, 2011).

Figure 4 illustrates the LEC in the maintenance of the atmospheric general circulation. The LEC controls two processes in the atmospheric general circulation: a process of baroclinic growth and another process of barotropic decay (Ma et al., 2021; Ulbrich and Speth, 1991). The primary source of energy for the atmospheric circulation is the P_M . The P_M is generated ($G(P_M)$) by the net radiative heating in low latitudes (e.g. incoming solar radiation and the latent heat release) and by the net cooling in high latitudes, which can

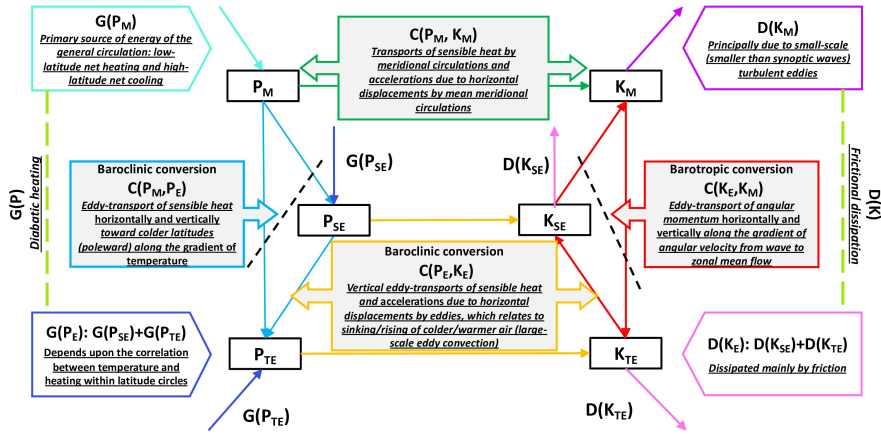


Figure 4: Schematic diagram of Lorenz energy cycle used in this thesis. P_s and K_s illustrate available potential and kinetic energy, respectively. C_s and their corresponding arrows denote energy conversion between the energy terms, and G_s and D_s are the generation and dissipation rates respectively. The same color of the boxes and corresponding arrows shows the evolving dynamical processes as presenting in the boxes, which summaries from Lorenz (1955) and Peixóto and Oort (1974). Equations for computing every term can be found in Oort (1964) and (Lembo et al., 2019b). Further information can be found in the main text.

be transferred to the P_E via baroclinic growth. The generation of P_E , both the P_{SE} and the P_{TE} ($G(P_{SE})$ and $G(P_{TE})$), is also via the heating processes, such as latent heat release in warm regions. The P_M can be converted to P_E ($C(P_M, P_E)$) by the eddy transport of the sensible heat horizontally and vertically in different latitudes. The P_E and the K_E conversion ($C(P_E, K_E)$) is mainly governed by warm air rising and cold air sinking at the same latitude, and the K_{SE} and the K_{TE} are transferred from the corresponding P_{SE} and P_{TE} . Lastly, the decay of energy is usually barotropic. The bulk of K_E is dissipated by the friction ($D(P_{SE})$ and $D(P_{TE})$) while the remaining part of the K_E is converted (or transferred) into the K_M ($C(K_E, K_M)$) through the eddy transport of the angular momentum horizontally and vertically, which are also related to the wave-mean flow interactions. In addition, the K_M is mainly dissipated by the friction of the small-scale turbulent eddies ($D(K_M)$) while the small remaining part of the K_M is converted into the P_M again by a direct (Hadley cell) or indirect (Ferrel cell) meridional circulations ($C(P_M, K_M)$). Overall, the general atmospheric energy cycle follows the path from the $P_M \rightarrow P_E \rightarrow K_E \rightarrow K_M$ (Kim and Kim, 2013; Peixóto and Oort, 1974).

The direction of the energy conversion relies on time and space as well (Kim and Choi, 2017). For example, energy from eddies reacts to the perturbation of energy generation promoting the mean circulations, and the kinetic energy can be transferred to higher latitudes to redistribute the potential energy (Kim and Choi, 2017). The conceptual LEC in Fig. 4 is a general summary of the energy cascading structure in the atmosphere, which separates physical and

dynamical processes in the view of energy transfer (Kim and Choi, 2017; Pan et al., 2017). The atmospheric energy cycle in Earth's atmosphere is much more complex, so the conceptual model should be used with care (Lorenz, 1955).

Nevertheless, the LEC can provide insights into the characteristics of atmospheric motion and circulation, which substantially influence the weather and the climate (Pan et al., 2017). Also, the LEC can be used to assess the performance of global atmosphere and climate models (Kim and Kim, 2013; Marques et al., 2010).

1.2.2 *Estimate of the Lorenz energy cycles and its applications*

An accurate inspection of the atmospheric energy cycle enables a better understanding of the dynamics of the atmosphere, and the diagnosis of the variations of the global circulation under a warming climate (Hernández-Deckers and Storch, 2010; Kim and Choi, 2017; Pan et al., 2017). Building on the idea of the LEC Lorenz (1955), atmospheric energetics has been assessed focusing on the mean state of the atmosphere in various fields, such as the hydrological cycle, climate change, and finding alternative energy sources to replace fossil fuels (Huang, 2014; Lucarini, 2009; Lucarini et al., 2014; Marques, 2011; Pan et al., 2017; Storch et al., 2012).

The LEC representation depends heavily on reliable observations. Due to the lack of observations over the Southern Hemisphere, early work on the LEC primarily focused on the Northern Hemisphere (Li et al., 2007; Marques, 2011). Oort (1964) provided one of the first tentatives to estimate the atmospheric energy cycle in a single year using a very sparse dataset aided by idealized models over the Northern Hemisphere. They also pioneered the discussion of atmospheric energy in different domains, including a space domain, a time domain, and a mixed space-time domain. Later, Krueger et al. (1965) identified the annual energy cycle in a region north of 20 °N using air temperature and geopotential height over a 5-year period. Based on data from more than 600 radiosonde stations, Oort and Peixóto (1974) and Peixóto and Oort (1974) extended the atmospheric energy cycle to the region north of 15 °S covering the tropical region. Oort (1983) further calculated the global atmospheric energy cycle using a 10-year radiosonde dataset, even though the accuracy is limited by the sparse observation network in the Southern Hemisphere. Although these studies are limited by the observations and have limited accuracy, the primary features of atmospheric energetics they uncovered still hold true today (Marques et al., 2010; Marques, 2011).

The accuracy of the LEC estimate has been improved in recent decades due to the introduction of various high-quality global atmospheric reanalysis datasets (Marques et al., 2010). In particular, since 1979, the satellite data in combination with operational model forecasts using data assimilation greatly improves the data availability over the Southern Hemisphere. The reanalysis

datasets provide information of the atmosphere all over the globe up to the stratosphere over a long period of time using state-of-the-art techniques, which reduces the error of LEC computations (Li et al., 2007). One of the important improvements from the reanalysis datasets is that they allow for the inclusion of some omitted terms in early studies (Oort, 1964; Oort and Peixóto, 1974; Peixóto and Oort, 1974). For example, Kim and Kim (2013) evaluated the variations of the LEC using the Modern-Era Retrospective analysis for Research and Applications (MERRA) and NCEP-DOE R2 reanalysis datasets over a 30-year period.

Accurate estimates of the LEC further extend the application of the LEC. The LEC is continuously assessed through observations (Hu et al., 2004; Pan et al., 2017) and atmospheric models (Lembo et al., 2019b; Marques et al., 2009), which can be used to analyze various atmospheric phenomena. For example, Hu et al. (2004) evaluated changes in the atmospheric circulation and surface temperatures using the LEC. Marques (2011) examined the LEC in five state-of-the-art climate models and also compared those results with three reanalysis datasets to evaluate the performance of the individual model. Hernández-Deckers and Storch (2010) studied how the LEC responds to the increasing greenhouse gas concentrations by using the atmosphere-ocean ECHAM5/Max Planck Institute Ocean Model. Lembo et al. (2019b) developed a software, named the Thermodynamic Diagnostic Tool (TheDiaTo), to compute the annual LEC to assess the performances of Coupled Model Intercomparison Project Phase 6 (CMIP6) model simulations.

Despite the better spatial and temporal observation coverage, reanalysis datasets still have biases (Li et al., 2007) and different reanalysis products have discrepancies due to their adopted methods, which leads to discrepancies in the LEC estimates (Marques et al., 2010). However, agreements in the estimates of the LEC of its variations, global climatology, and temporal and spatial structures between different reanalysis datasets show that the evaluation of the LEC is reliable, and the discrepancies are decreasing with the advancement of observations and models. With recent developments and the potential to further extend to other forms (Yamagami and HL, 2016), the LEC is still a valuable framework for the continued understanding of the global circulation, especially under climate change.

1.2.3 *Summary*

The conceptual model for the atmospheric energy cycle, the Lorenz energy cycle, is discussed, and the LEC is estimated since its introduction by Lorenz (1955). Restricted by observations, the majority of the studies put great efforts into the climatological mean of the atmospheric energy within a given time period instead of their variations (Kim and Choi, 2017; Pan et al., 2017). Pan et al. (2017) advocated the study of the long-term temporal characteristics of atmospheric energetics, and suggested a generally linearly increasing trend

of the atmospheric LEC from 1979 to 2013. The increasing trend is a result of the warming climate, and Pan et al. (2017) further concluded that as a heat engine, the Earth's global atmosphere has increased its efficiency during the studied period. The relationship between the eddy-related energies and the large-scale climate variabilities (like ENSO) is qualitatively described but their mechanisms are quite unclear, especially in a warmer climate, showing the need for further research (Li et al., 2011; Yamagami and HL, 2016).

Additionally, recent studies suggested that the classical process of the LEC holds true under a warmer climate (Hernández-Deckers and Storch, 2010; Perkins-Kirkpatrick and Lewis, 2020). The increased moisture content in the atmosphere due to the higher air temperature may extend the baroclinic system vertically by strengthening diabatic heating through latent heat release (Al-Ghussain, 2019; Kim and Choi, 2017). Meanwhile, baroclinic systems affect various weather systems and modes of climate variability. However, the vertical structure and the variations of moisture content within the troposphere are still in dispute (Gettelman et al., 2006; Po-Chedley et al., 2019). Hence, the changing moisture content contributes a high uncertainty in estimating the atmospheric energetics under climate change. In this sense, further improvements on observation and/or data assimilation of moisture content are needed, especially for the upper troposphere (Kim and Choi, 2017).

Climate models enable the comparison of the current and future atmospheric energy budget to evaluate the changes in global circulation. As the strengthening or weakening of the LEC could reflect the intensification or the decline of baroclinic activities (Hernández-Deckers and Storch, 2010), analysis of the intensity of the LEC between the present and future climate offers a reasonable way to investigate the changes of the circulation in the mid-latitudes under climate change. Moreover, the LEC can be analyzed over a specific region by an estimate of local energetics (Clément et al., 2017). This is of importance in understanding the regional weather disturbances and the eddy activities under a warmer climate.

1.3 CONTRIBUTIONS OF THIS DISSERTATION

1.3.1 *Maintenance mechanisms of heat waves*

The first contribution of this dissertation provides a way to diagnose the maintenance mechanism of regional heat waves. Numerous research on heat waves focus on their variations or the large-scale or regional-scale mechanisms that trigger heat waves, but few studies investigated the (thermo-)dynamic mechanisms and maintenance of heat waves. Thus, the first aim of this dissertation is to explore the maintenance mechanisms involved in persistent heat waves.

Heat waves are often associated with persistent large-scale circulation anomalies, i.e., blockings or (quasi-) stationary Rossby waves, as discussed

in Section 1.1.2. Without a stalling quasi-stationary Rossby wave, heat waves are unlikely to occur, even in the presence of already-desiccated expanses of soil (Zschenderlein et al., 2019). This stalling large-scale circulation can be described as a stationary anticyclone (hereafter, anomalous stationary waves) (Hannachi et al., 2017). Under the persisting anomalous stationary waves, heat waves tend to occur and last for several days or weeks. Therefore, the maintenance of the anomalous stationary waves can be regarded as a proxy to study persistent heat waves.

The large-scale circulation is often divided into the zonal mean and the zonally asymmetric components, where the zonally asymmetric component depends strongly on the zonal variations while the zonal mean component is less dependent on the zonal variations (Holton and Hakim, 2012a). The zonally asymmetric component is generally called the stationary wave (eddy). Thus, by using temporal and spatial decomposition, the anomalous stationary wave is defined as the deviation from the zonal mean of the time-mean flow (Ma and Franzke, 2021; Wang, 2010). These anomalous stationary waves explain the changes in the atmospheric general circulation. They are closely linked to the regional climate due to their positive correlation with the large-scale zonal variations in temperature (Liu et al., 1998; Wang, 2010), and play a significant role in the wave-driven zonal mean circulation as well (Simpson et al., 2016; Wang, 2010).

Based on the linear stationary Rossby wave theory (Hannachi et al., 2017; Simpson et al., 2016; Ting and Yu, 1998), stationary waves arise from the forcing of longitudinal asymmetries in the topography, the diabatic heating, the transient eddy heat and vorticity fluxes, and their interactions. Depending on the magnitude and location of the perturbation of the forcing, changes in any of the forcing terms or their nonlinear interactions between each other may modify the stationary wave patterns (Sobolowski et al., 2011). Both linear and nonlinear numerical models have been developed to simulate the observed stationary wave field (Held et al., 2002). The main idea of a stationary wave model is to simulate the stationary wave in the presence of a prescribed zonal mean flow and a zonally asymmetric forcing. A detailed review of the history of developing stationary wave models can be found in Wang (2010) and Held et al. (2002).

In this dissertation, a fully nonlinear stationary wave model (NSWM) developed by Ting and Yu (1998) is used to explain and understand the forcing and the maintenance of the observed anomalous stationary waves during heat waves. Although the NSWM has some limitations (Held et al., 2002), such as low horizontal and vertical resolutions, it enables us to identify causal relationships among different forcing terms and provides information about the nonlinear interactions among the forcings in maintaining stationary waves. Additionally, as mentioned in Section 1.1.2, the influence of tropical heating on the stationary waves and regional heat waves is still unclear. Hence, the NSWM is used to diagnose the contributions of tropical heating as well.

The observed increases in the frequency and the intensity of the extreme heat events have been found in most mid-latitude regions, linking to anthropogenic global warming (Coumou et al., 2018). In the mid-latitudes, European heat waves are generally associated with persistent blocking highs, which interrupt the prevailing westerlies from the North Atlantic and are associated with the fair weather and clear skies, bringing increased radiative forcing, and then leading to a temperature rise near the surface (Ma and Franzke, 2021). Moreover, due to anthropogenic global warming, heat waves in Europe will become more common by the end of the twenty-first century (Fragkoulidis et al., 2018). Therefore, the European heat waves require further research. Further details can be found in the first appendix or Ma and Franzke (2021).

Overall, the first part of this cumulative dissertation conducts a systematic study of the dynamical processes driving the circulation anomalies during persistent European heat waves using the NSWCM. Based on the Japanese Reanalysis (JRA-55) dataset (Kobayashi et al., 2015), a number of European heat wave events are selected and examined. Specifically, this dissertation contributes to a better understanding of the maintenance mechanisms of heat waves by addressing the following research questions. The below part is summarized from our first paper in Ma and Franzke (2021):

1. What are the significant forcing terms contributing to the observed anomalous stationary waves?

Transient vorticity fluxes play a dominant role in maintaining the observed anomalous stationary waves. Further decomposition of the transient vorticity fluxes reveals that they are dominated by the high-frequency rotational component, with the divergent component being much smaller. Different from the maintenance of the summer climatological stationary waves (Ting, 1994), our results indicate that diabatic heating tends to make negative contributions to the maintenance of the observed anomalous stationary waves during heat waves, especially over the UK and eastern Europe. Furthermore, through the nonlinear interaction with other forcings, the orographic effects make moderate contributions to the maintenance of the observed anomalous stationary wave, especially via the nonlinear interaction with diabatic heating.

2. What are the relative contributions from the different nonlinear interactions to the observed stationary waves?

Our model simulations show that the nonlinear interactions between the three forcing terms (orographic forcing, diabatic heating, and transient momentum fluxes) make substantial contributions to the observed stationary waves. In particular, while the diabatic heating as an individual forcing leads to rather small anomalous stationary wave responses, together with the transient fluxes, it makes a substantial contribution. This

indicates that all three forcings are necessary for maintaining anomalous stationary waves and European heat waves.

3. Which tropical region contributes most to forcing the anomalous stationary waves associated with European heat waves?

The NSWMM simulations show that the tropical heating located in the tropical Indian Ocean and the Western Pacific and the tropical Atlantic forces the observed anomalous stationary waves remotely, and the former plays a stronger role than the latter. Moreover, the heating over the mid-latitude North Atlantic also makes contributions to the anomalous stationary waves mainly over southwestern Europe.

Thence, the successful application of the NSWMM enabled us to examine the relative contributions of various nonlinear effects to the maintenance of regional heat waves. From a forecasting perspective, our research findings show that there is a potential for improving seasonal forecasts using selected predictors for the statistical forecasting of European heat waves. For example, we consider the forecasts by considering the nonlinear effects involved in the anomalous stationary waves and the heating sources in the nearby and the remote tropical regions. Our results also pave the way for research on persistent extreme weather events, like droughts or floods which are induced by large-scale circulation anomalies.

1.3.2 *Changes in the maintenance mechanisms*

The second contribution of this dissertation provides a way to investigate the changes in the maintenance mechanisms under a warmer climate. Motivated by the identified increasing trends in anticyclonic circulations (Barnes et al., 2014; Horton et al., 2015; Lee et al., 2017), the second aim of this dissertation is to explore the impact of recent climate warming on the maintenance mechanisms of large-scale circulation anomalies during heat waves.

The atmospheric large-scale circulation generally governs the surface weather variability. Horton et al. (2015) found significant trends in the occurrence of atmospheric circulation patterns since 1979. Observations show that these increasing trends in anticyclonic circulations have contributed to the frequent occurrence of summer heat waves over parts of Eurasia and North America (Lee et al., 2017; Screen and Simmonds, 2014). Inner East Asia, as one of those experiencing frequent occurrence of the anticyclonic circulation regions, is suffering from more frequent summer heat waves and droughts (Erdenebat and Sato, 2016; Hessel et al., 2018). Zhang et al. (2020) identified an intensified anticyclonic circulation anomalies over inner East Asia, associated with an enhanced land-atmosphere coupling and more frequent summer heat waves. They further warn that regional climate is shifting to hotter and drier, and is potentially irreversible. Although Zhang et al. (2020) indicated that the

enhanced land-atmosphere coupling could contribute to intensifying surface warming and anticyclonic circulation anomalies, the maintenance mechanisms involved in the circulation anomalies remain largely unclear, especially recent climate warming may play a role in causing dynamic and/or thermodynamic changes in the maintenance mechanisms.

Overall, the second part of this cumulative dissertation focuses on whether recent climate change has altered the maintenance processes of heat waves. Based on the JRA-55 reanalysis dataset, we find a significant warming trend over inner East Asia from 1958 to 2019. A breakdown of the period into 1958-1988 and 1989-2019, we confirm the significant regional warming trend is dominated by the intensified surface warming from 1989 to 2019. We thus identify heat waves for each of the two periods. Following our previous research in Ma and Franzke (2021), we conduct numerical simulations using the NSWMM to investigate the dynamical process in maintaining heat waves over inner East Asia, and then explore whether the recent climate warming has altered the maintenance mechanism of the large-scale circulations during heat waves.

This part of my dissertation contributes to a better understanding of climate warming impacts on heat waves from a maintenance perspective. More specifically, this part answers the following questions. The below part is summarized from our second manuscript (details see the second appendix):

1. How does climate warming affect regional large-scale circulations and related heat waves?

A significant warmer period with an intensified anticyclonic system is confirmed from 1989 to 2019 over inner East Asia. This anticyclonic system is causing more frequent and longer-lasting heat waves. Heatwaves are identified from 1958 to 1988 and from 1989 to 2019, respectively. The large-scale circulation anomalies are composited for each period during heat waves. The differences in the spatial patterns of the observed stationary waves for the two periods present a wavelike pattern, which resembles a strengthening Silk Road pattern over Eurasia (Ding and Wang, 2005). This Silk Road pattern has been proved to contribute frequent and longer-lasting heat waves over inner East Asia in (Wang et al., 2017a) and (Ding and Wang, 2005).

2. Which forcing process is affected most by regional climate warming?

The NSWMM can faithfully reproduce the observed anticyclonic system for both periods. The reproductivity of NSWMM is better from 1958 to 1988 than from 1989 to 2019. It is mainly due to the lack of land-atmosphere coupling process in the NSWMM, which is enhanced their role in intensifying regional anticyclonic circulation anomalies since the late 1990s (Zhang et al., 2020). Moreover, the transients are a dominant factor in reproducing the observed stationary waves for both periods, especially

the high-frequency transient vorticity fluxes. The nonlinear interaction between different forcing terms is also important to the maintenance of the observed anomalous stationary waves. Further, our results suggest that the maintaining mechanisms have changed in a warmer climate, mainly through the nonlinear interactions between different forcing terms. In particular, the nonlinear effects of diabatic heating become more dominant through its interaction with orography and transients.

3. Does tropical heating play a different role under a warmer climate?

The diabatic cooling due to the radiative cooling dominates over inner East Asia, indicating the persistence of the anti-cyclonic system with strong descending motions. The NSWMM simulations suggest that heating anomalies over the Indian Ocean and the Pacific are more important than the Atlantic in maintaining stationary waves during heat waves over inner East Asia. Under a warmer climate, the changes of the maintaining mechanisms between the two periods are generally forced by the heating anomalies mainly over mid-latitude North Pacific and the tropical Indian Ocean. Additionally, results imply that the SST decadal oscillation over the Pacific, the East Asian summer monsoon, and the tropical Indian Ocean are strengthening their role in rising surface temperatures over inner East Asia.

Thence, this part of the thesis attempts to provide a feasible way to indicate that the warming climate has changed the maintaining mechanisms of large-scale circulation patterns, during heat waves at least. Our findings may provide insights into improving climate models and building statistical methods in heat wave forecasting over inner East Asia, to cope with the rising risk of livestock and rangeland crisis under a hotter and drier climate (Zhang et al., 2020).

1.3.3 *Trends in atmospheric energy cycles*

The third contribution of this dissertation is a broader perspective on the understanding of climate change using the LEC. Previous studies focus on the mean states of the Lorenz energy cycle of the Earth's global atmosphere. However, as mentioned in Section 1.2, the long-term temporal variations of the global atmospheric energy cycle, especially the relationship between the temporal variations of the LEC and the key modes of climate variability, are less studied. Thus, the third aim of this dissertation is to provide an extensive analysis of the variability and trends in the atmospheric energy cycle.

The long-term temporal characteristics of the atmospheric LEC are examined using the JRA-55 reanalysis dataset (Kobayashi et al., 2015). The JRA-55 covers the period from 1958 when regular radiosonde observations began on a global basis, and it is a comprehensive atmospheric dataset suitable for studying

multi-decadal variability and climate change as well. The LEC is computed by the diagnostic tool, TheDiaTo, developed by Lembo et al. (2019b). The calculation in TheDiaTo follows the LEC framework proposed by Lorenz (1955) and extended by Ulbrich and Speth (1991). The advantage of TheDiaTo is that it allows for the systematic investigation of the energy exchanges embedded in the atmospheric general circulation within the troposphere (from 900 hPa to 100 hPa) across different spatial scales of motion. It should be noted that, similar to the formulation proposed by Lorenz and widely adopted afterward, motions are assumed to be quasi-hydrostatic and the approach used in this diagnostic tool assumes a dry atmosphere (Lembo et al., 2019b).

The computed energy terms inside TheDiaTo are depicted schematically in Fig. 4. Moreover, TheDiaTo allows the decomposition of stationary and transient eddy energies into waves with different zonal wavenumbers. Waves at different scales might contribute differently to the weather and climate variability by transferring the heat and the momentum fluxes (Chemke and Ming, 2020; Lembo et al., 2019a). Therefore, the variations of eddy energies in the LEC are considered on different zonal wavenumber regimes. In doing so, the stationary and the transient eddy energies are decomposed into three wave number groups: the planetary-scale waves (PW, zonal wave-number 1-3), the synoptic-scale waves (SW, wave-number 4-9), and the mesoscale waves (MW, wave-number 10-21).

Global- or regional-scale climate variables, such as the sea surface temperature, the surface pressure, or the wind speed, fluctuate more or less regularly in terms of spatial structures or patterns (De Viron et al., 2013; Stephenson et al., 2004). Many of these regular fluctuations are often referred to as modes of climate variability (Hernández et al., 2020), which are at most quasi-periodic with oscillations in a characteristic or phase and monitored using the scalar-valued climate indices (De Viron et al., 2013; Hannachi et al., 2007; Hernández et al., 2020). By modulating atmospheric circulation on different spatial and temporal scales, these modes have been proven to have a substantial impact on global and regional temperature extremes (Kenyon and Hegerl, 2008) and precipitation extremes (Kenyon and Hegerl, 2010). However, the relationship between these modes of climate variability and atmospheric energetics has not been fully investigated. Only a few previous studies discussed this relationship qualitatively. For example, Pan et al. (2017) reported that time series of the mechanical energies show not only long-term linear trends, but also some inter-annual variabilities like El Niño-Southern Oscillation signals; Li et al. (2011) analyzed the mechanical energies of the global atmosphere during the El Niño and La Niña years and revealed that mean energies increased during El Niño years and decreased during La Niña years.

In this dissertation, I thus provide an extensive analysis of the relationships between the variations of the LEC components and the key modes of climate variability, and discuss the potential physical processes regarding such relationships. Three types of climate indices representing modes of climate

variability are used in this study: atmospheric indices, oceanic indices, and temperature indices. Further, the non-parametric Mann-Kendall test is used to examine the trends of different components of the Lorenz energy cycle and the Sen's slope is used to estimate the magnitude of the trends (Mann, 1945; Sen, 1968). The considered modes of climate variability and other methods can be found in the third appendix or Ma et al. (2021).

Overall, the third part of this cumulative dissertation performs a comprehensive investigation into the variability of atmospheric energetics. By checking the statistical differences between the energies in the pre-satellite period and the satellite-era, a significant jump exists in the zonal mean and the eddy energies around 1979. It is likely that this jump introduces an inhomogeneity into the components of the Lorenz energy cycle. Thus, the results focus on the trends and the variability of the LEC between 1979 and 2019. This part of my dissertation contributes to a better understanding of climate change from a broader perspective. More specifically, I summarize the main results by answering the following questions. The below part is summarized from our paper in Ma et al. (2021):

1. What are the trends of the mechanic energies?

The total mechanic energy in the troposphere did not significantly change during the period 1979–2019. However, the eddy available potential energy exhibits a significant positive trend, especially the transient eddy available potential energy in the Southern Hemisphere. This is consistent with the increase in storm track strength in the Southern Hemisphere (Franzke and Harnik, submitted).

2. How efficient is the atmospheric energies conversion?

The conversion rate between the eddy available potential and the eddy kinetic energy, and between the zonal mean available potential and the zonal mean kinetic energy has significantly increased. The significant trend of the former is mainly through the transient eddies indicating a strengthening of baroclinic eddy activity in the climate system; the latter suggests the role of the expansion of the Hadley cell over the last few decades.

3. What is the scale of the wave-activity that dominates the eddy energies?

A decomposition of the eddy energies into different wave-number groups shows that the energies of planetary-scale waves dominate the stationary eddy energies; the energy carried by the synoptic-scale waves dominates the transient eddy energies with a significant increasing trend. Results confirm the recent findings on the intensification of eddy activity (Pan et al., 2017) and synoptic-scale waves (Chemke and Ming, 2020).

4. What key modes of climate variability have a close relationship with the atmospheric energetics?

A tight correlation exists between the temporal variations of most Lorenz energy cycle components and the atmospheric and oceanic indices. Among those modes, the El Niño-Southern Oscillation, the Arctic Oscillation, the Southern Annular Mode, and the Pacific Decadal Oscillation contribute the most to the interannual variability of the Lorenz energy cycle. The correlations with the temperature differences indicate that the variations are more related to the meridional heat transport over the Southern Hemisphere. While the highest correlations with modes of climate variability have modest correlation values, these modes nevertheless have a significant impact on the Lorenz energy cycle.

Thence, the third part of the dissertation contributes to an understanding of the variations of the atmospheric energetics and the changes in atmospheric circulations. The results provide a basis to evaluate general circulation models and can assist the diagnosis of eddy activities within the troposphere. Moreover, some key modes of climate variability are pointed out to play an important role in the variations of atmospheric energetics. However, it should be noted that these correlated results do not indicate any cause-effect relationship.

1.3.4 *Atmospheric energy cycles and heat waves*

Finally, the overarching theme of this dissertation is to discuss the mechanisms involving persistent heat extremes and the hints from the variation of atmospheric energy cycles. For this purpose, I present the potential linkage between atmospheric energy cycles and the maintenance of heat waves.

The surface weather conditions, especially the local temperature and precipitation extremes, are closely related to the occurrence of anomalous large-scale atmospheric circulations (Barnes et al., 2014; Coumou et al., 2014). Horton et al. (2015) reported that increasing trends in the occurrence of anticyclonic circulations have contributed substantially to the boreal summer hot extremes over parts of Eurasia and North America. They further concluded that the changes in the regional circulation patterns have altered the risk of extreme temperatures. However, the implications of these changes in the circulation to the variations in the atmospheric energetics and the intensity of the cyclones and the anticyclones are not clear. Hence, analysis of variations in atmospheric energy paves the way to an understanding of the strengthening or weakening of the circulations (Hu et al., 2004), and helps to illustrate the response of weather disturbances or extremes to a changing climate (Kim and Choi, 2017).

Baroclinic instability over the mid-latitudes is responsible for generating various weather systems. The instability grows by converting the available potential energy into eddy kinetic energy. The baroclinic process is maintained by the horizontal temperature gradient between the tropics and the polar regions (Galfi, 2018). The resulting eddy kinetic energy is often used to

measure the strengths and frequencies of cyclonic and anticyclonic systems (Coumou et al., 2015), and is used to represent storm track activity (Lehmann et al., 2014) since weather variation occurs when the mean atmospheric energy cascades into smaller eddies (Kim and Choi, 2017). The intensification and weakening of the cyclones and anticyclones is then linked to the gain or the loss of eddy kinetic energy (Lorenz, 1955). Therefore, the atmospheric circulation change derived from the energetics can assist the understanding of the changes of the weather extremes controlled by the large-scale cyclones and anticyclones (Hu et al., 2004).

Previous studies have examined the role of eddy kinetic energy in summer extremes. For example, Coumou et al. (2015) extracted the eddy kinetic energy by applying a 2.5- to 6-day bandpass filter to the observed wind field data, and revealed a general negative correlation between those two variables. They concluded that the warm summer months are associated with low eddy kinetic energy. This negative correlation is more significant over Eurasia and North America. Moreover, they reported a steady decline in the summertime eddy kinetic energy over the Northern Hemisphere, in particular, over the mid-latitudes. This decline was observed at all pressure levels, with the strongest in the lower to mid-troposphere. This decline is also projected by the CMIP5 climate models under a high-emission scenario (Lehmann et al., 2014). Coumou et al. (2015) further discussed that the low eddy kinetic energy creates favorable conditions for the buildup of heat and drought over the mid-latitude continents, and thus it might have contributed to more persistent heat waves in recent summers.

Similarly, by using the eddy kinetic energy as a measure of storm track activity, Lehmann and Coumou (2015) found that the monthly rainfall/wet extremes are associated with a strong storm track activity (high eddy kinetic energy) and a dry/heat extreme with low storm track activity (low eddy kinetic energy). They suggested that the low summer eddy kinetic energy implies low rainfall and high temperatures, which both have a drying effect on soil. Once the soil has dried out, the surface temperature can increase and lead to the heat waves through the positive soil-atmosphere feedback as explained in Section 1.1.2. Thus, the low summer eddy kinetic energy can influence temperature directly and indirectly. Moreover, Lehmann and Coumou (2015) also reported a general decreasing trend of eddy kinetic energy over mid-latitude continental land regions (Fig. 5), which might have contributed to the observed weather extremes, like the European heat wave in 2003, the Russian heat wave in 2010, and the American heat wave in 2012. Additionally, by regressing the eddy kinetic energy and geopotential height anomalies, Lehmann and Coumou (2015) found a significant negative correlation during the summer season as well. They then argued that low eddy kinetic energy creates favorable conditions for atmospheric blocking and hence persistent weather over the continental land at least in summer, in agreement with Dong et al. (2013) and Coumou et al. (2015).

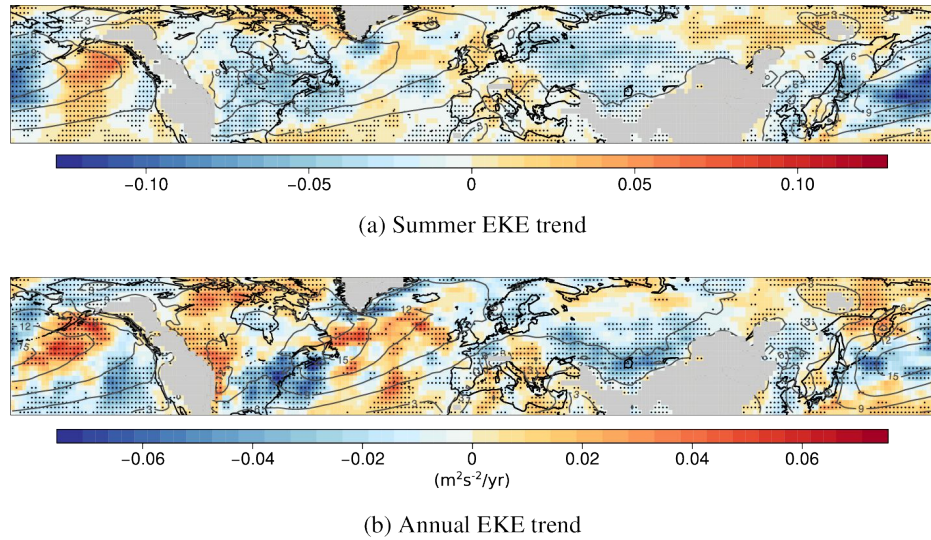


Figure 5: Trends in eddy kinetic energy (EKE) for the time period 1979-2014 in summer (a) and annual (b). Figure taken from Lehmann and Coumou (2015). Contour lines denote EKE climatology in the corresponding season and land regions higher than 1 km have been masked.

Our diagnosis in Ma et al. (2021) shows consistent results with the reported declining trend of eddy kinetic energy over the Northern Hemisphere (Coumou et al., 2015; Lehmann and Coumou, 2015; Lehmann et al., 2014). This provides further information that this downward trend can be accounted for a decrease in transient eddy kinetic energy. As shown in Fig. 6c, it confirms the correlations between summertime surface temperature anomalies and the estimated eddy kinetic energy during 1979-2019 similar to Lehmann and Coumou (2015) (Fig. 6a) and in Coumou et al. (2015) (Fig. 6b). Some discrepancies exist between the correlations obtained in this dissertation and previous studies mainly over Northern America and northern Russia. These discrepancies are due to the inclusion of the eddy kinetic energy data on the annual scale averaged over all seasons and also vertically averaged between 900 hPa to 100 hPa, which is different from the one used in the Lehmann and Coumou (2015) and Coumou et al. (2015). However, a general consistent negative correlation still can be found in Fig. 6a-c over the northern Atlantic and Europe. Therefore, this dissertation supports the conclusion that storm activity has weakened during the past few decades and suggests that this weakening might favor the occurrence and persistence of heat extremes over Eurasia.

Following the LEC framework, I further present the correlations between the decomposed eddy kinetic energy and the temperature anomalies in Fig. 7. By comparing Fig. 7 and Fig. 6, the results show that the negative correlations between eddy kinetic energy and temperature over the continental mid-latitudes are mainly due to the contributions from the stationary kinetic energy rather than the transient component, while both components contribute to the neg-

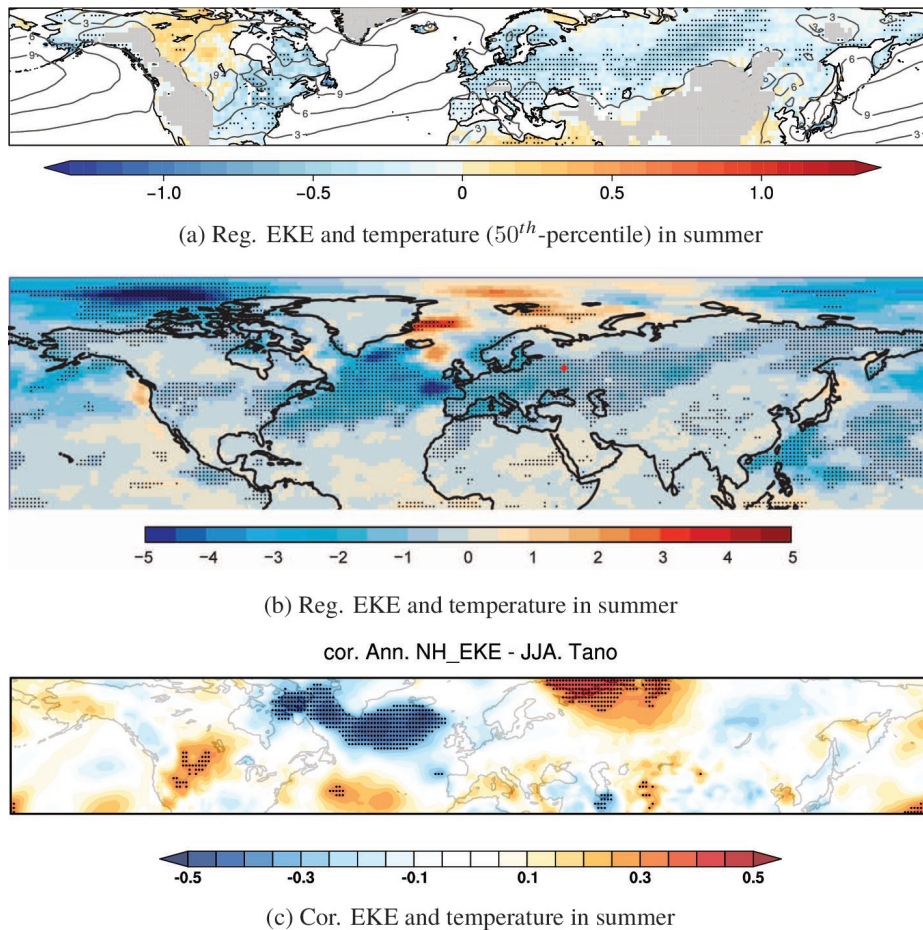


Figure 6: Relationship between EKE and surface temperature in summer. (a) Slope of quantile regression analysis selected of 50th-percentile and the EKE is estimated at 850 hPa during 1979-2014 (figure taken from Lehmann and Coumou (2015)). (b) Slope of regression analysis during 1979-2013 (figure taken from Coumou et al. (2015)). (c) Pearson correlation coefficients during 1979-2019. Both variables were linearly detrended, and stippling indicates significance at the 5% level.

ative correlation over the northern Atlantic. Based on the decomposition of the eddy kinetic energy into different wave-number groups, our results further suggest that the stationary energies embedded in the wavenumbers 4-9 (synoptic-scale) comprise the largest contribution to the negative correlation over the continent in the mid-latitude of the Northern Hemisphere. Thus, results suggest that it is the declining stationary eddy energy embedded in the synoptic-scale waves that have contributed to the more persistent heat waves in recent summers. This result could support the linkage between the amplified quasi-stationary planetary waves and the prolonged heat extremes at the surface in response to Arctic amplification as proposed by Coumou et al. (2015) and Lehmann and Coumou (2015).

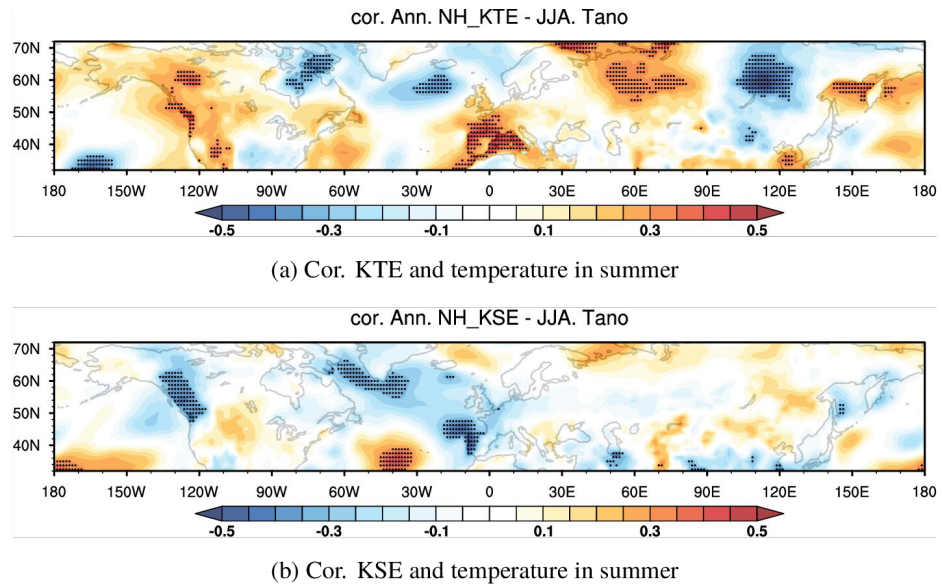


Figure 7: Same as Fig. 6c, but for the correlations between transient (a) and stationary (b) eddy kinetic energy and surface temperature anomalies.

Additionally, as stated in Section 1.3.3, this thesis supports the observed expansion of the Hadley cell over the last few decades from the increased conversion rates of the zonal mean available potential and the zonal mean kinetic energy. The expansion has been shown in Seager et al. (2010), where they indicate the reduced precipitation in the subtropics and mid-latitudes is due to the poleward expansion of the sinking branch of the Hadley cell. These drying trends in the subtropics could potentially increase the aridity, modify the soil moisture, and raise the risk of experiencing heat waves through land-atmosphere coupling processes (Horton et al., 2016). This inhomogeneous drying could redistribute precipitation and impact the regional hydrological cycle, then potentially alter the characteristics of heat waves under the background of climate change. However, the conversion rate of the zonal mean energies in this dissertation is calculated over the annual (temporal-resolution) and the global (spatial-resolution) scales. Further study is needed to quantify the expansion on a finer temporal and spatial scale.

This dissertation supports the argument that summer heat extremes are associated with low eddy kinetic energies, and the decreasing trends of the eddy kinetic energies might have contributed to more persistent heat waves in the mid-latitude Northern Hemisphere. The decrease of the eddy kinetic energies is mainly due to the transient eddy kinetic energy, while the stationary eddy kinetic energy embedded in the synoptic-scale waves may contribute the most to the maintenance of summer heat waves. Note that all results are obtained from the JRA-55 reanalysis product. It is important to bear in mind that using another reanalysis dataset may provide slightly different results at a regional scale. It is due to some known caveats in different reanalysis

datasets from the observational networks and the integrations of modern data systems (Coumou et al., 2014; Hu et al., 2004; Kobayashi et al., 2015).

1.4 CONCLUDING REMARKS AND PATHS FORWARD

1.4.1 *Concluding remarks*

A nonlinear stationary wave model has been successfully used to diagnose the maintenance mechanisms of large-scale circulations during heat waves. The diagnosed processes include examination of the contributions from different types of forcing and the investigation of the role played by tropical heatings over Europe. This dissertation further confirms that the maintenance mechanisms of the circulations might have been altered by regional climate warming. This warming caused significant changes in the nonlinear interactions among different forcing processes over inner East Asia. Thus, this thesis offers a new way to understand the dynamical and physical mechanisms of persistent weather extremes through anomalous stationary waves and deepen our understanding of the impact of climate warming on heat extremes. From a forecasting perspective, the research findings from this thesis show the potential of improving seasonal forecasts or which predictors to select for the statistical forecasting of heatwaves. Results can provide insights into improving global or regional climate models for predicting hot extremes under climate change.

This dissertation focuses then on the variations of the atmospheric circulation by the measure of atmospheric energetics. Results show an overall strengthening of baroclinic eddy activity in the climate system, especially over the Southern Hemisphere. Meanwhile, results support the observed expansion of the Hadley cell, which may lead to a drying trend in the subtropics. The large-scale modes of climate variability are linked with the variations of atmospheric energetics. The El Niño-Southern Oscillation, the Arctic Oscillation, and the Southern Annular Mode are proven to have an important role in modulating the atmospheric energy cycle, thus impacting the changes in global atmospheric circulations.

Finally, this dissertation discusses the potential linkage between atmospheric energetics and the summer heat extremes over the Northern Hemisphere mid-latitudes. The results are in agreement with previous studies as shown in Section 1.3.4. This potential linkage offers a promising way to understand changing circulations and persistent summer heat waves. The preliminary results are that the transient eddy kinetic energy is responsible for the overall decreasing trend in the eddy kinetic energy, while the stationary eddy kinetic energy accounts largely for the correlations between the eddy kinetic energy and persistent summer heat waves. Further decomposition indicates that the stationary eddy kinetic energies embedded in synoptic-scale waves contribute

the most to the persistent positive summer temperature anomalies over the mid-latitudes, especially over Europe.

1.4.2 *Paths forward*

Plenty of research can be carried out to move forward from this thesis towards a better understanding of heat waves and their relationship with atmospheric energetics. First, this thesis uses the nonlinear stationary wave model to simulate the large-scale circulation anomalies during heat waves and diagnose the maintenance mechanisms of heat waves. The model is developed on a low horizontal and vertical resolution. The orographic effect, for example, on both the background flow and its nonlinear interactions with the diabatic heating may be restricted by the current low-resolution model. Also, the simplicity of the current model cannot truthfully simulate certain teleconnection patterns (e.g. the NAO) in the climate (Ma and Franzke, 2021). Thus, using a higher spatial resolution may provide a more complete and precise insight into our understanding.

Working with a more advanced climate model may extend our conclusions as it includes feedbacks with other components affecting heat waves. For example, coupling the model with a land model may improve the quality of the numerical simulations and the accuracy of the simulated stationary waves, especially the amplitude of these waves. As land-atmosphere coupling is strengthening during heat waves, quantifying the contribution of this enhanced coupling to the maintenance mechanisms of large-scale circulations anomalies is also essential under a warmer climate.

The current model is under the assumption of a dry atmosphere, which does not consider the effect of the moisture content, which plays an important role in maintaining heat waves. Under anthropogenic global warming, the moisture content may increase in the lower troposphere, which may result in higher latent heat release and frequent convective activities. Thus, including moisture information in the simulation would be helpful to evaluate the impact of global warming on the thermodynamics of heat waves.

The relationship between atmospheric energetics and the characteristics of heat waves can be further explored. For example, atmospheric energy is also affected by the moisture content, and that is not considered in this study. With the multi-scale approach, the Lorenz energy cycle can also be used to investigate other extreme events, such as floods and droughts.

Finally, this dissertation draws conclusions based on reanalysis data to investigate the physical mechanisms of heat waves and variations in atmospheric energetics. Using data from long-term climate projections should provide insight into the future trends and changes of these physical phenomena, which could be used for climate change mitigation and adaptation.

APPENDICES

A

THE ROLE OF TRANSIENT EDDIES AND DIABATIC HEATING IN THE MAINTENANCE OF EUROPEAN HEAT WAVES: A NONLINEAR STATIONARY WAVE PERSPECTIVE

Appendix A comprises a paper, which has been published in the journal of *Climate Dynamics* as:

Ma, Q., Franzke, C.L.E. (2021), "The role of transient eddies and diabatic heating in the maintenance of European heat waves: a nonlinear quasi-stationary wave perspective", *Climate Dynamics* 56, 2983–3002. doi: <https://doi.org/10.1007/s00382-021-05628-9> (last accessed on 30th of May 2021).

My and other's contributions to this paper are as follows:

I performed the numerical simulations and the analysis, plotted figures, conceived the work, and wrote the manuscript. C.F. contributed to conceive the work, review, and write the manuscript.

The role of transient eddies and diabatic heating in the maintenance of European heat waves: a nonlinear stationary wave perspective

Qiyun Ma^{1,2}, Christian L. E. Franzke^{1,3}

¹Meteorological Institute, University of Hamburg, Hamburg, Germany

²School of Integrated Climate System Science, University of Hamburg, Hamburg, Germany

³Center for Earth System Research and Sustainability, University of Hamburg, Hamburg, Germany

ABSTRACT

European heat waves result from large-scale stationary waves and have major impacts on the economy and mortality. However, the dynamical processes leading to and maintaining heat waves are still not well understood. Here we use a nonlinear stationary wave model (NSWM) to examine the role played by anomalous stationary waves and how they are forced during heat waves. For our study, we use the Japanese Reanalysis (JRA-55) data for the period 1958 through 2017. We show that the NSWM can successfully reproduce the main features of the observed anomalous stationary waves in the upper troposphere. Our results indicate that the dynamics of heat waves are nonlinear, and transient momentum fluxes are the primary drivers of the observed anomalous stationary waves. The contribution from orographic forcing is moderate and mainly through nonlinear interactions with diabatic heating. Further decomposition of the transients indicates that the high-frequency transient vorticity fluxes make dominant contributions. Furthermore, our results reveal that the response to heating located in the tropical Indian Ocean and the west Pacific region is primarily responsible for maintaining the observed anomalous stationary waves linked to European heat waves. This is confirmed by exploring the relationship between heat waves and the Indian Ocean Dipole strength. The heating in the mid-latitude and tropical Atlantic region plays a secondary role. Our results suggest that European heat waves are potentially predictable by considering the nonlinear effects involved in anomalous stationary waves and the heating sources in the nearby and remote tropical region.

A.1 INTRODUCTION

Mid-latitude heat waves are expected to become more frequent and intense due to anthropogenic global warming (Kornhuber et al., 2019; Perkins, 2015). Over the last few decades, heat waves had significant impacts on human health, terrestrial ecosystems, and global crop production (Deng et al., 2018b; Horton et al., 2016). For instance, the 2003 European and the 2010 Russian heat waves produced significant socio-economic damages (Russo et al., 2015). In the context of anthropogenic global warming, heat waves in Europe will become commonplace by the end of the twenty-first century (Carril et al., 2008; Fragkoulidis et al., 2018). Hence, a better understanding of the physical and dynamical processes governing European heat waves is essential for improved predictability and adaptation measures.

In general, European heat waves are associated with persistent large-scale circulation anomalies, i.e., anti-cyclones or blocking highs (Stefanon et al., 2012; Woollings et al., 2018), which interrupt the prevailing westerlies from the North Atlantic and are associated with fair weather and clear skies, bringing an increase of radiative forcing, and then leading to temperature rises near the surface. For example, Zschenderlein et al. (2019) investigated the processes determining European heat waves using Lagrangian analysis and found that co-located anti-cyclones are quite important in establishing high temperatures near the surface due to the subsidence of air. Wolf et al. (2018) demonstrated that European heat waves have a clear connection with localized blocking anti-cyclones, which are also zonally elongated. However, the dynamical mechanisms involved in persistent anti-cyclonic circulations are still unclear.

The identification of the drivers of persistent anti-cyclones is complicated due to the complexity of the dynamical and physical processes involved. Blocking events can be attributed to internal atmospheric dynamics, but also can be triggered or forced by remote anomalous heating over tropical regions (Dole et al., 2011; Park and Lee, 2019). Recent global climate change also contributes to the difficulty in examining the mechanisms, owing to the strongly nonlinear feedbacks in the thermodynamic and physical components of the climate variability (Nakamura and Huang, 2018; Risbey et al., 2018; Schär et al., 2004).

Over Europe, persistent blocking anti-cyclones are part of slow-moving planetary waves or quasi-stationary Rossby waves (Kornhuber et al., 2017). These quasi-stationary waves are the primary drivers of the mid-latitude weather variations on weekly or monthly timescales, and their activities further impact on the position of the jet streams and act as guides for transient perturbations such as storms and blocking events (Held et al., 2002; Sellevold et al., 2016). Petoukhov et al. (2016) and Kornhuber et al. (2019) illustrate that persistent stationary waves can be explained by a phase-locked quasi-resonant amplification. This quasi-resonant amplification leads to persistent extreme circulation events and temperature anomalies through circumglobal wave

patterns as well. Large-scale teleconnection patterns are also associated with stationary waves (Feldstein and Franzke, 2017; Franzke and Feldstein, 2005; Hannachi et al., 2017). For example, Luo et al. (2007) points out that the decay of the positive phase of North Atlantic Oscillation (NAO) events can result in blockings over Europe via enhanced downstream energy dispersion. Li et al. (2020) further demonstrates that the atmospheric circulation during European blocking and positive NAO events leads to a favorable circulation pattern for heat waves over northern and western Europe.

Furthermore, tropical diabatic heating is a major Rossby wave source (Teng and Branstator, 2019). Heating from a tropical region has a significant influence on atmospheric blocking conditions which are necessary to cause anomalous summer heat waves over Europe (Della-Marta et al., 2007). The important tropical regions have been identified as the tropical Atlantic (Cassou et al., 2005), the tropical Indian Ocean and the northwest Pacific regions (Behera et al., 2013). Numerical studies by Bader and Latif (2005) also showed that anomalous Indian Ocean sea surface temperatures have an impact on the NAO and Europe based on a coupled GCM, which has a strong connection to the quasi-stationary waves over Europe (Wolf et al., 2018). However, there is no consensus regarding the locations where heating can force persistent blocking systems over Europe. Building on these findings, our study aims to investigate the dynamical mechanism of maintaining anomalous stationary waves and identify the key region of tropical heating related to European heat waves.

Based on linear stationary Rossby wave theory, stationary waves are defined here as departures from the climatological- and zonal-mean state, which arise from three forcing components: topography, diabatic heating, and transient eddy fluxes (Simpson et al., 2016; Ting, 1994) and their interactions. Changes in any of the forcing terms or their nonlinear interactions between each other may modify the stationary wave patterns, depending on the magnitude and location of the perturbation of the forcing (Sobolowski et al., 2011). Models of intermediate complexity have been used to successfully explain and understand the forcing and maintenance of stationary waves (Held et al., 2002). In this study we use a fully nonlinear stationary wave model (NSWM) developed by Ting and Yu (1998). While this model has some limitations (Held et al., 2002), it enables us to decompose the response to given forcings to help identify causal relationships among the three forcing terms (Simpson et al., 2016). As a nonlinear diagnostic tool, NSWM has been used widely in investigating the maintenance mechanisms of stationary waves in seasonal or climatological settings (Simpson et al., 2016; Ting, 1994), and has also been used in reproducing some basic features of observed waves for specific circulation anomalies (Liu et al., 1998; Schubert et al., 2014). An advantage of the NSWM is that it allows us to diagnose the nonlinear interactions among different forcings in maintaining the stationary waves. To our knowledge,

there are no previous studies that provide a dynamic analysis of the nonlinear effects of European heat waves.

Here, we conduct a systematic study of the dynamic processes driving the circulation anomalies during persistent European heat waves using the NSWMM. While most previous studies focused on individual heat wave events, here we will examine a large set of European heat wave events. Building upon previous studies, we hypothesize that the meteorological aspects of European heat waves are caused by anomalous stationary waves (blocking highs) in the upper troposphere. Specifically, we seek to address the following questions: 1) What are the significant forcing terms of the observed anomalous stationary waves? 2) What are the relative contributions from the different nonlinear interactions to the observed stationary waves? and 3) Which tropical region contributes most in forcing anomalous stationary waves associated with European heat waves? While Ghosh et al. (2017, 2019) found that the heating of North Atlantic mid-latitudes related to the positive Atlantic Multi-decadal Oscillation sea surface temperature is important for European heat waves, in this present paper we find that the heating in the tropical Indian Ocean and the west Pacific region is also important for maintaining a blocking anticyclone over Europe linked to European heat waves. The remainder of this paper is organized as follows: Section A.2 describes the data, the NSWMM and the experimental design, and the decomposition method of the nonlinear interactions of the NSWMM. The results of the identification of persistent European heat wave events and our diagnostic analysis are presented in section A.3. The conclusions are given in section A.4.

A.2 DATA, METHODS, AND MODEL EXPERIMENTS

A.2.1 *Data source*

For our study we obtain the reanalysis data from the 6-hourly JRA-55 (Japanese 55-year Reanalysis) data-set (Kobayashi et al., 2015), with a horizontal resolution of $1.25^\circ \times 1.25^\circ$. We use the JRA-55 data for the period from 1958 to 2017, i.e., 60 years in total. Daily mean fields are obtained from these 6-hourly fields. We limit the analysis to the extended boreal summer period from June through August (JJA). The heating rates provided by JRA-55 can be used to calculate diabatic heating rates directly, by adding of the convective, large-scale condensation, solar and long-wave radiation, and vertical diffusion heating rates (Shi et al., 2020). The diabatic heating rate is a key parameter in the NSWMM, and the resulting total diabatic heating is consistent with other reanalysis products (Zhang et al., 2017).

We use 2 m daily mean air temperature to identify European heat wave events. To examine large-scale circulation anomalies during heat waves, anomalous stationary waves are obtained in the upper troposphere using 200 hPa streamfunction. For each grid point, the daily climatological mean of the

200 hPa streamfunction field ($\overline{\Psi}$) is determined by calculating the mean of the 60-year JJA data. The daily zonal mean of $\overline{\Psi}$ is subtracted at each grid point to obtain the daily climatological stationary wave $\overline{\Psi}^*$. Then, the daily stationary wave Ψ^* is calculated at each grid point by subtracting the zonal mean for each day. Finally, the daily anomalous stationary wave is derived by subtracting $\overline{\Psi}^*$ from Ψ^* for the corresponding day of the year. We average the daily anomalous stationary wave during the respective heat wave event period as the observed anomalous stationary wave for that heat wave event. As for the model simulations, we use the three-dimensional wind, temperature, relative vorticity, surface pressure, diabatic heating, and realistic orographic data.

Moreover, to explore the links between European heat waves and large-scale teleconnection patterns and corresponding sea surface temperature anomalies, the daily North Atlantic Oscillation (NAO) index, and the monthly index representing the strength of the Indian Ocean Dipole (IOD) and the NINO3.4 index which describes El Niño and La Niña events are obtained from the National Center for Environmental Prediction/Climate Prediction Center <https://www.cpc.ncep.noaa.gov/>.

A.2.2 Definition of heat waves

No universal definition exists for a heat wave event due to the fact that various societal sectors are impacted differently by heat waves (Perkins, 2015). Hence, the definition of a heat wave is usually based on the research question at hand (Horton et al., 2016). In general, one can define heat wave events as a period of consecutive days when the daily temperature is above a certain threshold or percentile of the long-term temperature distribution (Deng et al., 2018b; Russo et al., 2015; Stefanon et al., 2012).

In this study, we focus on heat wave events in the European region ($35^\circ - 60^\circ$ N, 10° W - 40° E) over the period 1958 – 2017. A heat wave event here has to satisfy two key criteria: 1) the temperature has to be above a threshold, and 2) this threshold has to be crossed for a certain duration. We define that abnormally high temperatures occur when:

$$\widehat{TG} > \widehat{TG}_{90} \quad (\text{A.1})$$

where the hat represents an area-average over the European region, \widehat{TG} is the area-averaged daily 2 m air temperature, \widehat{TG}_{90} is the 90th percentile of the time series of \widehat{TG} over the period 1958 – 2017.

We identify 80 heat wave events using the above definition (Eq. A.1). We change the duration criterion from 3 to 10 days in steps of 1 day. Nearly half of the 80 heat wave events (38 events) can be identified by increasing the threshold to 5 days (Fig. A.1). These 38 events are sufficient to represent the dynamical processes behind the 80 events. Also, as stated by Guo et al. (2017), the relaxation of the threshold of the heat wave duration will not modify

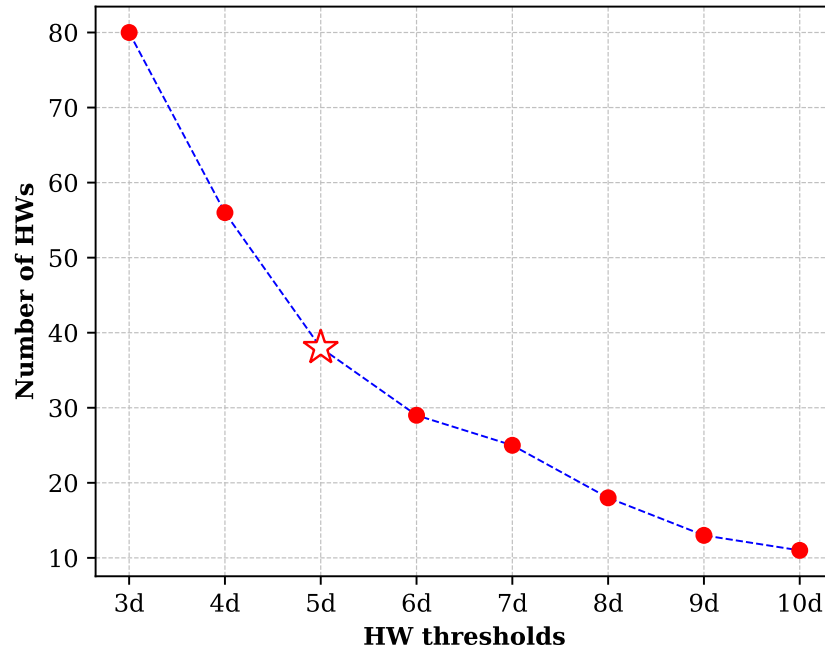


Figure A.1: Number of heat wave events identified by using different duration thresholds.

the heat wave impacts on mortality. Thus, our threshold of 5 days is a good compromise between the duration, to satisfy our assumption of a stationary wave, and the number of heat wave events to analyze. Therefore, we conduct model simulations only focused on these 38 events to facilitate computation. Sensitivity experiments for heat wave events with a longer duration threshold revealed similar results. From this, we derive a heat wave list in section A.3.1, with corresponding start dates, end dates, and durations for each heat wave event.

Moreover, we measure the averaged magnitude of heat wave events by using the daily heat wave magnitude index ($HWMI_d$) from Russo et al. (2015). This index can measure the magnitude of a heat wave event at each grid point based on the corresponding inter quartile range of TG (Fragkoulidis et al., 2018). We averaged this index for each identified heat wave over the European region for easy comparison due to the different durations among the identified events.

A.2.3 Model and experimental design

We focus on the maintenance mechanisms of anomalous stationary waves associated with European heat waves. The nonlinear stationary wave model (NSWM) by Ting and Yu (1998) is used to simulate the observed anomalous stationary waves and diagnose the various nonlinear effects in maintaining

anomalous stationary waves. This idealized model is a time-dependent baroclinic model, which solves the three-dimensional nonlinear primitive equations for deviations from a prescribed zonal mean basic state in response to zonally asymmetric imposed forcings in σ -coordinates (P/P_s), where P denotes the pressure level and P_s the surface pressure. The horizontal resolution is rhomboidal truncation R30 (about $2.25^\circ \times 3.75^\circ$) with 14 unevenly spaced vertical σ levels. The spectral form of the primitive equations has four prognostic equations for vorticity (ζ), divergence (D), temperature (T), the logarithm of surface pressure ($\ln P_s$) and two diagnostic equations for the geopotential (Φ) and vertical velocity ($\dot{\sigma}$):

$$\frac{\partial \zeta}{\partial t} = -\nabla \cdot \{(f + \zeta) \cdot \mathbf{V}\} - \mathbf{k} \cdot \nabla \times \left\{ RT \nabla \ln P_s + \dot{\sigma} \frac{\partial \mathbf{V}}{\partial \sigma} \right\} - \varepsilon \zeta - \nu \nabla^4 \zeta \quad (\text{A.2a})$$

$$\begin{aligned} \frac{\partial D}{\partial t} &= \mathbf{k} \cdot \nabla \times \{(f + \zeta) \cdot \mathbf{V}\} - \nabla \cdot \left\{ RT \nabla \ln P_s + \dot{\sigma} \frac{\partial \mathbf{V}}{\partial \sigma} \right\} - \nabla^2 \left\{ \frac{1}{2}(u^2 + v^2) + \Phi \right\} \\ &\quad - \varepsilon D - \nu \nabla^4 D \end{aligned} \quad (\text{A.2b})$$

$$\frac{\partial T}{\partial t} = -\mathbf{V} \cdot \nabla T - \dot{\sigma} \frac{\partial T}{\partial \sigma} + \frac{\kappa T}{\sigma} \dot{\sigma} + \kappa T \{ (\mathbf{V} - \tilde{\mathbf{V}}) \cdot \nabla \ln P_s - \tilde{D} \} - \varepsilon T - \nu \nabla^4 T \quad (\text{A.2c})$$

$$\frac{\partial \ln P_s}{\partial t} = -\tilde{\mathbf{V}} \cdot \nabla \ln P_s - \tilde{D} \quad (\text{A.2d})$$

$$\frac{\partial \Phi}{\partial \sigma} = -\frac{RT}{\sigma} \quad (\text{A.2e})$$

$$\frac{\partial \dot{\sigma}}{\partial \sigma} = -(\mathbf{V} - \tilde{\mathbf{V}}) \cdot \nabla \ln P_s - (D - \tilde{D}) \quad (\text{A.2f})$$

where the tilde denotes the vertically averaged quantities, $f = 2\Omega \sin \phi$ the Coriolis parameter, Ω the angular velocity of the Earth, ϕ the latitude, \mathbf{V} the 2-D horizontal wind field, and R the specific gas constant.

To describe the evolution of the anomalous variables from a climatological state, the NSWCM decomposes all model variables into the climatological state (represented by an over-bar) and the deviation (represented by a prime), and then removes the climatological state equation from Eq. A.2. The resulting

anomaly equations are (the primes have been omitted in the follow equations for brevity):

$$\begin{aligned} \frac{\partial \zeta}{\partial t} = & -\nabla \cdot \left\{ (f + \bar{\zeta}) \cdot \mathbf{V} + \zeta \bar{\mathbf{V}} + \zeta \mathbf{V} \right\} - \mathbf{k} \cdot \nabla \times \left\{ RT \nabla \overline{\ln P_s} + R \bar{T} \nabla \ln P_s \right. \\ & \left. + RT \nabla \ln P_s + \dot{\sigma} \frac{\partial \bar{\mathbf{V}}}{\partial \sigma} + \bar{\sigma} \frac{\partial \mathbf{V}}{\partial \sigma} + \dot{\sigma} \frac{\partial \mathbf{V}}{\partial \sigma} \right\} + TF_V - \varepsilon \zeta - \nu \nabla^4 \zeta \quad (\text{A.3a}) \end{aligned}$$

$$\begin{aligned} \frac{\partial D}{\partial t} = & \mathbf{k} \cdot \nabla \times \left\{ (f + \bar{\zeta}) \mathbf{V} + \zeta \bar{\mathbf{V}} + \zeta \mathbf{V} \right\} - \nabla \cdot \left\{ RT \nabla \overline{\ln P_s} + R \bar{T} \nabla \ln P_s + RT \nabla \ln P_s \right. \\ & \left. + \dot{\sigma} \frac{\partial \bar{\mathbf{V}}}{\partial \sigma} + \bar{\sigma} \frac{\partial \mathbf{V}}{\partial \sigma} + \dot{\sigma} \frac{\partial \mathbf{V}}{\partial \sigma} \right\} - \nabla^2 \left\{ \frac{1}{2} (u^2 + v^2) + u\bar{u} + v\bar{v} + \Phi \right\} \\ & + TF_D - \varepsilon D - \nu \nabla^4 D \quad (\text{A.3b}) \end{aligned}$$

$$\begin{aligned} \frac{\partial T}{\partial t} = & -\bar{\mathbf{V}} \cdot \nabla T - \mathbf{V} \cdot \nabla \bar{T} - \mathbf{V} \cdot T - \bar{\sigma} \frac{\partial T}{\partial \sigma} - \dot{\sigma} \frac{\partial \bar{T}}{\partial \sigma} - \dot{\sigma} \frac{\partial T}{\partial \sigma} + \frac{\kappa T}{\sigma} \bar{\sigma} + \frac{\kappa \bar{T}}{\sigma} \dot{\sigma} + \frac{\kappa T}{\sigma} \dot{\sigma} \\ & + \kappa T (\mathbf{V} - \bar{\mathbf{V}}) \cdot \nabla \ln P_s + \kappa \bar{T} (\mathbf{V} - \bar{\mathbf{V}}) \cdot \nabla \ln P_s + \kappa T (\mathbf{V} - \bar{\mathbf{V}}) \cdot \nabla \overline{\ln P_s} \\ & + \kappa \bar{T} (\bar{\mathbf{V}} - \bar{\bar{\mathbf{V}}}) \cdot \nabla \ln P_s + \kappa \bar{T} (\mathbf{V} - \bar{\mathbf{V}}) \cdot \nabla \overline{\ln P_s} + \kappa T (\bar{\mathbf{V}} - \bar{\bar{\mathbf{V}}}) \cdot \nabla \overline{\ln P_s} \\ & + \kappa T (\bar{\mathbf{V}} - \bar{\bar{\mathbf{V}}}) \cdot \nabla \ln P_s - \kappa \bar{T} \bar{D} - \kappa T \bar{D} - \kappa T \bar{D} + TF_{TEMP} - \varepsilon T - \nu \nabla^4 T \quad (\text{A.3c}) \end{aligned}$$

$$\frac{\partial \ln P_s}{\partial t} = -\bar{\mathbf{V}} \cdot \nabla \ln P_s - \bar{\mathbf{V}} \cdot \nabla \overline{\ln P_s} - \bar{\mathbf{V}} \cdot \nabla \ln P_s - \bar{D} - TF_{P_s} \quad (\text{A.3d})$$

$$\frac{\partial \Phi}{\partial \sigma} = -\frac{RT}{\sigma} \quad (\text{A.3e})$$

$$\frac{\partial \dot{\sigma}}{\partial \sigma} = -(\bar{\mathbf{V}} - \bar{\bar{\mathbf{V}}}) \cdot \nabla \ln P_s - (\mathbf{V} - \bar{\mathbf{V}}) \cdot \nabla \overline{\ln P_s} - (\mathbf{V} - \bar{\mathbf{V}}) \cdot \nabla \ln P_s - (D - \bar{D}) \quad (\text{A.3f})$$

where TF_{TEMP} denotes the transient heat flux convergence terms, TF_{P_s} the surface pressure term, TF_V the transient vorticity forcing term, and TF_D the transient divergence forcing term. The orographic forcing term is in the hydrostatic equation in Eq. A.3e as the lower boundary condition (Ting, 1994), and also involved in the transient divergence equation in Eq. A.3b through geopotential height. Furthermore, various damping terms including Rayleigh friction and Newtonian cooling (ε), and bi-harmonic diffusion (ν) are used in the NSWMM to prevent baroclinic instability and eliminate small-scale noise. The model coefficients used in this study are identical with those used in Held et al. (2002).

For the simulations in our study, all the NSWMM inputs are from JRA-55. The basic state is a 60-year-average (1958-2017) zonal mean flow consisting of u , v , T , and P_s , first interpolated onto the model σ levels before taking the zonal mean. The period of the basic state is event-dependent; that means that for each heat wave event we use the 60-year climatological mean state corresponding for that event period. For example, if an identified heat wave lasts from 5th-15th June 2003, the basic state will be chosen as 5th-15th June

from the 60-year-averaged zonal mean flow. Therefore, the NSWMM simulates only the response of the zonally asymmetric components, which means the zonal-mean anomalies generated by zonal-mean forcing terms are excluded (Liu et al., 1998). We also tested other definitions of the mean state such as using the climatological JJA mean or the JJA mean in the respective year of the heat wave and the two week period of the respective heat wave. Using those mean states produced very similar results (not shown). This suggests that our results are robust concerning the particular choice of the mean state.

There are three different forcing components for the NSWMM in simulating anomalous stationary waves: diabatic heating (Q), transient momentum fluxes (M), and orography (O). The TF_{TEMP} is included in the diabatic heating forcing following Simpson et al. (2016), given the close linkage between the transient heat fluxes and the tendency for the transients to act diffusively on temperature gradients induced by other diabatic sources. We regard the TF_V and TF_D as transient momentum fluxes forcing, which are computed as in Ting and Yu (1998):

$$TF_V = -\nabla \cdot (\overline{V'\zeta'}) \quad (\text{A.4})$$

and

$$TF_D = \mathbf{k} \cdot \nabla \times (\overline{V'\zeta'}) - \frac{1}{2} \nabla^2 (\overline{V' \cdot V'}) \quad (\text{A.5})$$

where V is the horizontal wind. And the realistic orographic data is from JRA-55. These forcings are then linearly interpolated onto the σ -coordinates of the NSWMM.

We simulate the observed anomalous stationary wave using a time step of 30min. The NSWMM reaches a (quasi-) steady-state after being integrated for around 20 days (Held et al., 2002). Therefore, we take the day 31-50 average for each simulation to ensure that our results are insensitive to the choice of the averaging period. To easily compare with reanalysis data, we also interpolate model results from the σ -coordinate to pressure coordinates.

As discussed in section A.2.2, we first simulate the observed anomalous stationary wave for each of the 38 heat wave events, and the NSWMM is driven by all the forcing terms for each simulation. These simulations for each heat wave event refer to the model sensitivity analysis (see section A.3.2.1). Then, the composite analysis method (Boschat et al., 2016) is used to determine the robust mechanism of the maintenance of the anomalous stationary wave. We composite the observed anomalous stationary wave for the 38 events, and also the corresponding forcing terms to run the NSWMM as the composite experiment.

A.2.4 Decomposition of the forcing terms in the NSWMM

The NSWMM enables us to perform simulations with just a subset of the forcings to systematically identify the relevant forcings and their interactions.

Following Ting et al. (2001), the total nonlinear response of the NSWAM to the three forcings could simply be due to the nonlinear effect of an individual forcing or could be caused by more complex interactions due to various combinations of the three forcing terms and their nonlinear interactions. Hence, we need to quantify these complex mechanisms arising from these forcings in the NSWAM. To this end, we use the factor separation method (Cleveland et al., 2020; Stein and Alpert, 1993) to calculate the NSWAM response to individual forcings and the nonlinear interactions among the different forcings. Ting et al. (2001) and Sobolowski et al. (2011) have already used this method to decompose the results of the NSWAM.

Based on the factor separation method, we can decompose the total nonlinear effect (TNE) between two forcings into individual nonlinear effects (INE) and total effects of nonlinear interactions (TENI):

$$\text{TNE}_{f_i, f_j} = \text{INE}_{f_i} + \text{INE}_{f_j} + \text{TENI}_{f_i, f_j} \quad (\text{A.6})$$

where the subscripts f_i and f_j represent two different forcings, TNE_{f_i, f_j} is the total nonlinear effect of the forcings f_i and f_j , INE_{f_i} and INE_{f_j} are the individual nonlinear effects of forcings f_i and f_j respectively, and TENI_{f_i, f_j} is the total effect of nonlinear interactions between forcing f_i and f_j . Using Eq. A.6, we can quantify the total effect of nonlinear interactions between two forcings (TENI_{f_i, f_j}). Then, the nonlinear interactions between three forcings can be derived as:

$$\text{TENI}_{f_i, f_j, f_k} = \text{TNE}_{f_i, f_j, f_k} - (\text{INE}_{f_i} + \text{INE}_{f_j} + \text{INE}_{f_k} + \text{TENI}_{f_i, f_j} + \text{TENI}_{f_i, f_k} + \text{TENI}_{f_j, f_k}) \quad (\text{A.7})$$

And if we substitute Eq. A.6 into Eq. A.7, we can get the individual total nonlinear effect (ITNE) of a given forcing, for example, f_k . It can be obtained as

$$\text{ITNE}_{f_k} = \text{TNE}_{f_i, f_j, f_k} - \text{TNE}_{f_i, f_j} \quad (\text{A.8})$$

In this way, various mechanisms of the nonlinear responses in the NSWAM can be qualitatively examined. For our simulations, the forcing input in the NSWAM are Q, M, and O. Thus, to get the total linear nonlinear effect of three (TNE_QMO) or two forcings (TNE_QM, TNE_QO, and TNE_MO), the model is run with three or two forcing components. To get the individual nonlinear effects (INE_Q, INE_M, and INE_O), the model is driven by only one forcing. All the total effects of nonlinear interactions (TENI_QM, TENI_QO, TENI_MO, and TENI_QMO) are decomposed following Eq. A.6 and Eq. A.7, as also for the individual total nonlinear effects (ITNE_Q, ITNE_M, and ITNE_O).

Using reanalysis data for our stationary wave analysis has the advantage that our model results can directly be compared with the reanalysis data. However, the reanalysis data might have some dynamical inconsistencies with

the NSW dynamics (Wang and Ting, 1999). A comprehensive comparison of the numerical model and the reanalysis, therefore, is difficult because of the brevity of the reanalysis data set (Teng et al., 2013). Here, an area-weighted spatial pattern correlation (hereafter referred to as pattern correlation) (Ting et al., 2001) is used to determine how well the NSW simulates the spatial structure of the observed anomalous stationary wave. This pattern correlation can further be used to examine the relative contributions of the various mechanisms to maintain the observed anomalous stationary wave while we analyze the decomposed results. The weights are the square of the cosine of latitudes. Note that the pattern correlation measures the similarity between observed and simulated spatial patterns of anomalous stationary wave without considering the magnitude of each pattern. Besides, the statistical significance test is conducted for the pattern correlation following Walsh (2008).

A.3 RESULTS AND DISCUSSION

A.3.1 Identification of heat waves

We devote our attention to the 38 heat wave events which last at least 5 days. Table A.1 describes the characteristics of these heat wave events, including dates, duration, region-averaged temperature anomalies (T_{ano}), and heat wave magnitudes (HWMId). These identified heat waves are in general consistent with recent studies (Petoukhov et al., 2013; Schubert et al., 2014). Specifically, 29 out of 38 (76.3%) events occurred after 2000, which is likely due to anthropogenic global warming. Furthermore, the frequency of heat waves occurring in one year is increasing, for example, 3 events in 2003, and 4 events in 2012 and 2015 respectively. Similarly, the increasing trend is also evident for characteristics of duration, T_{ano} , and HWMId. These increasing trends over Europe may be attributed to regional manifestations of global warming or changes in land-use and associated reductions in soil moisture (Behera et al., 2013). According to T_{ano} and HWMId, the heat waves in 2007, 2010 and 2016 were the most extreme in the last 60 years. Research also shows that these heat wave events were the most extreme over the last 500 years (Barriopedro et al., 2011; Casty et al., 2005).

The composite of surface temperature anomalies (Fig. A.2) for the 38 heat wave events clearly shows that the positive T_{ano} over our defined European region (green box in Fig. A.2a) has a magnitude of up to 4K. This is the composite mean, individual events can reach higher anomalous temperatures. The composite of HWMId exhibits identical spatial patterns with the temperature anomaly as well. By examining the corresponding large-scale circulation conditions, we composite the observed anomalous stationary wave for each event in Fig. A.2b. An upper-level anti-cyclonic system is in phase with the positive temperature anomalies over Europe. This system favors the occurrence and persistence of regional heat waves (Deng et al., 2018b). The persistent blocking

location over Europe blocks the weather disturbances from the Atlantic which could alleviate local summer high temperatures (Behera et al., 2013), and strengthens the advection of warm air masses from northern Africa and the Mediterranean basin (Cassou et al., 2005). Figure A.2b is also consistent with Li et al. (2020), in which they find that European heat waves are corresponding more to a typical European blocking during positive NAO events. We confirm that European heat waves are dominated by an anti-cyclonic circulation aloft. Thus, we conduct a further numerical investigation for the maintenance of this dynamic linkage in the following.

Large-scale teleconnection patterns play an important role in the modulation of European temperatures, especially the NAO, and the atmospheric response to El Niño and IOD events (Cassou et al., 2005; Della-Marta et al., 2007; Schneidereit et al., 2012). Table A.1 shows the values of the corresponding indices of the large-scale teleconnection patterns during each heat wave period. For the NAO index, we averaged the daily NAO index for the duration of the heat wave events; The monthly value of NINO_{3.4} and IOD is shown for the month when the heat wave occurred. Generally, European heat waves tend to occur during the positive IOD phase (30 out of 38 events), negative NAO period (23 out of 38), and positive NINO_{3.4} period.

We also examine this relationship by two-dimensional probability distribution function (PDF) plots of T_{ano} and each corresponding indices for the summer season from 1958 to 2017 and the identified heat wave periods, respectively (Fig. A.2c-e). We estimate the PDFs in a non-parametric way by using a kernel density estimator (Silverman, 1986). There is a clear positive linear relationship between T_{ano} and IOD when all days are considered. But for a given value of IOD, T_{ano} is much stronger on heat wave days than it normally is, indicating that factors other than IOD must also contribute to persistent heat waves (Teng et al., 2013). There is a slight negative relation between T_{ano} and NINO_{3.4} for all summer months. There is no evident relationship between NAO and T_{ano} but high-temperature anomalies have a slight tendency for negative NAO events.

Our results are consistent with Behera et al. (2013) who also explored the relationship between European heat waves with the IOD and NINO_{3.4} indices. Their research demonstrated that IOD events have a significant influence on summer heat waves over western Europe. They also indicated El Niño and La Niña events play a role in the extreme Eastern European events. The role of El Niño and La Niña in European heat waves is also examined in Trenberth and Fasullo (2012) and Schneidereit et al. (2012). They found that the 2010 Russian heat wave had a strong link to La Niña conditions which is also shown in Table A.1. The linkage of IOD, El Niño and La Niña events reveals the influence of the tropics on European summer heat waves. This motivates us to further examine the role of different tropical regions in forcing and modulating heat waves in the following section.

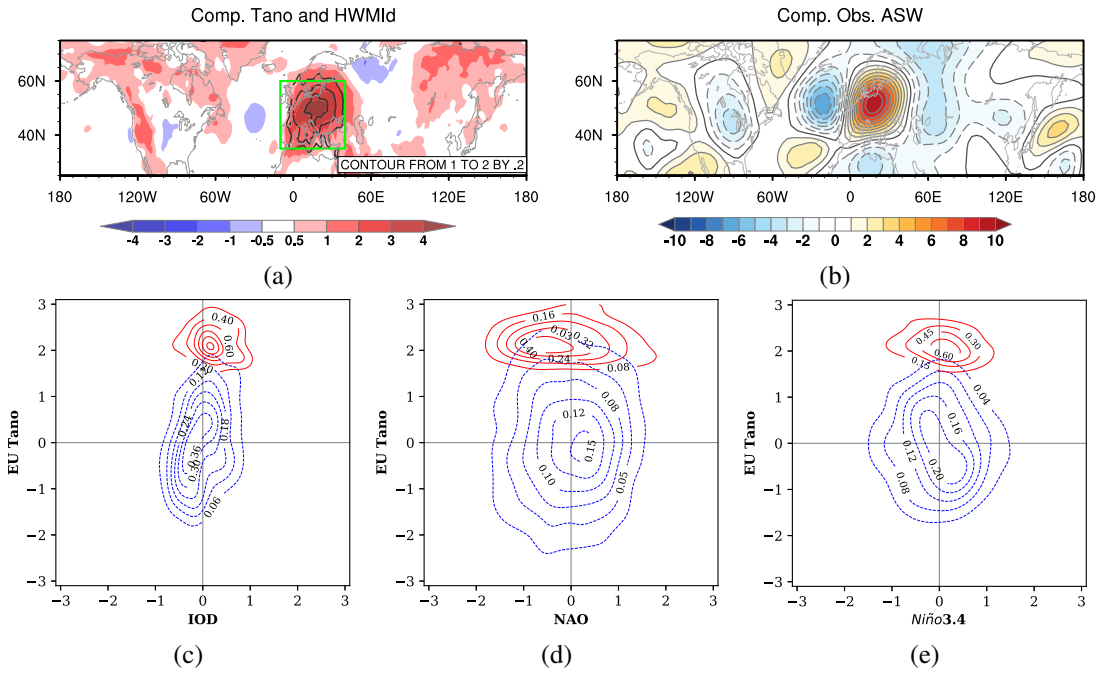


Figure A.2: **(a)** Composite spatial pattern of temperature anomalies T_{ano} (shading) and the heat wave magnitude HWMId (contour); the green dashed box depicts the used European region of our study. **(b)** The corresponding composites of the 200 hPa streamfunction anomaly; contour interval is $1 \times 10^6 m^2 s^{-1}$. Probability density functions of daily Europe T_{ano} versus NAO **(c)**, NINO3.4 **(d)** and IOD **(e)** index for JJA (blue) and the heat wave events stated in Table A.1 (red).

However, our results indicate that heat waves have no clear relationship with the NAO, which is inconsistent with previous studies like Li et al. (2020), Behera et al. (2013) and Folland et al. (2009). However, there are distinct differences between our study and the studies mentioned above. Our area of heat waves is in central Europe which has significant positive correlations with the summer NAO in the north and significant negative correlations in the south (not shown). These opposite correlations between north and south in our heat wave area likely causes the weak relationship with the NAO. The different role of the NAO for different areas is also found in Behera et al. (2013), where they investigated heat waves for western and eastern Europe and found the role of the NAO is not obvious for eastern Europe while it has a weaker influence on western European summers. The whole of western Europe and part of eastern Europe in their research are contained in our defined region, which could also result in this disagreement. Besides, the composite spatial pattern of the observed anomalous stationary wave (Fig. A.2b) shows resemblance to the combination of the positive NAO and the Atlantic low regime rather than solely the positive NAO as shown in Cassou et al. (2005).

Table A.1: The selected heat wave events and their features over Europe ($35^{\circ}N - 60^{\circ}N$ and $10^{\circ}W - 40^{\circ}E$) with corresponding indices of the NAO, NINO_{3.4}, and IOD indices. *Dur.* is the duration of a heat wave event, T_{ano} and HWMId are the regional averaged surface temperature anomaly and heat wave magnitude over land-surface, respectively.

HWs	Start Date	End Date	Dur.	T_{ano}	HWMId	NAO	NINO _{3.4}	IOD
HW 01	1982-06-01	1982-06-06	6 d	2.03	4.22	0.19	0.72	0.37
HW 02	1992-08-27	1992-08-31	5 d	2.07	4.23	-0.21	0.09	-0.66
HW 03	1994-07-12	1994-07-16	5 d	1.89	4.25	1.62	0.44	0.65
HW 04	1994-07-25	1994-08-01	8 d	1.73	4.29	1.36	0.44	0.79
HW 05	1994-08-03	1994-08-12	10 d	1.83	4.41	0.63	0.43	0.92
HW 06	1996-06-06	1996-06-12	7 d	2.46	4.42	0.79	-0.30	-0.28
HW 07	1997-06-10	1997-06-14	5 d	2.04	4.07	-0.89	1.22	0.20
HW 08	1998-06-04	1998-06-09	6 d	2.15	4.02	-1.34	-0.13	0.26
HW 09	1999-07-02	1999-07-14	13 d	2.03	4.30	-0.28	-1.10	0.21
HW 10	2001-07-25	2001-08-01	8 d	1.95	4.45	-0.45	-0.11	-0.12
HW 11	2002-06-16	2002-06-24	9 d	2.48	4.29	0.59	0.65	-0.08
HW 12	2003-06-05	2003-06-15	11 d	2.57	4.55	-0.27	-0.16	0.25
HW 13	2003-07-15	2003-07-24	10 d	1.77	4.33	0.45	0.08	0.23
HW 14	2003-08-02	2003-08-15	14 d	2.01	4.79	0.37	0.21	0.22
HW 15	2006-06-18	2006-07-02	15 d	2.26	4.32	0.55	0.08	0.10
HW 16	2006-07-09	2006-07-14	6 d	2.20	4.38	1.21	0.12	0.14
HW 17	2006-07-19	2006-07-27	9 d	2.02	4.63	-0.03	0.12	0.14
HW 18	2007-06-13	2007-06-20	8 d	2.00	3.86	-0.53	-0.41	0.14
HW 19	2007-08-22	2007-08-26	5 d	2.83	5.31	0.14	-0.84	0.35
HW 20	2009-06-28	2009-07-04	7 d	2.01	4.43	-0.84	0.41	0.06
HW 21	2010-06-29	2010-07-05	7 d	2.10	4.28	-0.53	-0.81	0.04
HW 22	2010-07-08	2010-07-23	16 d	2.84	5.18	-0.12	-1.03	0.10
HW 23	2010-08-07	2010-08-16	10 d	2.45	4.84	-0.29	-1.38	0.05
HW 24	2012-06-16	2012-06-23	8 d	2.26	3.98	-0.73	0.05	0.12
HW 25	2012-07-03	2012-07-09	7 d	2.22	4.36	-0.73	0.27	0.64
HW 26	2012-07-25	2012-07-29	5 d	2.42	4.80	-0.14	0.27	0.64
HW 27	2012-08-17	2012-08-21	5 d	1.91	4.66	-1.24	0.33	0.76
HW 28	2013-06-16	2013-06-21	6 d	2.13	3.98	0.90	-0.34	-0.38
HW 29	2014-06-06	2014-06-12	7 d	2.45	4.51	-0.41	0.23	0.09
HW 30	2014-08-09	2014-08-13	5 d	1.61	3.86	-0.67	0.03	-0.26
HW 31	2015-07-01	2015-07-08	8 d	2.51	4.65	-1.24	1.54	0.32
HW 32	2015-07-17	2015-07-22	6 d	1.60	3.85	-2.16	1.54	0.32
HW 33	2015-08-03	2015-08-14	12 d	2.45	4.86	0.21	1.83	0.68
HW 34	2015-08-27	2015-08-31	5 d	2.62	4.67	-0.89	1.83	0.68
HW 35	2016-06-21	2016-06-27	7 d	3.06	5.11	0.79	0.00	-0.33
HW 36	2016-08-21	2016-08-31	11 d	2.18	4.46	-1.06	-0.57	-0.33
HW 37	2017-06-18	2017-06-28	11 d	1.89	4.04	0.40	0.38	0.54
HW 38	2017-07-31	2017-08-06	7 d	2.39	4.91	-1.12	0.01	0.54

A.3.2 NSWAM responses to heat waves

A.3.2.1 Sensitivity analysis of NSWAM

The identified 38 heat wave events have different durations (Table A.1). Correspondingly, the performance of the NSWAM may vary depending on the duration. As stated in section A.2.3, we perform a composite experiment using the NSWAM with composite forcing terms for all 38 events. To test the robustness of our results, we carry out a sensitivity analysis for the performance of the NSWAM. We first run the NSWAM for each event with all the anomalous forcings, that is, global diabatic heating (Q), transient momentum fluxes (M), and orography (O). The pattern correlation is used to examine the reproducibility of the NSWAM in simulating the observed anomalous stationary wave and is calculated for each simulation over Europe and in the mid-latitudes ranging from 25°N to 75° N. After that, we divide these 38 events into different groups based on their duration. The duration for each group is extended from 5 to 10 days. We then compare the spread, mean and median value of the pattern correlations for these groups.

For the pattern correlations over Europe, variations of the pattern correlations tend to be rather stable for all duration thresholds (Fig. A.3). As regards the mid-latitudes, the mean and median are slightly lower than those over Europe, but the values remain as stable as for over Europe. Most of the pattern correlations are statistically significant. Our results suggest that the performance of the NSWAM for these 38 events is independent of the duration threshold in terms of the mean and median. The pattern correlation for the composite experiment is about 0.50 over Europe and larger than the significance threshold. Therefore, results from the composite experiment are robust for interpreting and analyzing the dynamic mechanisms in the NSWAM.

A.3.2.2 NSWAM responses to total forcings

We use the NSWAM for simulating the observed anomalous stationary wave (Fig. A.2b) and diagnosing various nonlinear effects involved in maintaining the anomalous stationary waves. Before decomposing the different contributions, we have to verify that the NSWAM is capable of reproducing the observed anomalous stationary wave (Fig. A.2b). As stated above, the pattern correlation (0.50), between the simulated anomalous stationary wave from the NSWAM forced by all forcing terms and the observed anomalous stationary wave, indicates that the NSWAM faithfully reproduces the observed upper-level anomalous stationary wave in the composite experiment. Some differences are to be expected given the simplifications of the nonlinear model (Sobolowski et al., 2011), and also the composite forcing terms might miss some individual forcing information.

To corroborate the consistency between the NSWAM and the reanalysis, we compare spatial patterns of the simulated and observed anomalous stationary

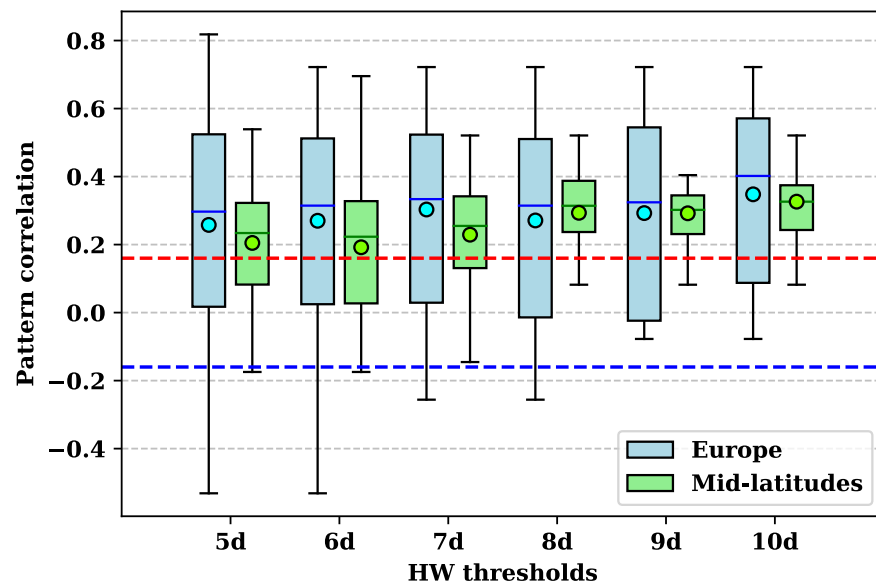


Figure A.3: Sensitivity analysis using pattern correlations of the NSWMM based on different heat wave thresholds. The NSWMM is forced by all the forcings: global diabatic heating (Q), transient momentum fluxes (M), and orography (O). The red (blue) dashed line represents the threshold of the statistically significant positive (negative) pattern correlation. Above (below) the red (blue) dashed line indicates statistically significant values. The filled circles represent the mean value for each pattern correlations over all events.

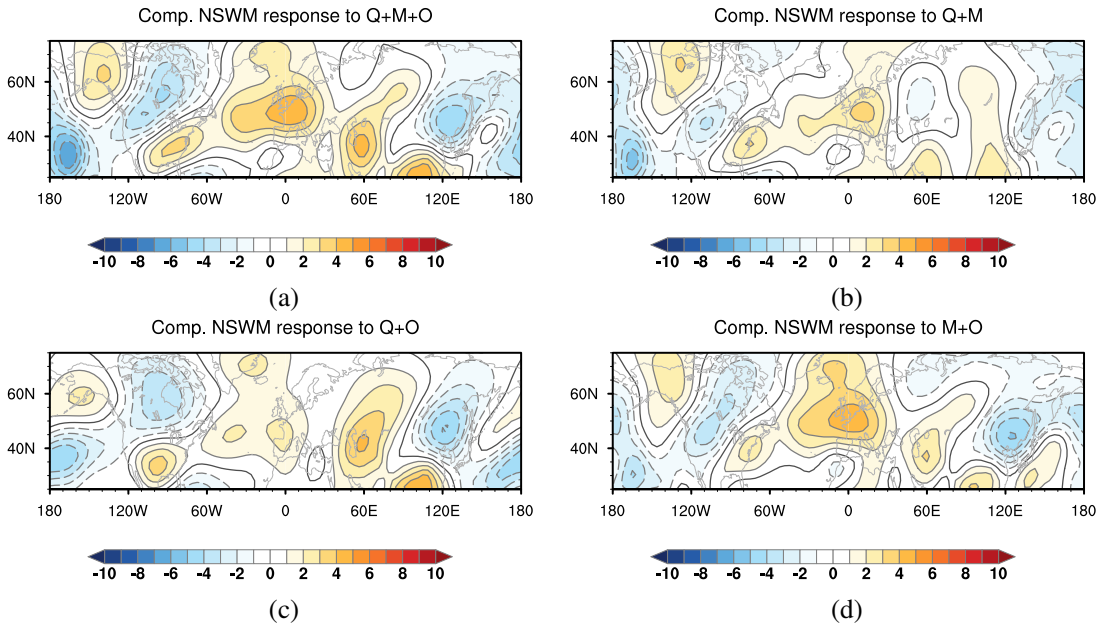


Figure A.4: The simulated anomalous stationary waves streamfunction fields of the NSW. **(a)** NSW forced by all the forcings as depicted in Fig. A.3. **(b)-(d)** The NSW is forced by different combinations of two terms in Q, M, and O. The contour interval is $1 \times 10^6 m^2 s^{-1}$.

wave (Fig. A.4a and Fig. A.2b). An obvious anti-cyclonic system is captured over Europe with a relatively lower amplitude compared with the observed anomalous stationary wave. This indicates that the streamfunction response of the NSW subjected to all three forcings reproduces the robust features of the observed anomalous stationary wave during heat wave events well over Europe by visual inspection. The simulated result in Fig. 4a presents also European blocking with a weaker positive NAO pattern over Europe, in agreement with Li et al. (2020). However, clear discrepancies exist in simulated responses over the North Atlantic, for example, the NSW fails to reproduce the cyclonic system located in the North Atlantic in Fig. A.2b. These discrepancies in simulating the observed anomalous stationary wave may be attributed to the inaccuracy of the dissipation parameterization or other missing physical processes, such as land-ocean-atmosphere interactions (Behera et al., 2013; Liu et al., 1998; Ting et al., 2001). The deficiency of the NSW in accurately modeling NAO events could also be responsible for these discrepancies (not shown). Overall, the NSW can provide us with plausible results to simulate the anti-cyclonic system over Europe. To better understand the contributions from the different components, we will further decompose the total stationary nonlinear effects based on the method described in section A.2.4.

A.3.3 *Decomposing the processes in NSWMM*

A.3.3.1 *Combined forcing effects*

We first decompose the NSWMM responses to two combined forcings as stated in section A.2.4, i.e., diabatic heating and transient momentum fluxes (TNE_QM), diabatic heating and orography (TNE_QO), and transient momentum fluxes and orography (TNE_MO). This means we input two forcing terms in each simulation, thus the response of the NSWMM not only exhibits the response to individual forcings but also includes their nonlinear interactions. The NSWMM streamfunction responses due to the combined forcing mechanisms are shown in Figs. A.4b-d. Generally, all the nonlinear responses generated from the combined forcings display a similar spatial pattern to the simulated anomalous stationary wave and all of them show a clear anti-cyclonic system over Europe as the observed anomalous stationary wave (Fig. A.2b). However, the response to transient momentum fluxes and orography exhibits the largest response (Fig. A.4d), in terms of magnitude, with smaller contributions coming from diabatic heating and orography (Fig. A.4c).

Moreover, the center of the anti-cyclonic system is slightly shifted towards the Iberian Peninsula for the response to diabatic heating and orography, but for the other two, the locations of the center are nearly identical and closely resemble the observed and simulated anomalous stationary wave. These differences indicate that transient momentum fluxes and its nonlinear interaction with other forcings make major contributions to the simulation of the observed anomalous stationary wave, as its combinations with the other two forcings have a propensity for generating larger responses and capturing similar centers for the anti-cyclonic system over Europe. Similarly, diabatic heating might play a damping role in the simulations.

The pattern correlations between the NSWMM responses to the combined forcing and the observed anomalous stationary wave can provide extra information that examination of the spatial maps might miss (Sobolowski et al., 2011). Results of the correlations confirmed that the contribution from the combined diabatic heating and transient momentum fluxes (0.59) and transient momentum fluxes and orography (0.48) are the two major contributors to the total NSWMM response. The two correlation values have passed the significance test. The contribution from the combined diabatic heating and orography plays a smaller role with an insignificant pattern correlation of 0.005. We then investigate which individual mechanisms play an important role in the combined forcings.

A.3.3.2 *Direct nonlinear effects*

The NSWMM streamfunction responses due to the forcing by the individual mechanisms are shown in the left panel in Fig. A.5. These responses represent the direct contributions from individual nonlinear effects to simulate the

observed anomalous stationary waves; these are INE_Q, INE_M, and INE_O. Our results reveal that the NSWAM response to transient momentum fluxes and orographic forcing have a larger response. In particular, the response of the transient momentum fluxes can generate a consistent anti-cyclonic system compared with the observed anomalous stationary wave (compare Figs. A.5b and A.2b). As for the responses generated by orography, they show an extended anti-cyclonic system from the North Atlantic to Europe (Fig. A.5c). This extended anti-cyclonic system constitutes a downstream flow emanating from the Tibetan Plateau. This is in agreement with Ting et al. (2001) and Held et al. (2002). Orographic forcing effects tend to strengthen the cyclonic flows downstream of the major northern hemispheric mountain chains.

However, the responses of the NSWAM to diabatic heating are more complex over Europe and has the smallest magnitude (Fig. A.5a). Cyclonic systems are visible over the UK and southern Europe, while an extended anti-cyclonic system reaches and dominates over the Iberian Peninsula. Generally, the role of diabatic heating is somehow different from Ting (1994), where she pointed out that the diabatic heating played a dominant role in maintaining the climatological summer stationary waves. The main reason for this disagreement lies in the fact that the climatological stationary waves during summertime have been removed in our study since we only focus on the anomalous stationary waves. This suggests that diabatic heating plays a major role in driving the zonal mean response.

We then calculate the pattern correlations between the nonlinear responses due to the individual forcing terms and the observed anomalous stationary wave over Europe. Consistent with those described above, transient momentum fluxes are the key contributor to simulate the observed anomalous stationary wave with a significant pattern correlation of 0.52. The pattern correlation for the response to orography is insignificant (0.08), although the responses have the same magnitude with transient momentum fluxes. The pattern correlation reveals that the diabatic heating makes a negative contribution to the total responses of the NSWAM due to the significant negative pattern correlation (-0.18).

Interestingly, our results suggest that nonlinear interactions between transient momentum fluxes and diabatic heating exist, and should make a significantly positive contribution to the simulation. This is because the pattern correlation for combined transient momentum fluxes and diabatic heating with the observed anomalous stationary wave is 0.59, which is larger than their individual contributions, especially the damping role of diabatic. We will investigate the role of various nonlinear interactions in the following section.

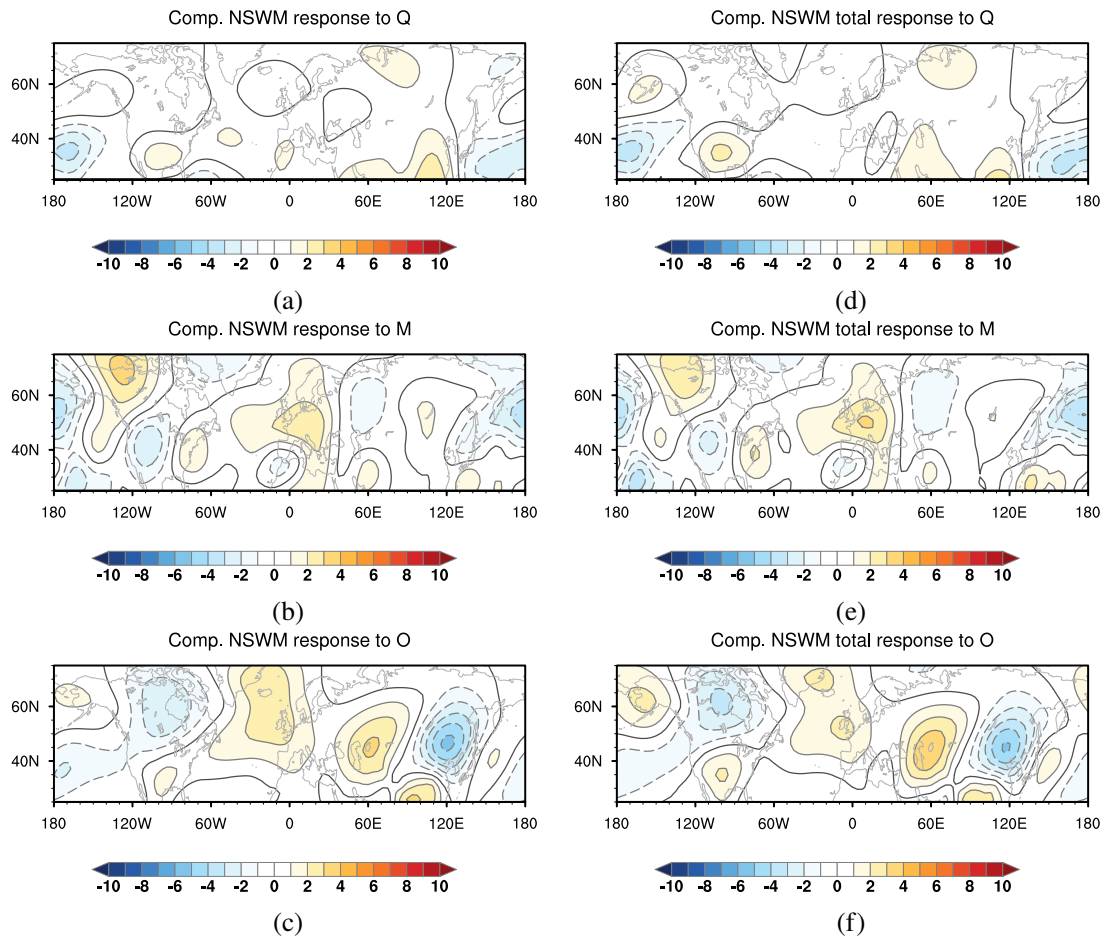


Figure A.5: Same as Fig. A.4. **(a)-(c)** (left panel) The NSWM is forced by the individual Q, M, and O forcings. **(d)-(f)** (right panel) The NSWM responses to the total nonlinear effects of Q, M, and O.

A.3.3.3 *Individual total nonlinear effects*

Before analyzing the effect of the nonlinear interactions between the three forcings, we first explore the individual total nonlinear effects to demonstrate whether they play an important role in our simulations. These are expressed by Eq. A.8, i.e. ITNE_Q, ITNE_M, and ITNE_O. This individual total nonlinear effect represents the nonlinear response due to the particular forcing and all its interactions with the other forcing terms.

The right panel in Fig. A.5 shows the nonlinear response of the NSWM due to the total effects of each forcing term. They should be compared with the corresponding direct nonlinear effects in section A.3.3.2. By including the nonlinear interaction effects, the magnitude of both positive and negative responses is increased to some extent. Particularly in the total nonlinear effects of transient momentum fluxes (ITNE_M, Fig. A.5e), a clear anti-cyclonic center, which resembles the observed one (Fig. A.2b), becomes more evident than due to its direct nonlinear effect (INE_M, Fig. A.5b). Considering the total nonlinear effects of orography, the extended anti-cyclonic system over the North Atlantic from the direct nonlinear effects of the orography is split into two centers and the southern center locates around the UK (Fig. A.5f). The response due to the total effects of the diabatic heating exhibits a more complex structure with lesser magnitude, enhancing the total response over northwestern and southeastern Europe while mitigating the total response over the southwestern Iberian Peninsula (compare Fig. A.5d with Fig. A.5a).

When comparing these pattern correlations with their direct nonlinear effects, all the correlation values are increased by including their nonlinear interactions with other forcings. Especially for diabatic heating, the pattern correlation value increases from -0.18 to -0.01, from significant to insignificant. Due to the lowest correlation, the contribution from the total effects due to diabatic heating is more modest and, as shown in the streamfunction response, more complex than the other two forcings for maintaining the observed anomalous stationary wave. The significant positive pattern correlation of transient momentum fluxes slightly increases from 0.53 to 0.58, and as for the orography, the pattern correlation increases from 0.08 to 0.13 but remains insignificant.

Diagnosis of these pattern correlations combined with the spatial patterns of the streamfunction shown in Fig. A.5, suggests that the total nonlinear effects of each forcing are more important than any of the individual direct forcings, especially for the investigation of diabatic heating. We then decompose and examine the role of the various nonlinear interactions between different forcings.

A.3.3.4 *Nonlinear interactions*

As shown in Eqs. A.6 and A.7, there are four nonlinear interaction terms that contribute to the total effects of nonlinear interactions in simulating

and maintaining anomalous stationary waves, namely, TONI_QM, TONI_QO, TONI_MO, and TONI_QMO. These nonlinear interactions represent nonlinear interference between flows forced by different forcings. Note that if the dynamic process is completely linear, then the nonlinear interaction terms will be identically zero.

The contributions of each of the interaction terms are shown in Fig. A.6. Note that, for display purposes, the range of the contour is 4 times smaller than for the previous figures. The nonlinear interferences between diabatic heating and orography (Fig. A.6b) and transient momentum fluxes and orography (Fig. A.6c) exhibit clearer spatial patterns with a larger magnitude over the northern hemisphere. These spatial patterns are broadly similar in North America as the downstream extensions emanated from the Tibetan Plateau. However, the responses over Europe have lesser amplitude. This indicates that the flow forced by orography plays an important role in these nonlinear interaction effects in maintaining the anomalous stationary waves. This is consistent with earlier findings (Ting et al., 2001) that emphasize the effect of orography in maintaining climatological and anomalous stationary waves during the NH winter. Our results suggest that the effect of orography is also important in maintaining anomalous stationary waves during heat waves via nonlinear interactions with other forcings.

It should be noted that the realistic orography is spectrally truncated in the NSWCM. This truncation leads to a low spatial resolution of the orography in the model, for example, small orographic features such as those over the Arabian region and South Africa may not be well resolved (Ting, 1994). The low representation of the orography therefore would potentially influence the related nonlinear individual and nonlinear effects with other forcings. As shown in Fig. A.6, the existence of orography is indeed the most important source for the nonlinear interactions. Thus, the orography could induce significant changes in thermal forcing (Ting, 1994) and affect the distribution of transient eddy flux (Held et al., 2002). However, we speculate that the lower spatial resolution of orography does not have a great impact on our results, at least for the generation of anomalous stationary waves over Europe. On one hand, the NSWCM responses to the nonlinear interaction effects between orography and other forcings tend to be largest in the Pacific-North American sector, which is beyond the scope of this paper, in agreement with Held et al. (2002). On the other hand, Iles et al. (2019) suggest that increasing the resolution of the orography and coastlines in climate simulations have limited benefits for temperature extremes over Europe, except in reducing hot biases over mountainous regions.

Examination of the pattern correlation, the responses due to interactions involving diabatic heating and transient momentum fluxes (0.60), and orography and transient momentum fluxes (0.45) make a significant positive contribution to the simulation of the observed anomalous stationary waves. This significant pattern correlation of the nonlinear interference between diabatic

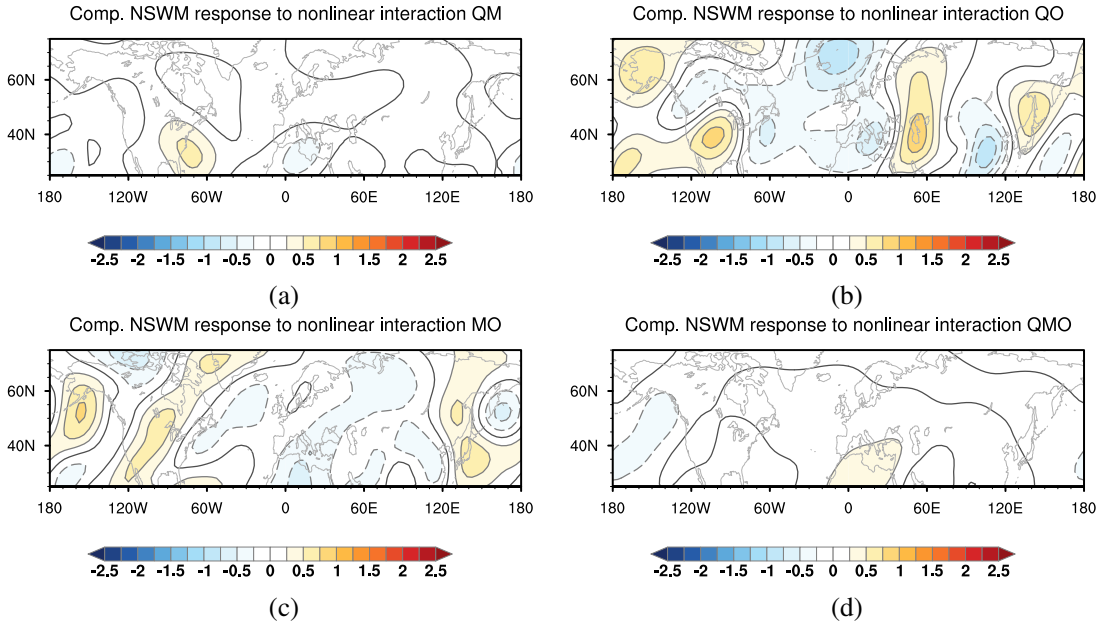


Figure A.6: Same as Fig. A.4, but for the NSWAM response to nonlinear interactions between the three different forcing terms.

heating and transient momentum fluxes proves our assumption in section A.3.3.2. Moreover, the contribution of the three-way interaction term is also non-trivial and surprisingly makes a significant damping contribution (-0.63). The streamfunction responses due to the nonlinear effect between diabatic heating and orography makes a modest contribution to the total response. However, the results of the pattern correlation should be interpreted cautiously as the magnitude of the responses is relatively low. By inspecting Fig. A.5a-c and Fig. A.5d-f, we can confirm that the nonlinear interference between diabatic heating and transient momentum fluxes and orography and transient momentum fluxes dominate more than the others (Fig. A.5d-f). While the magnitude of these interaction terms are rather small, the larger magnitude of the response to the total forcing indicates that a nonlinear resonance is amplifying the anomalous stationary wave response.

A.3.4 *Interrelationship between various nonlinear effects*

To explore further the robustness of the above results, we examine the interrelationship between all the nonlinear combinations, direct, individual total, and interaction effects involved in the NSWAM for all the simulations for all 38 heat wave events (Table A.1). Table A.2 shows the pairwise correlations for pattern correlations based on Spearman's rank correlation. The pattern correlation is calculated for each simulation and decomposition between the response of the NSWAM to every nonlinear effect and the observed anomalous stationary wave for the 38 events.

The dominant role of the transient momentum fluxes is corroborated. Obviously, the total response of the NSWAM (driven by all forcings, TNE_QMO) has a significant positive correlation with most nonlinear effects of the transient momentum fluxes, for example, the direct (INE_M, 0.81) and individual total nonlinear effects (ITNE_M, 0.88), and its combinations with diabatic heating (TNE_QM, 0.92) and orography (TNE_MO, 0.87). The individual total nonlinear effect of orography (ITNE_O) has a significant positive correlation with the nonlinear interaction effect involving transient momentum fluxes and orography (TNE_MO, 0.59). The significant positive correlations also exist in the direct nonlinear effect of diabatic heating (INE_Q) with its total nonlinear effect (ITNE_Q, 0.62) and its combination with the orography (TNE_QO, 0.74). However, consistent with our previous results, other nonlinear effects including diabatic heating, which can cause negative contributions to the total response of NSWAM, albeit these negative responses do not pass the significant test as shown in the second column in Table A.2.

A.3.5 *The role of transient momentum fluxes*

The transient momentum fluxes consist of two components: vorticity and divergence fluxes as expressed in Eq. A.4 and Eq. A.5. We have shown the dominant role of transient momentum fluxes in maintaining the anomalous stationary waves. Thus, it is of importance to identify which of the components are more vital in this dynamic process. For this purpose, we conduct simulations similar to section A.3.2.2. We employ the same global diabatic heating (Q) and orography (O) but replace the transient momentum fluxes (M) by the transient divergence (Fig. A.7a) and transient vorticity fluxes (Fig. A.7b), respectively. As shown in Fig. A.7, the spatial pattern of the responses to both components is quite similar and shows an extended anti-cyclonic system over Europe. However, the response to the transient vorticity fluxes can capture the similar location of the center of the anti-cyclonic system compared with the simulated anomalous stationary waves (Fig. A.4a) and the observed anomalous stationary waves (Fig. A.2b). The result demonstrates the contributions from transient vorticity fluxes to the total responses in the NSWAM are more important than those from divergence fluxes.

The pattern correlations support the importance of transient vorticity fluxes in maintaining the anomalous stationary wave over Europe. The pattern correlation between the response of transient vorticity fluxes with the observed anomalous stationary waves is 0.48 and is larger than the value of 0.07 of the transient divergence fluxes. This suggests that convective processes, driving divergent flows, play a rather minor role during European heat wave events.

We further decompose transient vorticity fluxes into high- (periods of less than 10 days) and low-frequency (periods between 10 and 30 days) eddies.

Table A.2: Correlations between the various decomposed forcing components of the NSWM for simulated anomalous stationary waves of the 38 simulations. The asterisk (*) indicates the correlation value is statistically significant at the 5% level.

Variables	V1	V2	V3	V4	V5	V6	V7	V8	V9	V10	V11	V12	V13	V14
V1	TNE_QMO	-												
V2	INE_Q	0.20	-											
V3	INE_M	0.81*	-0.14	-										
V4	INE_O	0.08	-0.16	-0.01	-									
V5	ITNE_Q	0.21	0.62*	-0.20	-0.23	-								
V6	ITNE_M	0.88*	-0.06	0.89*	0.00	0.08	-							
V7	ITNE_O	0.08	-0.03	-0.10	0.40	0.01	-0.08	-						
V8	TNE_QM	0.92*	0.19	0.84*	-0.08	0.14	0.88*	-0.22	-					
V9	TNE_QO	0.39	0.74*	-0.01	0.27	0.48	0.03	0.27	0.25	-				
V10	TNE_MO	0.87*	-0.09	0.96*	0.13	-0.17	0.88*	0.04	0.83*	0.13	-			
V11	TENI_QM	0.01	-0.13	-0.07	0.14	0.41	0.15	-0.22	0.06	-0.04	-0.11	-		
V12	TENI_QO	0.02	-0.20	0.05	-0.05	0.09	-0.07	0.15	-0.09	0.09	0.16	-		
V13	TENI_MO	0.08	0.07	-0.05	0.18	-0.09	-0.07	0.59*	-0.11	0.19	-0.25	0.07	-	
V14	TENI_QMO	0.01	0.17	-0.18	0.05	0.27	0.02	0.35	-0.09	0.03	-0.17	-0.44	-0.11	-

Thus, Eq. A.4 is decomposed into four nonlinear interaction components among different frequency scales:

$$TF_V = -\nabla \cdot (\overline{\mathbf{v}'_L \zeta'_L}) - \nabla \cdot (\overline{\mathbf{v}'_L \zeta'_H}) - \nabla \cdot (\overline{\mathbf{v}'_H \zeta'_L}) - \nabla \cdot (\overline{\mathbf{v}'_H \zeta'_H}) \quad (\text{A.9})$$

where the subscript L denotes low- and H high-pass filtered eddies.

Broadly, the responses of the NSWMM to these four components present a similar spatial pattern in terms of the magnitude and locations of anti-cyclonic and cyclonic systems (Fig. A.8). The responses to the terms in Fig. A.8b and Fig. A.8d generate an anti-cyclonic system with weak positive NAO patterns (Li et al., 2020), but the other two terms just play a modest role. Moreover, the responses to high-frequency transient vorticity fluxes (Fig. A.8d) exhibit an identical anti-cyclonic system compared with the observed anomalous stationary wave in Fig. A.2b. By comparison of Fig. A.7b, contributions from high-frequency transient vorticity fluxes dominate the response of the NSWMM to the total transient vorticity fluxes regarding the location of the center of the anti-cyclonic system over Europe.

The above analysis is also confirmed by the calculation of the pattern correlation. The significant pattern correlation between the responses to high-frequency transient vorticity fluxes and the observed anomalous stationary wave is 0.78 over Europe, which is larger than other components and also than the total responses to transient vorticity fluxes. The other three components, representing the nonlinear interactions between low- and high-frequency transient waves, either play a damping role or make only modest contributions as shown in the pattern correlations (Fig. A.8a-c). The pattern correlation of Fig. A.8b and Fig. A.2b has a negative value (-0.29) over Europe while the other two show no clear pattern correlations with the observed anomalous stationary wave.

Our results reveal that high-frequency transient vorticity fluxes dominate in the maintenance of observed anomalous stationary waves, which is consistent with Schubert et al. (2014). They found that the submonthly transient vorticity flux forcing dominates in the leading modes of boreal summer stationary Rossby waves which account for more than 60% of the surface temperature variability. Teng et al. (2013) also stated transient vorticity fluxes are instrumental during the life cycle of U.S. heat waves by contributing to the maintenance of streamfunction anomalies. Further research is needed to clarify the dynamic mechanisms of the transient vorticity fluxes in maintaining anomalous stationary waves, since this may be due to reduced low-frequency variability and persistent extreme events (Coumou et al., 2015) or by maintaining the waveguide teleconnections in summer (Teng and Branstator, 2019).

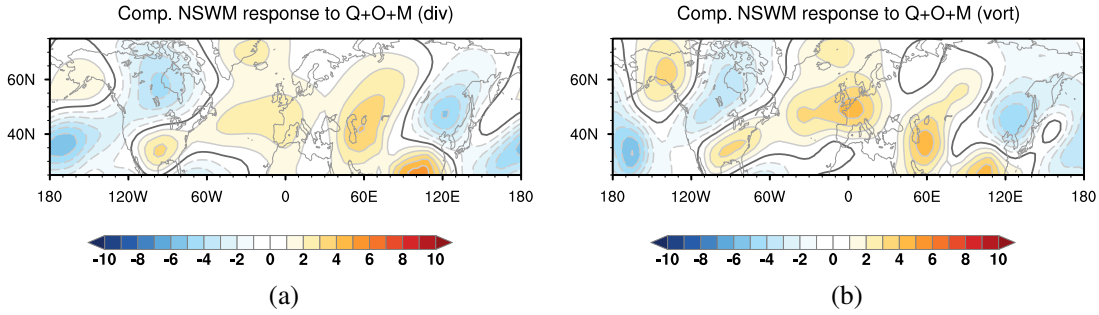


Figure A.7: Same as Fig. A.4a, but the transient momentum fluxes is replaced by separate transient divergence fluxes (a) and vorticity fluxes (b).

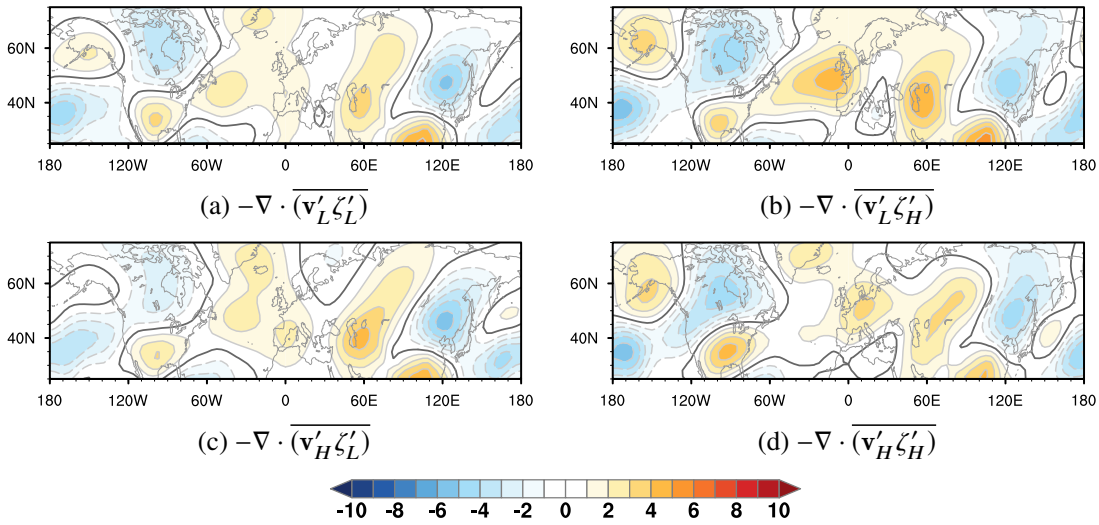


Figure A.8: Same as Fig. A.7b, but now the transient vorticity flux is decomposed into different nonlinear interaction parts stemming from different frequency ranges: **a)** $-\nabla \cdot (\mathbf{v}'_L \zeta'_L)$, **b)** $-\nabla \cdot (\mathbf{v}'_L \zeta'_H)$, **c)** $-\nabla \cdot (\mathbf{v}'_H \zeta'_L)$, and **d)** $-\nabla \cdot (\mathbf{v}'_H \zeta'_H)$.

A.3.6 *The role of diabatic heating*

A.3.6.1 *Distribution of diabatic heating*

Simulations with the NSWCM show that global diabatic heating anomalies contribute to the maintenance of the anomalous stationary waves and heat waves mainly due to nonlinear interactions with the other two forcings. Both local and remote diabatic processes in the troposphere could contribute to the responses of the NSWCM. Thus, we first investigate the spatial distributions of diabatic heating during European heat waves. Figure A.9a shows the vertically averaged (900-150 hPa) diabatic heating anomalies for the composite of the 38 heat wave events (Table A.1). Diabatic cooling dominates over Europe, except over the UK which experienced diabatic heating. The main reason for the diabatic cooling is the radiative cooling in the free atmosphere (Binder et al., 2017). Note that diabatic cooling is pervasive over Europe but with positive temperature anomalies (Fig. A.2a). This is explained by the blocking systems in the upper-level troposphere. Zschenderlein et al. (2019) demonstrated that the descending motions of the air parcels lead to adiabatic warming which can overcompensate the diabatic cooling. Hence, the surface temperatures are anomalously high over Europe. As for the UK, diabatic warming may result from surface sensible heat fluxes, which is crucial in determining high temperatures near the surface.

Another important feature in Fig. A.9a is that the diabatic heating anomalies are concentrated over the mid-latitude North Atlantic region ($30^{\circ}N - 60^{\circ}N$) and over tropical regions ($30^{\circ}S - 30^{\circ}N$). Heating in different regions may play different roles in influencing the large-scale circulation anomalies in nearby or remote regions (Teng and Branstator, 2019). Hence, elucidating the impact of various heating regions on European heat waves is fundamental for a better understanding of the physical mechanisms and can also provide insight into improving the predictable skill of European heat waves.

A.3.6.2 *Diabatic heating in the mid-latitude North Atlantic*

There is a strong positive diabatic heating anomaly over the mid-latitude North Atlantic (MATL) (Fig. A.9a). This motivates us to perform NSWCM simulations to determine the contribution of this heating source to the maintenance of European heat waves. A control simulation is first conducted, by running the NSWCM with the climatological mean (60-yr) of the JJA diabatic heating and keeping the transient momentum fluxes and the orography identical, similar to the simulation in section A.3.2.2. We then extract the anomalous diabatic heating over the considered MATL region from the global anomalous diabatic heating field which we used in the simulations in section A.3.2.2. This extracted diabatic heating is added to the 60-yr mean diabatic heating data in the control simulations. Based on these data, the new simulation is set up and all other forcings remain the same as in the control simulation. Then the

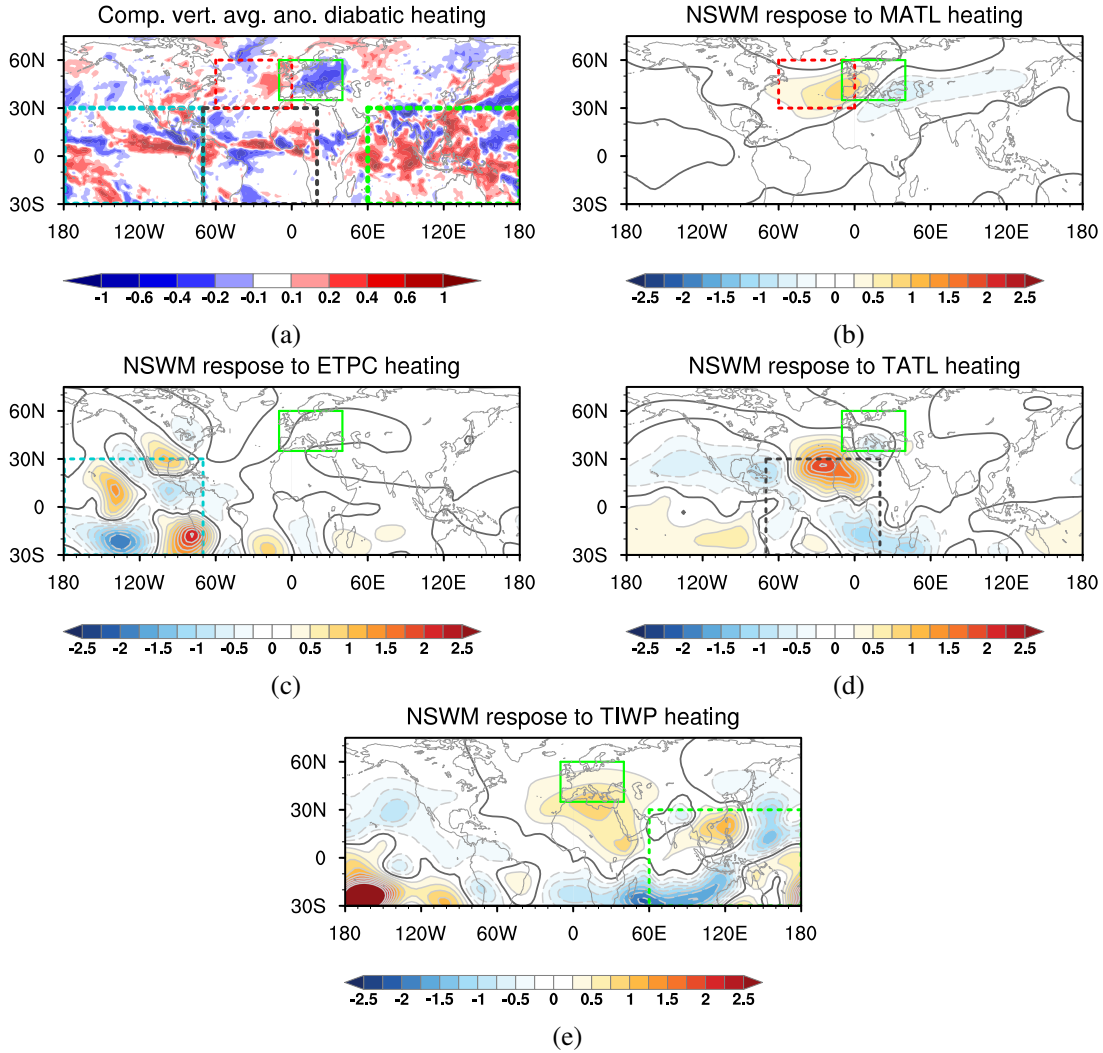


Figure A.9: **(a)** Vertically averaged (900 hPa to 150 hPa) diabatic heating anomalies. **(b)-(e)** The NSWM response to different regional sources of mid-latitude and tropical diabatic heating. The dashed boxes represent the regions used for regionally decomposing the diabatic heating fields: Mid-latitude North Atlantic (MATL, 0° - 60°W; red), East Tropical Pacific (ETPC, 70°W - 180°W; blue), Tropical Atlantic (TATL, 70°W - 20°E; black), and the Tropical Indian Ocean and West Pacific (TIWP, 60°E - 180°E; green). The contour interval is $1 \times 10^6 m^2 s^{-1}$.

responses of the control simulation are removed from the new simulation, by doing so, we can obtain the sole contributions from the MATL heating source in maintaining the observed anomalous stationary waves over Europe.

The responses of the NSWCM to the MATL heating regions are shown in Fig. A.9b. A clear anti-cyclonic system is generated that extends from the mid-latitude North Atlantic to western Europe over the heat wave region (Fig. A.2a). This anti-cyclonic system could partly contribute to the observed anomalous stationary waves over Europe in Fig. A.2b. Our results confirm the role of heating over the MATL region in maintaining European heat waves, in agreement with Ghosh et al. (2017, 2019). However, the positive response over the MATL region is in contrast to the observed cyclonic system over this region (compare Fig. A.9b with Fig. A.2b). This indicates that heating over other regions makes likely substantial contributions as well. Our result is consistent with Black et al. (2004) to some extent. By using a wind trajectory model, they demonstrated that air masses trapped within the anticyclonic systems over western Europe can travel very short distances, mainly from the MATL region for example during the summer 2003 European heat wave event.

A.3.6.3 *The various sources of tropical diabatic heating*

We then focus on the contributions from different regions of tropical diabatic heating. As previous studies indicated, tropical heating can drive large-scale circulation anomalies and trigger intensified subsidence in remote regions over mid- and high-latitudes (Bader and Latif, 2005; Cassou et al., 2005; Park and Lee, 2019). Building upon these previous studies and our analysis in section A.3.1 about large-scale climate patterns and European heat waves, three tropical heating sources are considered to ascertain their contributions, as shown in Fig. A.9a: the east tropical Pacific (ETPC), the tropical Atlantic (TATL), and the tropical Indian Ocean and West Pacific (TIWP).

With similar simulations as used for obtaining the response displayed in Fig. A.9b, the responses of the NSWCM to the three tropical heating regions are shown in Figs. A.9c-e, respectively. Generally, the responses to the three sources of tropical diabatic heating all lead to a wave-like response over the mid-latitudes at the upper-level troposphere, regardless of the magnitude. One of the most prominent responses is the one where the NSWCM is forced by heating over the TIWP region (Fig. A.9e). The response to this forcing generates an approximately circumglobal pattern with different amplitudes and locations of anomalous stationary waves. An anti-cyclonic system is fostered with its center located over the Mediterranean region. The maintenance of this system could be responsible for high-temperature extremes in western and southern Europe, especially around the Mediterranean region. Our diagnosis of heating in the TIWP region confirms the important role of IOD events in modulating temperatures in Europe, as discussed in section A.3.1. This tropical-extratropical connection is also consistent with Behera et al. (2013).

They demonstrated that European heat waves are associated with a Rossby wavetrain via a circumglobal teleconnection. This wavetrain is determined by the anomalous diabatic heating over the TIWP region. This anomalous diabatic heating could trigger perturbations in the upper tropospheric Asian jet and transmit this signal to western Europe from the west through the mid-latitude wave-guide during the positive IOD events, and then making major contributions to heat waves in western Europe.

Concerning the anomalous diabatic heating over TATL, we find that an anti-cyclonic system is produced off the coast of north-western Africa (Fig. A.9d). This system can reach the Iberian Peninsula and could be accountable for the high-temperature anomalies over there. This result is partly in agreement with Cassou et al. (2005), where they pointed out that tropical Atlantic anomalous heating could increase the probability for hot days to occur over Europe associated with the intraseasonal variability of the heating. They also stated that the tropical Atlantic heating acts to amplify the residence frequency of positive NAO events and the Atlantic low events, however, we do not capture these mechanisms by using the NSWMM. Perhaps the main reason is that the NSWMM seems to underestimate the role of transients in the positive feedbacks between the eddy mixing associated with wave breaking and both the deformation and deflection of jet stream (Held et al., 2002), which are crucial during the summer NAO life cycle (Franzke et al., 2004; Luo et al., 2007). Besides, our results demonstrate that the responses to tropical heating in the ETPC region are confined to local areas and the strong responses are mainly over the East Pacific (Fig. A.9c). Although the positive responses appear over Europe, the magnitude is rather small.

To sum up, while previous studies indicated that the North Atlantic mid-latitude sea surface temperature forcing is important for European heat waves (Cassou et al., 2005; Ghosh et al., 2017, 2019), here we demonstrate that IOD and tropical heating in west Pacific are also responsible for long-lived European heat waves (38 cases at least with a threshold of 5 days). Thus, our study provides another new understanding of what leads to long-lived European heat waves.

A.4 CONCLUSIONS

In this study we examined the dynamical mechanisms involved in the maintenance of European heat waves from a nonlinear anomalous stationary wave perspective. For this purpose, we first identified 80 heat wave events, which lasted at least 3 days, for the period 1958-2017. Most events (76.3%) occurred after 2000, indicating the effect of global warming over Europe. We use 38 heat wave events, which lasted at least 5 days, to explore their relationships with large-scale teleconnection patterns. We find that European heat waves tend to occur during positive IOD events. This relationship is confirmed

by examination of the two-dimensional probability distribution function of surface temperature anomalies and the IOD index.

Composite analysis of the 38 heat wave events shows a clear observed anomalous stationary wave located over Europe. We use the NSWMM to simulate the observed anomalous stationary waves to better understand the maintenance mechanisms involved. While there are some discrepancies, the main features of the observed anomalous stationary waves over Europe are reproduced well when forced by global anomalous diabatic heating, transient momentum fluxes, and orography.

We then use the factor separation method to decompose the total responses from the NSWMM. This method also enables us to further examine the nonlinear interactions in maintaining anomalous stationary waves and heat waves. Based on a visual inspection and pattern correlation, it is found that transient momentum fluxes play a dominant role in maintaining the observed anomalous stationary waves. But the NSWMM responses to transient momentum fluxes are alleviated by the nonlinear interaction between the three forcings. Further decomposing the transient momentum fluxes reveals that transient vorticity fluxes are more important than transient divergence fluxes. We also find that transient momentum fluxes are dominated by the high-frequency rotational component, with the divergent component being much smaller.

Different from the maintenance of summer climatological stationary waves (Ting, 1994), our results indicate that diabatic heating tends to make negative contributions to maintaining the observed anomalous stationary waves during heat waves, especially over the UK and eastern Europe. Furthermore, through nonlinear interaction with other forcings, orographic effects make moderate contributions to maintaining the observed anomalous stationary wave, especially via the nonlinear interaction with diabatic heating.

Our results show that the nonlinear interactions between the three forcing terms make substantial contributions. In particular, while diabatic heating as a individual forcing leads to rather small anomalous stationary wave responses, together with the transient fluxes it makes a substantial contribution. This indicates that all three forcings are necessary for maintaining anomalous stationary waves and European heat waves.

We further investigate the distribution of diabatic heating and find that strong diabatic cooling dominates over Europe during heat wave periods. This diabatic cooling indicates strong descending motions due to a persistent anti-cyclonic system. This system can lead to a large magnitude of adiabatic warming overcompensating the diabatic cooling and increasing the surface temperature. Further NSWMM simulations show that tropical heating located in the tropical Indian Ocean and Western Pacific (TIWP) and tropical Atlantic (TATL) forces the observed anomalous stationary waves remotely, and the former plays a stronger role than the latter. Moreover, heating over mid-latitude North Atlantic also makes contributions to the anomalous stationary waves mainly over southwestern Europe.

Overall, our results in this study offer a new dynamical perspective on understanding the maintenance of anomalous stationary waves associated with heat waves. The successful application of the NSWMM enabled us to examine the relative contributions due to various nonlinear effects in maintaining heat waves. From a forecasting perspective our research findings show the potential of improving seasonal forecasts or which predictors to select for statistical forecasting of European heat waves.

B

CHANGES IN THE MAINTENANCE MECHANISMS OF HEAT WAVES OVER INNER EAST ASIA OVER THE LAST FEW DECADES

Appendix B comprises a paper, which is intended to be submitted to the journal of *Journal of Climate* as:

Ma, Q., Franzke, C.L.E. (2021), "Changes in the maintenance mechanisms of heat waves over Inner East Asia over the last few decades", *Journal of Climate* (to be submitted)

My and other's contributions to this paper are as follows:

I performed the calculations and the analysis, plotted figures, conceived the work, and wrote the manuscript. C.F. contributed to conceive the work, review, and write the manuscript.

Changes in the Maintenance Mechanisms of Heat Waves over Inner East Asia over the last few Decades

Qiyun Ma^{1,2}, Christian L. E. Franzke^{3,4}

¹School of Integrated Climate System Science, University of Hamburg, Hamburg, Germany

²Meteorological Institute, University of Hamburg, Hamburg, Germany

³Center for Climate Physics, Institute for Basic Science (IBS), Busan, Republic of Korea

⁴Department of the Climate System, Pusan National University, Busan, Republic of Korea

ABSTRACT Heat waves constitute a weather risk to vulnerable groups, agriculture and the economy. Over the last few decades high-pressure anomalies have intensified over inner East Asia, which are linked to more frequent and persistent heat waves. However, the impacts of anthropogenic global warming on the maintenance mechanisms involved in the changes in atmospheric circulation during heat waves remains unclear. Here we provide evidence for a significant intensification of anticyclonic systems over inner East Asia within a strengthened Silk Road pattern over the last 3 decades. To investigate the changes in maintenance mechanisms, we use the Japanese reanalysis data set JRA-55 and a nonlinear stationary wave model (NSWM). We find that heat waves have become more persistent over the last few decades. Model simulations indicate that transient momentum fluxes are the dominated factors of the observational anomalous stationary waves, especially the transient vorticity flux. Our results reveal that recent climate warming has altered the maintenance mechanisms mainly through the nonlinear interactions between different forcing components. Particularly, diabatic heating becomes more dominant via its nonlinear interactions with orography and transient momentum fluxes. Diabatic heating anomalies over the mid-latitude Pacific, the tropical Indian Ocean, and the tropical western Pacific region contribute to the changes of circulations over inner East Asia under a warmer climate.

B.1 INTRODUCTION

More frequent extreme weather events have been reported over the last few decades (Franzke and Czupryna, 2020; Lee et al., 2017; Zhang et al., 2020). Among the extreme weather events, heat waves are a main reason for weather-related deaths (Franzke and Sentelles, 2020; Robinson, 2001), which are projected to become more intense and last longer (Deng et al., 2018a). As heat waves can cause huge detrimental impacts on our society and natural systems, great efforts have been made to understand the underlying physical and dynamical mechanisms (Horton et al., 2016; Perkins, 2015; Schubert et al., 2011; Trenberth and Fasullo, 2012).

The atmospheric large-scale circulation generally controls the surface weather variability (Horton et al., 2015). Changes in circulations are closely associated with the occurrence, intensity, and persistence of heat waves (Barnes et al., 2014; Lehmann and Coumou, 2015). For example, atmospheric blocking systems can lead to a persistent heat waves lasting for days to weeks, by suppressing convection and increasing radiation which favors persisting heat waves. As observations show an increase in the frequency of heat waves, this may indicate that the occurrence of certain atmospheric circulation patterns has increased.

Indeed, Horton et al. (2015) reported a significant trend in the occurrence of anticyclonic circulations during summer over parts of Eurasia and North America. This increasing trend can explain the observed trend in surface hot extremes to some degree. Lee et al. (2017) detected a dramatically increasing trend of the occurrence of a zonal wave-number-5 pattern. The high-pressure centers embedded in that wave-number-5 pattern are responsible for the increasingly frequent regional hot extremes. Although there is a strong link between the frequent heat waves and the increasing trend of anticyclonic circulations, the maintenance mechanisms remain largely unknown (Horton et al., 2015). Particularly, how these mechanisms have been altered by climate warming is still unknown (Teng and Branstator, 2019).

Mid-latitude large-scale circulation changes are closely associated with stationary wave changes (Simpson et al., 2016; Wills et al., 2019). The changes in stationary Rossby waves govern persistent heat waves in the mid-latitudes (Coumou et al., 2015; Fragkoulidis et al., 2018; Screen and Simmonds, 2014). Building upon this relationship, we employ a fully nonlinear stationary wave model (NSWM) developed by Ting and Yu (1998). The large-scale circulation anomalies arise from three forcing components and their nonlinear interactions: topography, diabatic heating, and transient momentum fluxes, based on linear stationary Rossby wave theory (Held et al., 2002; Simpson et al., 2016; Ting, 1994). The NSWM simulates the response to a given forcing based on a prescribed zonal mean basic state (Held et al., 2002) and allows us to identify causal relationships to a certain forcing (Simpson et al., 2016). Ma and Franzke (2021) used the NSWM to reproduce the anomalous stationary waves and

diagnose the maintenance mechanisms during European heat waves. Based on this research, NSWMM is used not only for investigating the maintenance mechanisms during heat waves but also to offer a feasible way to compare the changes of the mechanisms under climate change.

Located in a semi-arid region, Inner East Asia (including Mongolia and northern China) experienced rapid warming with increasing trends of the occurrence of droughts and heat waves over the last few decades (Hessl et al., 2018; Zhang et al., 2020). Characterized by complex geographical and climatic conditions (Dashkhuu et al., 2015), recent strong warming-related extremes have caused huge impacts on society and ecosystems (Tao et al., 2015; Zhang et al., 2020).

Observations have shown more intense high-pressure anomalies over inner East Asia (Horton et al., 2015; Zhang et al., 2020), resulting in more frequent and persistent heat waves and droughts. The enhanced land-atmosphere coupling likely contributed to the strengthened anticyclonic circulations since the 1990s (Zhang et al., 2020). However, the dynamical maintenance mechanisms of the anticyclonic circulation anomalies are still unknown.

In section C.2, we introduce the data and used analysis methods. Results of the identification of heat waves and observed features of anomalous stationary waves are shown in B.3. Section B.4 discusses the selection of numerical experiments and the model results, and decomposition of the total responses from NSWMM are presented in section B.5. The decomposition of the transient momentum fluxes is shown in section B.6, and section B.7 illustrates the spatial distribution of diabatic heating and detection of the key heating regions. Then section B.8 explores the impacts of modes of climate variability. The summary and conclusions in this study are given in section B.9.

B.2 DATA AND METHODS

B.2.1 *Data and study domain*

This study uses the daily Japanese 55-year Reanalysis (JRA-55) dataset in $1.25^\circ \times 1.25^\circ$ horizontal resolution from 1958 to 2019. The reanalysis dataset has been shown to have qualitatively similar characteristics to station-based observations in identified temperature extreme events (Donat et al., 2013; Horton et al., 2015). Thus, the JRA-55 dataset is used to identify and analyze summertime heat waves. Moreover, JRA-55 allows for the investigation of changes in the atmospheric circulations related to heat waves. Relevant variables are identical to Ma and Franzke (2021). Those variables are used to obtain the observed anomalous stationary waves and to carry out numerical experiments.

We focus on summer heat waves for the months June, July, and August (JJA) over inner East Asia ($35^\circ\text{N} - 55^\circ\text{N}$, $90^\circ\text{E} - 120^\circ\text{E}$). Figure B.1a shows the time series of the regionally and seasonally averaged temperature. The temperature

shows a significant increase (p -value < 0.001) during the period of 1958 - 2019 (WH). A clear discontinuity exists in the time series of the temperature. If we break the time period of 1958 - 2019 into two periods: 1958 - 1988 (H1) and 1989 - 2019 (H2), we can see the existence of a significant difference in the temperature among H1 and H2 using the non-parametric Mann-Whitney U test (Nachar, 2008). The test reveals that the temperature differences are significant between the H2 and H1 periods (p -value < 0.001). The statistical difference is confirmed using a two-sample t -test by Ye and Ahammed (2020) as well.

We can also justify the breakdown of the WH period into the H1 and H2 period using 200 hPa streamfunction and diabatic heating. As shown in Fig. B.2, all the quantities indicate that significant differences exist between both periods based on the two-tailed Student's t -test. Compared with the H1 period, the H2 period experienced significant warming with strengthened anticyclone aloft especially over northwestern inner East Asia, and a significant diabatic cooling (heating) pattern over north and northwestern (south and southeastern) inner East Asia. The amplified high-pressure anomalies at the upper troposphere over inner East Asia are consistent with the observed trends (Wang et al., 2013; Zhang et al., 2020). This strengthened anticyclonic system will further increase surface warming and foster the formation of heat waves through enhanced downward shortwave radiation.

B.2.2 Identification of heat waves

Regionally averaged temperature anomalies are used to define the occurrence of heat waves. Specifically, three criteria are used to define a heat wave event:

- Threshold: the temperature is above a pre-defined threshold;
- Duration: the threshold is continuously exceeded for a set length;
- Interval: two heat waves are separated in time by a sufficiently long period otherwise they are considered to be the same heat wave.

We use the 90th percentile of daily mean temperature over a reference period, centered on a 31 day window (Russo et al., 2015) as the threshold. The threshold on a given day d is the 90th percentile of the temperature data (A_d) selected by

$$A_d = \bigcup_{y=y_{str}}^{y_{end}} \bigcup_{i=d-15}^{d+15} T_{s,y,i} \quad (\text{B.1})$$

where y_{str} and y_{end} denote the start and end of the reference period, \cup represents the union of sets, and $T_{s,y,i}$ represents 2m air temperature of the day i in the year y . Figure B.1b presents the calculated 90th percentile

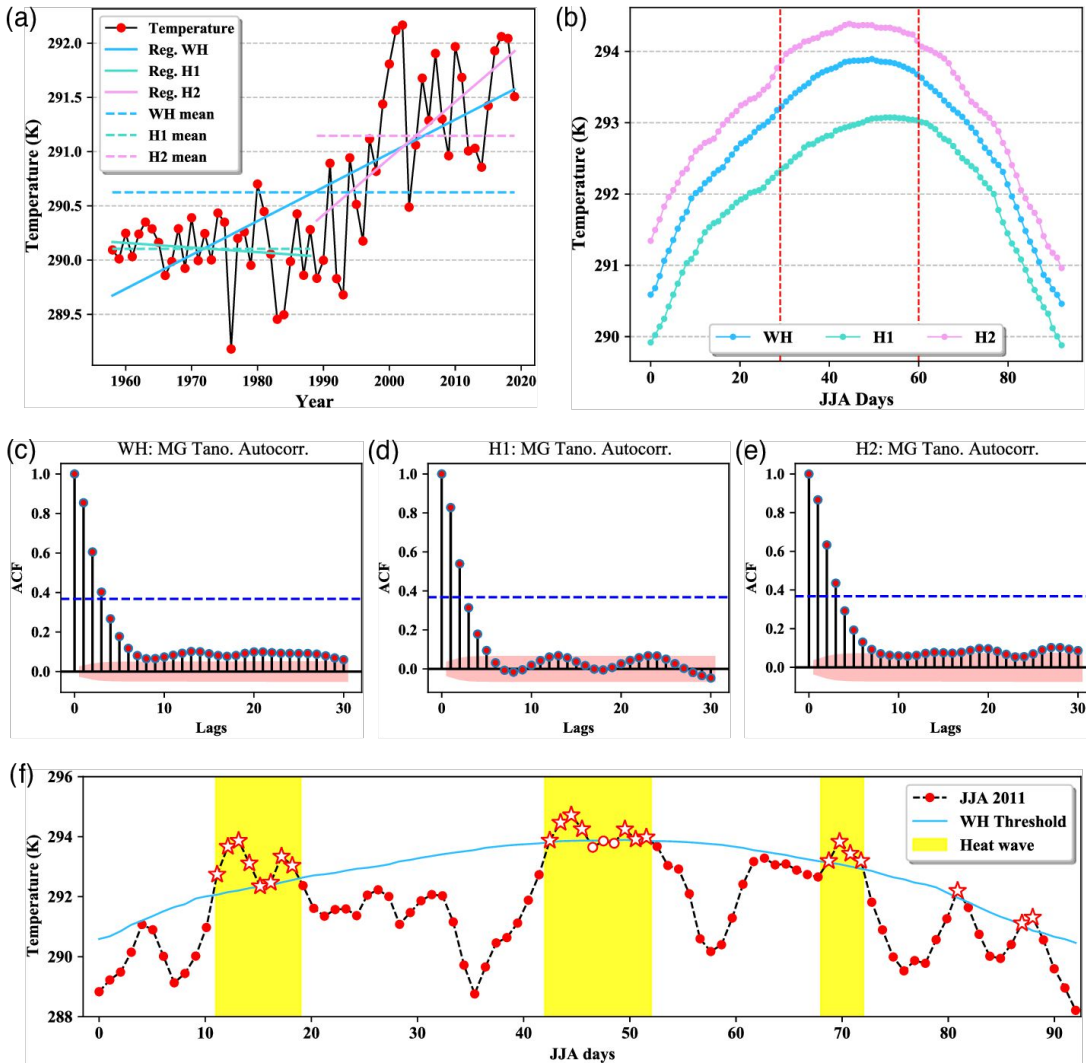


Figure B.1: Summer mean temperatures and identification of heat waves over inner East Asia. **(a)** Regional averaged temperatures from 1958 to 2019. **(b)** The 90th percentile value of temperature within the corresponding reference period. Vertical red-dashed lines separate the summer months. **(c-e)** The auto-correlations of temperature anomalies during different reference period. Blue lines denotes the $1/e$ value. Auto-correlations that fall within the shading zones are not significant at 5% level. **(f)** The example of identified heat wave events (yellow shading) in 2011, based on the reference period 1958-2019.

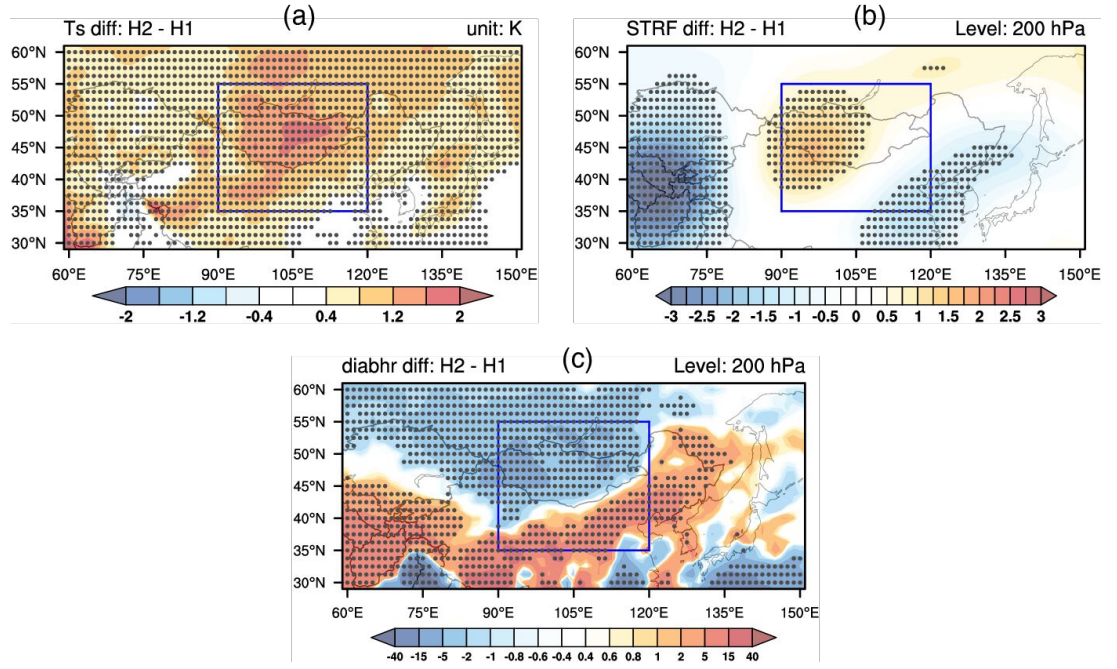


Figure B.2: The statistically significant difference test for (a) surface temperature (T_s , K), 200 hPa (b) streamfunction (STRF, $1.0 \times 10^6 m^2 s^{-1}$), and 200 hPa (c) diabatic heating (diabhr, K/day). Grid cells with statistically significant difference between H1 and H2 periods (5% significance level) are stippled. Blue frame represents the defined research domain of Inner East Asia.

threshold for different reference periods. The significant difference test shows that the time series of the threshold among different reference periods are all significant (p -value < 0.001).

We use 3-days as the duration criterion in this study, as beyond this duration heat waves have similar health impacts (Guo et al., 2017). The stress of human health due to heat events is reduced for short periods of intermittent events, which implies that the interval time between two heat events should be under consideration (Guo et al., 2017). Here, the interval time between two heat events is based on the e -folding ($1/e$) time of the auto-correlation of regionally averaged temperature anomalies (Berner et al., 2020). Figure B.1c-e shows the auto-correlation coefficients of the detrended temperature anomalies for different periods. We then use the e -folding time as the criterion for considering the interval time.

Figure B.1f presents an example of how we identify heat waves using the aforementioned three criteria in summer 2011 for the WH period. The 90th percentile threshold is calculated using Eq. (B.1) for WH (from 1958 to 2019). If the temperature exceeds the threshold (the cyan line in Figure B.1f), we consider the corresponding day hot. A heat wave event occurs when at least 3 consecutive days are hotter than the threshold. However, for the second event the temperature drop for three days below the threshold but since this is

below our duration threshold, these and the following hot days are considered to constitute one event.

B.2.3 Trends analysis of heat wave magnitude

We analyze trends of the monthly and seasonal heat wave magnitude using a modified daily heat wave index (HDMI_d) by Russo et al. (2015). The HDMI_d measures the exceedance of the daily temperature over the defined interquartile range of maximum daily temperature TG at each grid point (Fragkoulidis et al., 2018; Ma and Franzke, 2021). In this study, the interquartile range of TG is obtained from each considered period. The daily magnitude of HDMI_d is given by:

$$M_d = \begin{cases} \frac{TG - TG_{lt25p}}{TG_{lt75p} - TG_{lt25p}} & \text{if } TG > TG_{lt25p} \\ 0 & \text{if } TG \leq TG_{lt25p} \end{cases} \quad (\text{B.2})$$

where M_d denotes the daily magnitude of heat waves on day d ; TG_{lt25p} is the 25th percentile and TG_{lt75p} the 75th percentile of the climatological distribution of TG on each grid point, respectively. The difference of $TG_{lt75p} - TG_{lt25p}$ is the corresponding interquartile range of TG . We then compute the sum of M_d at each grid point for each summer month.

The trend of the monthly and seasonal magnitudes of a heat wave for each grid point is detected by the modified MK test (Kendall, 1948; Mann, 1945; Praveen et al., 2020; Yue and Wang, 2002), and the impact of the serial correlation on the trend is eliminated as in Yue and Wang (2002). The false discovery rate (FDR) correction (Benjamini and Hochberg, 1995; Wilks, 2016) is applied to verify the significant test results. Following Wilks (2016), we set $\alpha_{FDR} = 2\alpha$ for the significance tests with a global α level of 0.05.

B.2.4 Model Simulations

The NSWCM is a dry dynamical core of a nonlinear time-dependent atmospheric general circulation model. It has rhomboidal truncation at wave-number-30 in the horizontal and 14 unevenly spaced σ levels in the vertical, approximately $2.25^\circ \times 3.75^\circ$. As an idealized baroclinic model, NSWCM is built upon the three-dimensional nonlinear primitive equations. All the variables are deviations from a prescribed zonal mean basic state. The NSWCM then produces the response to a certain zonally asymmetric imposed forcing (Simpson et al., 2016). Rayleigh friction, biharmonic diffusion, and Newtonian relaxation are used as damping terms to obtain a steady-state solution (Ma and Franzke, 2021). The model equations and coefficients are identical to Held et al. (2002). A quasi-steady solution is reached by around day 30. Thus, our simulation results are shown by averaging the field from days 30 to 50.

The NSWAM inputs are computed from the JRA-55 reanalysis data. The inputs are a prescribed basic state and three forcing components (Ma and Franzke, 2021): diabatic heating (Q), orography (O), and transient momentum fluxes (M). The climatological mean is based on the respective used period.

The climatological mean and zonal mean of each reference period are removed when we calculate the forcing terms of Q and M . Many previous studies (Li et al., 2020; Schubert et al., 2011; Yang et al., 2021) have shown that precursors of heat waves can appear several days before a heat wave starts and these signals might persist for a few days after the termination of a heat wave. Therefore, we test the sensitivity of the NSWAM simulations to the selected periods of the study. The period is an extension of the heat wave period by several days. This extension only has an effect on the calculation of Q and M . Table B.1 lists the experiments used to test the sensitivity of NSWAM for extended heat wave periods.

Moreover, another sensitivity analysis is conducted for the orography, as the location of inner East Asia is close to the Himalayan-Tibet region ($25^{\circ}\text{N} - 40^{\circ}\text{N}$, $70^{\circ}\text{E} - 105^{\circ}\text{E}$). This region has been shown to exert significant influence on the summer South Asian monsoon by acting as an elevated heat source (Duan and Wu, 2005; Yeh, 1957). However, the narrow range of the Himalayas cannot be well resolved in numerical models (Ma et al., 2014). Boos and Hurley (2013) found that a smoothed model topography could cause a negative model bias in simulating monsoon strength. In order to gauge the sensitivity of model bias to the orography, we test our simulations by gradually reducing the height of orography by 10% until 50% of its original height (Table B.2).

Several other methods are used in this study. We quantify the accuracy of NSWAM's simulations by the domain-wide area-weighted pattern correlation between the NSWAM outputs and observed anomalous stationary waves (Ma and Franzke, 2021). We use the factor separation method (Cleveland et al., 2020; Stein and Alpert, 1993) to decompose the the total responses of the NSWAM to all forcings and the involved nonlinear interactions (Ma and Franzke, 2021). Then, the relative contribution of different forcings to the observed anomalous stationary waves can be quantified by the pattern correlation as well. The method in Walsh (2008) is used to obtain the statistical significance of the pattern correlations.

B.3 IDENTIFICATION OF HEAT WAVES AND OBSERVED STATIONARY WAVES

B.3.1 *Identification of heat waves*

Figure B.3 displays the characteristics of the identified heat waves for different periods. We identify 59, 35, and 32 heat waves for WH, H1, and H2, respectively. The frequency of heat waves in each year is shown in Fig. B.3a. For WH, the maximum frequency occurs in 2002 with 5 heat waves, and the average frequency for the total 62 years is 0.95 yr^{-1} . Three heat waves occur

Table B.1: List of experiments of the sensitivity test for extending heat wave period discussed in the main text.

Name	Description
EXBO0d	Calculating the forcing terms during heat wave period without extension
EXBO3d	Calculating the forcing terms by extending heat wave period lag ± 3 days
EXBO5d	Calculating the forcing terms by extending heat wave period lag ± 5 days
EXBO7d	Calculating the forcing terms by extending heat wave period lag ± 7 days
EXPR3d	Calculating the forcing terms by extending heat wave period lag +3 days
EXPR5d	Calculating the forcing terms by extending heat wave period lag +5 days
EXPR7d	Calculating the forcing terms by extending heat wave period lag +7 days

Table B.2: List of experiments of the sensitivity test for the altered orography over Himalayan–Tibet region (25°N - 40°N , 70°E - 105°E).

Name	Description
QMOori	Keeping the raw orography over HTB, without any modification
QMO90	Reducing the orography over HTB region by 10%
QMO80	Reducing the orography over HTB region by 20%
QMO70	Reducing the orography over HTB region by 30%
QMO60	Reducing the orography over HTB region by 40%
QMO50	Reducing the orography over HTB region by 50%

in 1970 and 1972 for H1 with the average frequency of 1.13 yr^{-1} . For H2 the maximum frequency is in 2001 with 4 heat waves, and the averaged frequency is 1.03 yr^{-1} . Note that those frequencies are not comparable since they refer to different reference periods.

There is a clear difference concerning the inter-annual variations of the frequencies. During the WH period, only 4 heat waves are identified from 1958 to 1988, and all the remaining 55 events are found between 1989 and 2019 with the most after 2000. In terms of the H1 and H2 periods, the time series does not show clear inter-annual variation, which is mainly due to the existence of the significant difference of the used threshold (Fig. B.1b) in identifying heat waves. A comparison of the variations among the three periods indicates that the used threshold has an impact on the analysis of heat wave characteristics over inner East Asia. In agreement with Erdenebat and Sato (2016), our results imply that the region is experiencing clear climate warming over the last few decades.

Figure B.3b shows the total duration of heat waves in each year. A total of 350 days are found for the WH period, with an average of 5.65 days per event. The maximum duration is 29 days in 2000, indicating one-third of summer days experienced heat waves. Similarly, the years 2002, 2005, 2010, and 2017 had more than 25 days of heat wave. This analysis is consistent with the regional drought period (Erdenebat and Sato, 2016; Zhang et al., 2020). For the H1 and H2 periods, a total of 161 and 176 days of heat waves occurred in these 31 years, with an average duration of 5.19 and 5.68 days per event. Moreover, a clear increasing trend of the annual duration of heat waves can be seen. Heat waves tend to last longer with climate warming in the inner East Asia region. This implies that regional warming is producing long-lasting heat waves, which did not occur previously (Vogel et al., 2021; Zhang et al., 2020).

The trend of the magnitude of heat waves for the WH period is presented in Fig. B.4. A prevailing significant increasing trend is observed in summer (Fig. B.4a-d). The overwhelming significant warming trend is detected in August (Fig. B.4c) compared with June (Fig. B.4a) and July (Fig. B.4b). The trend in August dominates the overall increasing trend in summer as shown in Fig. B.4d. This increase is consistent with the surging regional temperature during 1958-2019 as shown in Fig. B.1a. Further analysis of the heat wave magnitude for WH indicates the overall increasing trend is mainly caused by the significant warming period in the H2 period, in agreement with Fig. B.1a. Results support the circulation change with an intensified anticyclonic system over inner East Asia in Fig. B.2b, which leads to the significant rising of regional heat wave magnitude.

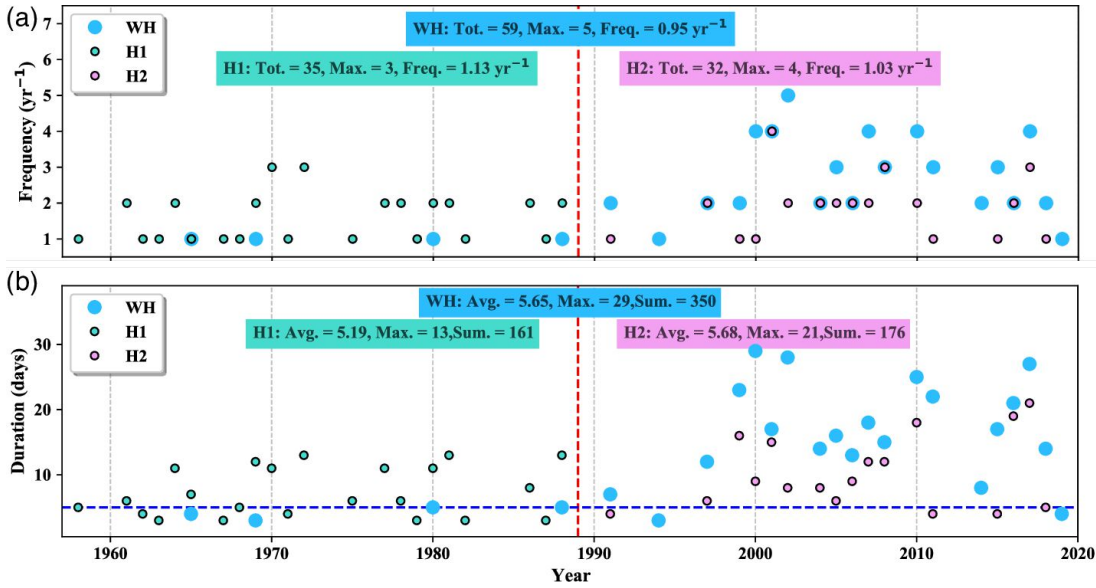


Figure B.3: Time series of identified heat waves frequency (**(a)**, yr^{-1}) and duration (**(b)**, day). Big blue dots denote the identified heat waves for the WH period, green and pink dots for H1 and H2 periods, respectively. The vertical red dashed line is the boundary between H1 and H2 period. The horizontal blue dashed line is the threshold which duration equals to 5 days. Details see the main text.

B.3.2 Observed anomalous stationary waves

Figures B.5a, b and c show the composite of observed temperature anomalies during heat waves for the WH, H1, and H2 periods. For each period, clear positive temperature anomalies can be found over inner East Asia. Moreover, a composite of observed anomalous stationary waves shows a strong anticyclonic system located over inner East Asia at 200 hPa for both periods. This provides favorable circulation conditions for the occurrence and persistence of regional heat waves (Deng et al., 2018a; Horton et al., 2016).

A closer inspection on the 200 hPa anomalous stationary waves shows that a wavelike pattern extends from western and northern Europe to the inner East Asia region with a set of highs and lows for both periods. This wavelike pattern shares some similar features over inner East Asia where the anticyclonic system tilts southwest-northeast for WH and H2 (Figs. B.5a and c), except for H1 which is broadly zonally stretched (Fig. B.5b). Although differences exist in the spatial patterns, the amplitudes of the anticyclonic centers are similar, and the locations of the centers are also almost the same for the three periods.

To investigate the changes of the large-scale circulation between H1 and H2, we present their differences in Fig. B.5d. The amplitudes of the differences are nearly half of the amplitude in Figs. B.5b and c, and the spatial patterns are similar with the observed features for the H2 period in Figs. B.5c. A

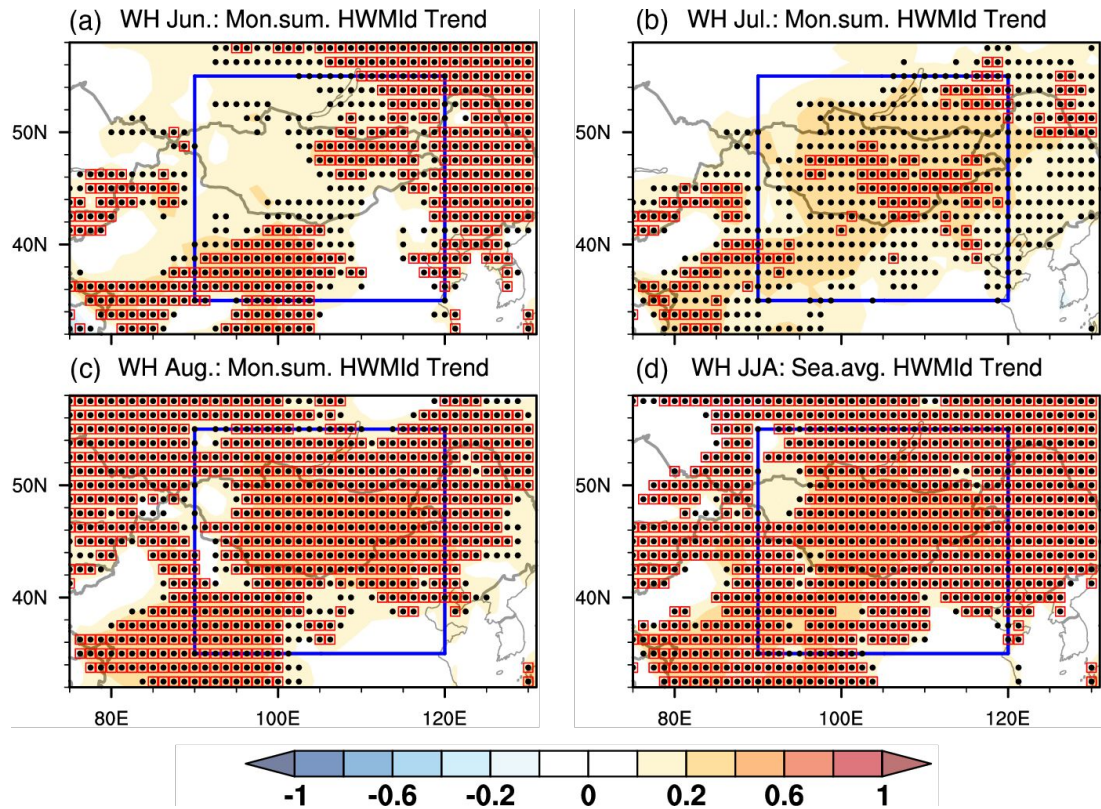


Figure B.4: Trends of heat wave magnitude for WH period in June (Jun., (a)), July (Jul., (b)), August (Aug., (c)), and JJA averaged (Sea.avg., (d)). Black dots denotes that the trend of the grid is significant at the p -value < 0.05 level. Red squares represent that the significant trends meets the FDR criteria.

wavelike pattern extending from eastern Europe into the inner East Asia region is also visible. This wavelike pattern is quite similar to a strengthened Silk Road pattern along the Eurasian jet stream (Ding and Wang, 2005; Wang et al., 2017a), which contributes to frequent and longer-lasting heat waves. This strengthened pattern is consistent with the observations in Kim and Lee (2021) and Wang et al. (2017a), and the climate model predictions in Chowdary et al. (2019). Interestingly, compared to Fig. B.2b, the differences are an intensification of the climatological differences with the center slightly shifting southeastward.

To further diagnose the forcing mechanisms, we next turn to the NSWM to reproduce the anomalous stationary waves in Figs. B.5a-d, for better investigating the maintenance mechanisms involved.

B.4 NUMERICAL EXPERIMENTS AND DIAGNOSTIC RESULTS FROM NSWM

B.4.1 *Selections of Experiment*

As shown in Fig. B.3b, we select heat wave events that last for at least 5 days for the numerical simulations. There are 32, 16, and 15 heat waves for WH, H1, and H2, respectively. On one hand, these chosen events account for around 50% of the total identified heat wave events for each period. These heat waves are sufficient to represent the dynamical processes of heat waves (Ma and Franzke, 2021). On the another hand, the 5-day threshold is a good compromise for our study of stationary waves compared with 3 days, which can be influenced by other localized processes, such as a short warm advection process or Foehn effect in the vicinity region (Chen and Lu, 2015).

We perform sensitivity analysis for the WH period at first, as stated in section B.2.4. The impact of the length of the period under study and the orographic effect over the Himalayan-Tibet region are examined. The spatial pattern correlation between model results and reanalysis over inner East Asia is used for measuring the performance of the NWSM.

As shown in Fig. B.6a, all pattern correlations are statistically significant. We find a clear increase in the pattern correlation by including circulation information prior to the start of the heat wave. Our results indicate that considering the synoptic disturbances prior to heat waves will improve the model simulations. This is to some extent in agreement with Chen and Lu (2015). Their results support that the synoptic disturbances prior to heat waves play a main role in leading to heat waves. Concerning the sensitivity of the orography, reducing the orographic height indeed increases the correlation in a range from 0.1 to 0.2 (Fig. B.6a), while this increase is slow after reducing 30% of the height over the Himalayan-Tibet region. Similarly, we show in Figs. B.6a and b the computed pattern correlations for the H1 and H2 periods. Overall, Figs. B.6a, b, and c suggest that we could select EXPR3d with a 30%

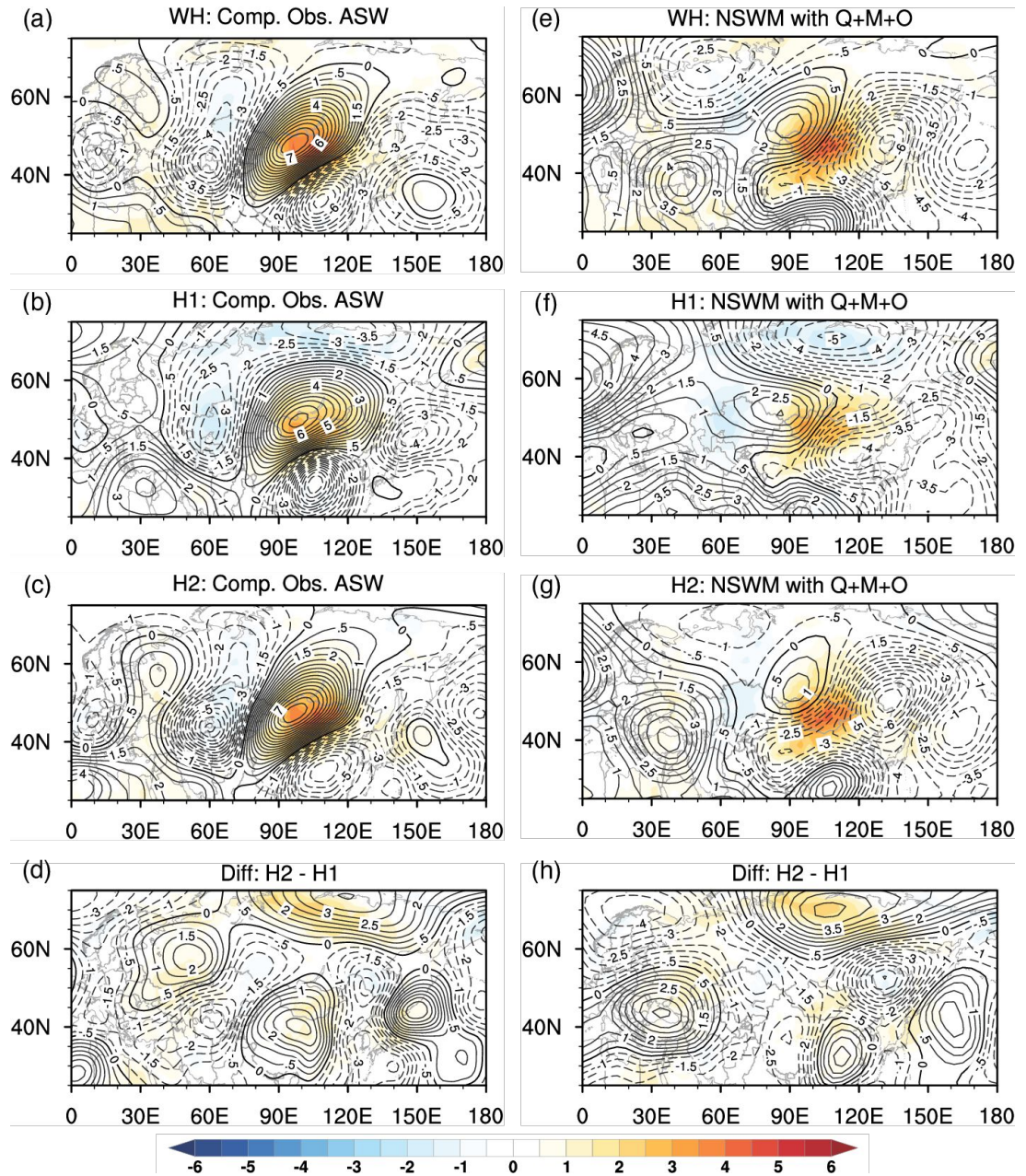


Figure B.5: The observed (a,c,e) and simulated (b,d,f) anomalous stationary waves streamfunction fields (contours) at the 200 hPa for WH, H1, and H2 period, respectively. g and h The difference of anomalous stationary waves streamfunction fields between H1 and H2 period in observations (g, i.e. e-c) and simulations (h, i.e. f-d). Shading represents the temperature anomalies referencing to each period. The contour interval is $0.5 \times 10^6 m^2 s^{-1}$.

reduced orographic height over the Himalayan-Tibet region (QMOR70) to conduct the numerical simulations.

Therefore, we will present and analyze the numerical experiments based on EXPR3d and QMOR70 in the following sections. We note that experiments with the largest correlations have been analyzed as well, e.g. EXPR5d for WH, EXPR3d for H1, and EXPR7d for H2, and the results are very similar to EXPR3d (not shown).

B.4.2 NSWMM responses to total forcing

As shown in section B.4.1, significant spatial pattern correlations are identified when we force the NSWMM with all the forcings (TNE_QMO). Figures B.6a and b shows that the correlations for WH and H1 are nearly the same, around 0.75, while for the H2 period it is 0.51 (Fig. B.6c). They are all statistically significant, indicating the model can provide useful results in simulating the observed anomalous stationary waves. The relatively smaller correlation for the H2 period could be due to the intensified contributions from land-atmosphere coupling during this period as shown by Zhang et al. (2020), which is a missing process in NSWMM (Ma and Franzke, 2021).

We then compare the spatial patterns generated by the NSWMM and the observed circulation patterns. As shown in Figs. B.5e, f, and g, the model can produce a similar anticyclonic system over inner East Asia with a smaller amplitude. The tilts of the observed anticyclonic system in WH and H2 are well captured and the zonally confined anticyclonic system for H1 is also reasonably reproduced. Moreover, Fig. B.5h displays the simulated differences in spatial patterns between H1 and H2. Comparing Fig. B.5h with Fig. B.5g, we see that generally a similar wavelike pattern is reproduced.

Discrepancies between the simulations and the observations exist regarding the simulated location of the anticyclonic centers and also the amplitude. Large discrepancies present in the simulations for H2 and also for the differences between H1 and H2. Possible causes are the quality of the input forcing data, the chosen parameters of the dissipation, the model resolution, and the lack of some physical processes (Held et al., 2002; Liu et al., 1998; Ma and Franzke, 2021). However, the significant spatial correlations and the captured anticyclonic systems confirm that the NSWMM can capture the basic features of the observed anticyclonic systems for all periods. This provides a basis for further elucidating the effect of the various forcing mechanisms involved during heat waves. To explore the effects of climate warming, we will then concentrate on decomposing the NSWMM responses into various forcing mechanisms for the H1 and H2 periods.

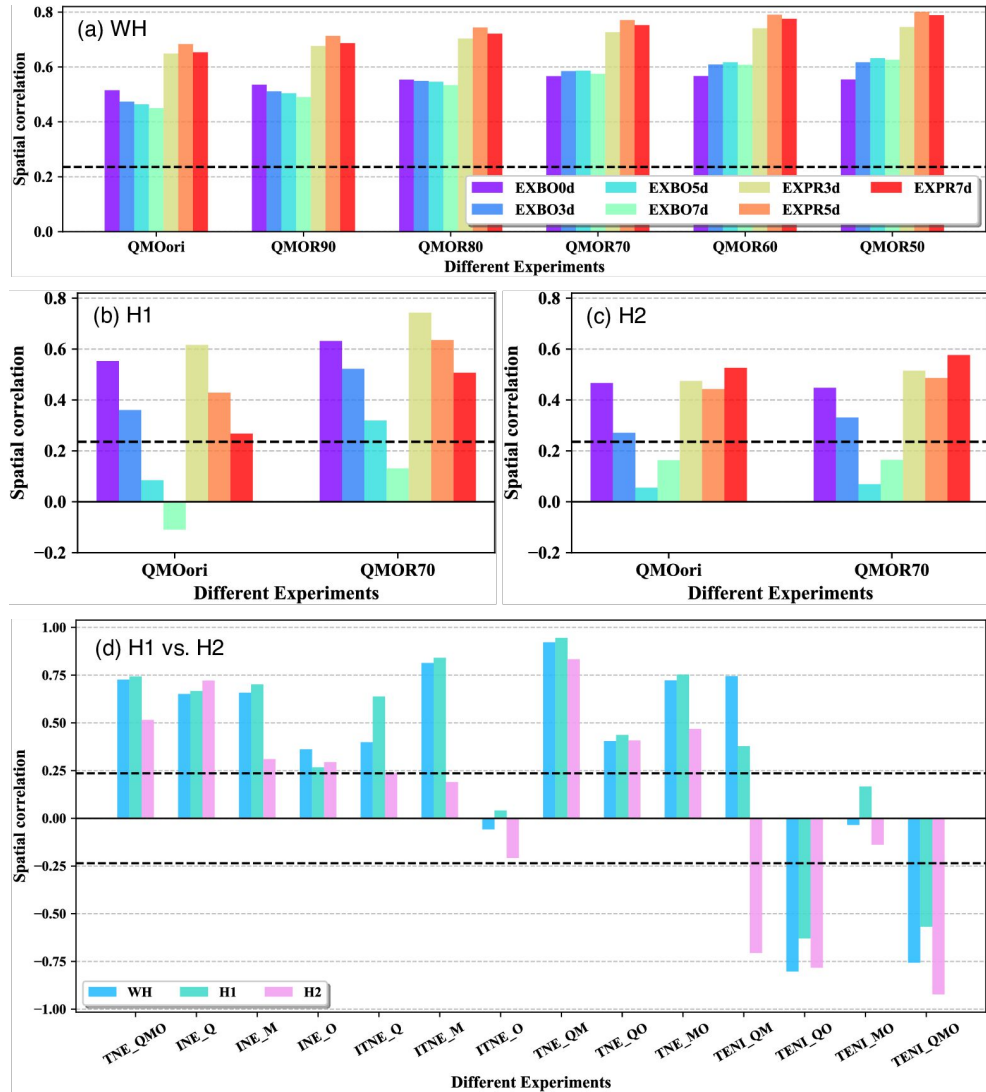


Figure B.6: Spatial pattern correlation between observational and simulated anomalous stationary waves at 200 hPa over inner East Asia. (a-c) Correlations are obtained from the NSWCM sensitivity analysis, where the NSWCM is driven by: diabatic heating (Q), transient momentum fluxes (M), and orography (O). The experiment settings see Tables B.1 and B.2. (d) Correlations are obtained from different decompositions of results from NSWCM for the H1 and H2 period. The black dashed lines denote the statistically significant pattern correlation threshold followed the methods by Walsh (2008). Significant positive (negative) correlations are above (below) the threshold. See the main text for more details.

B.5 DECOMPOSING VARIOUS FORCING MECHANISMS IN NSWMM

B.5.1 *Direct nonlinear effects*

Using the factor separation method (Ma and Franzke, 2021), we first decompose the NSWMM streamfunction responses into individual nonlinear effects: INE_Q, INE_M, and INE_O. Upon comparison of Figs. B.5 and B.7a-c, it is evident that the anticyclone over inner East Asia is mainly forced by the transients (Fig. B.7b). The effects of diabatic heating play a secondary role for H1 (Fig. B.7a), while it tends to generate the cyclonic systems extending from the western Pacific into inner East Asia for H2. Responses to the orography (Fig. B.7c) are almost the same for all periods since it has only interaction with the basic state for each period (Ma and Franzke, 2021). Moreover, the effect of the transients dominates in simulating the differences between H1 and H2 (Figs. B.7b and B.5h). Although the transients play the dominant role, the simulated wave trains over Eurasia for all periods are results of the integrated effects from all forcing terms.

The pattern correlations are shown in Fig. B.6d. All correlations are statistically significant. The effects of diabatic heating and transients tend to have the same contributions to the simulated spatial patterns for H1. In contrast to the simulated spatial patterns (Fig. B.7b), the effects of diabatic heating present relatively higher correlations for H2. This is due to that diabatic heating seems to cause the observed cyclonic system over southeastern inner East Asia. Furthermore, the contribution of transients decreases for H2 compared with H1. The model reproduces the anticyclone which has an opposite tilt with the observed one (compared Fig. B.7b with Fig. B.5c), which could explain the relatively lower correlation of the NSWMM responses to the transients for the H2.

B.5.2 *Individual total nonlinear effects*

We then decompose the model responses into individual total nonlinear effects (ITNE), by including all the nonlinear interactions for each forcing component. The results are named ITNE_Q, ITNE_M, and ITNE_O. Comparing Figs. B.7d-f with Figs. B.7a-c, we find similar spatial patterns for simulated stationary waves for all the corresponding periods. However, generally lesser amplitudes are identified, which are clear for the response of diabatic heating in H1, for the response of transients in H2, and for the response of orography in all periods. For the differences in Figs. B.7d-f, an intensified anticyclone is identified over southeastern inner East Asia, which is likely responsible for the shifted anticyclonic system (Fig. B.5g and Fig. B.5h).

Considering the pattern correlations, Fig. B.6d illustrates that a general decrease occurs by including the nonlinear interactions for each forcing component, except for the transients for H1. The most dominant features are that

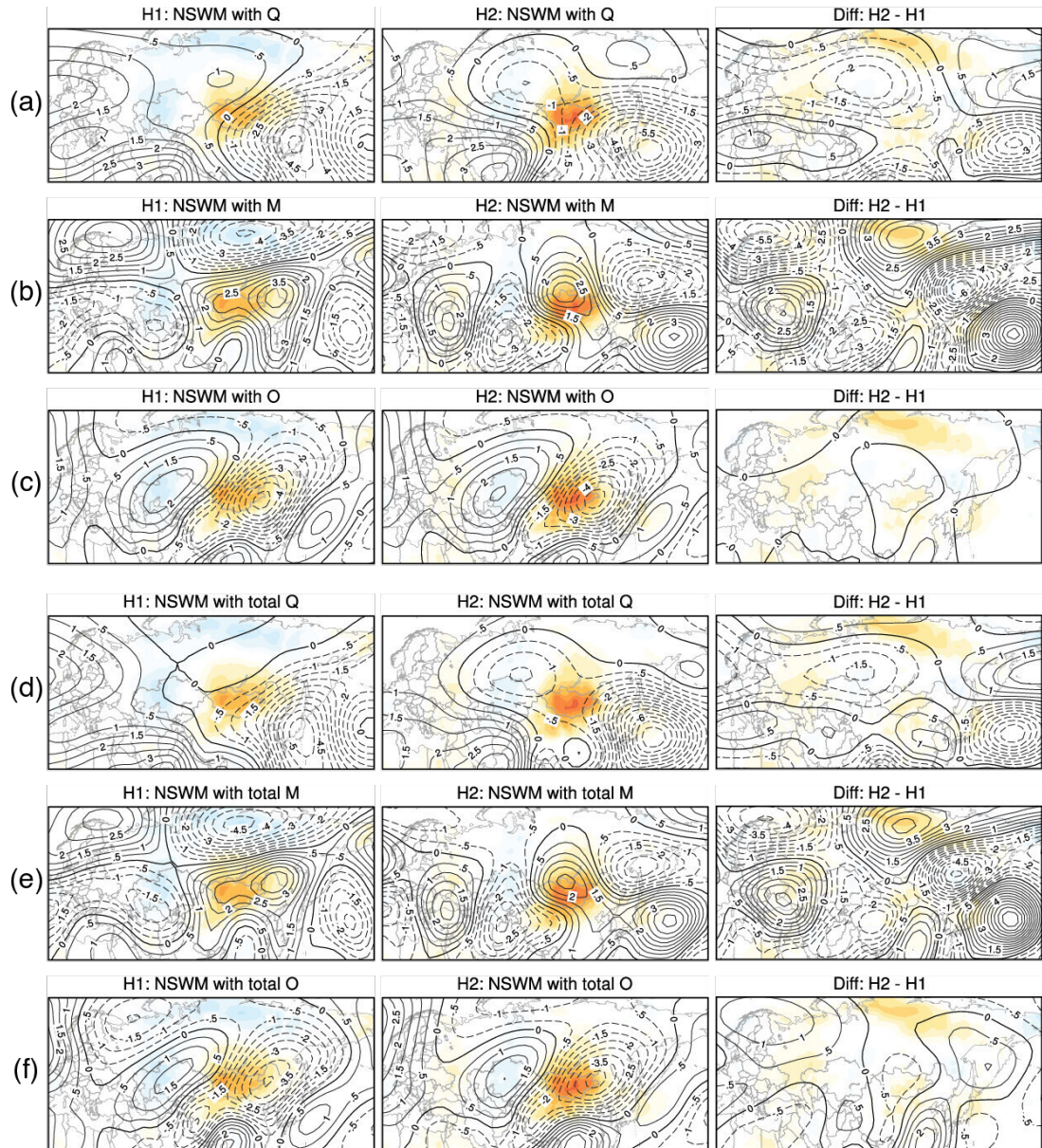


Figure B.7: Same as the right panel in Fig. B.5, but the NSWM is forced by the individual forcing term (a-c) and (d-f) responses to the total nonlinear effects of each forcing term for H1 and H2 periods.

the correlation of the nonlinear effect of orography becomes insignificant for all periods, and the correlation for the response to the transients during H2 turns insignificant. Our results imply that the nonlinear interactions among different forcing components play crucial roles not only in reproducing the observed stationary waves but also are responsible for the difference in the maintenance mechanisms.

B.5.3 *Nonlinear interactions*

We then simulate the combined forcing effects by driving NSWMM with two forcing components at the same time. The spatial patterns of the combined effect for diabatic heating and transients (TNE_QM) and for the transients and orography (TNE_MO) are similar to the observed stationary waves in Fig. B.5. The response to the combined effect for diabatic heating and orography (TNE_QO, not shown) is more similar to Fig. B.7c. For the response to the combined effect between the transients and diabatic heating, the correlation is larger than the response to their individual nonlinear effects. In contrast, correlations for the response to the combined effect between diabatic heating and orography are generally smaller than the response to the individual nonlinear effect of diabatic heating (Fig. B.6d). All the correlations are significant and nearly equal in the different periods, while the combined effects between transients and orography tend to decrease from H1 to H2. Therefore, our results indicate that the nonlinear interactions play a significant role in the heat wave dynamics.

Four nonlinear interaction components are considered: TENE_QM, TENE_QO, TENE_MO, and TENE_QMO. The response to the nonlinear interaction terms will be identically zero if the involved dynamic process is linear (Sobolowski et al., 2011). Figure B.8 displays the contributions of each of the nonlinear interaction terms to the maintenance of anomalous stationary waves. The responses to the nonlinear interaction between diabatic heating and orography (Fig. B.8b) and between transients and orography (Fig. B.8c) have a relatively larger amplitude. Results indicate that the orographic effect plays an important role in maintaining the stationary waves by nonlinear interaction with other forcings. This is in agreement with previous studies, the orographic effect could have significant impacts on the distribution of thermal forcing (Ting, 1994) and transient eddy fluxes (Held et al., 2002).

Regarding the spatial patterns, the response to the nonlinear interaction between diabatic heating and orography generates an anticyclonic system for all periods although the centers and extensions of the simulated systems vary. The responses due to nonlinear interactions involving transients and orography reproduce the observed anticyclone only for H1 (Fig. B.8c). The response to the nonlinear interactions between diabatic heating and transients (Fig. B.8a) lead to a cyclonic system for H2 only. Contributions of the three-way interactions (Fig. B.8d) are modest in terms of their amplitude, although

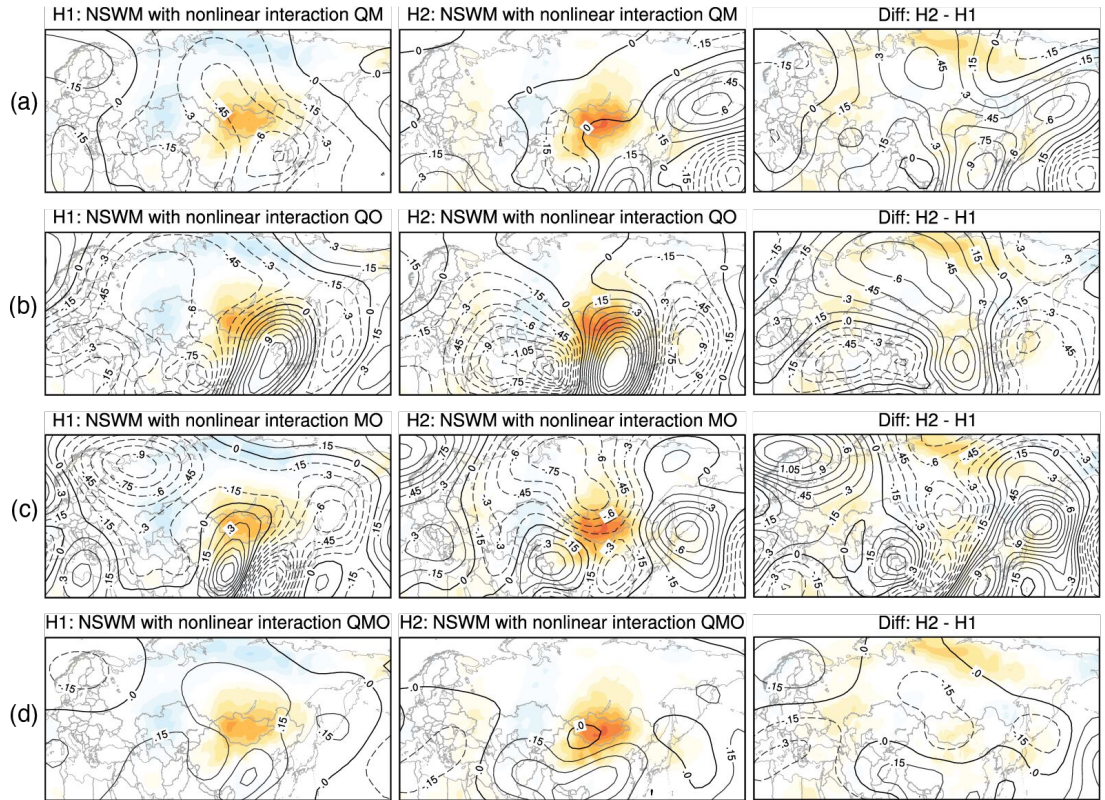


Figure B.8: The NSW responses to the nonlinear interactions between the three different forcing terms. Contour interval is $0.15 \times 10^6 m^2 s^{-1}$.

they play different roles in different periods. Moreover, by inspecting the differences between H1 and H2, we find that only the response to the nonlinear interaction between diabatic heating and orography could broadly simulate the observed difference in Fig. B.5.

As shown in Fig. B.6d, except for the correlations from the interaction between transients and orography, all others are significant. The clearest feature is that the significant positive correlations for H1 with the nonlinear interactions between diabatic heating and transients, while the correlation value for H2 is negative. All other terms present significant negative correlations, with the values for H2 larger than those for H1.

In summary, based on the pattern correlation and spatial patterns, the decomposition results show that the transients are a dominant factor in reproducing the anticyclonic systems for both periods. The nonlinear interactions between different forcing terms are also crucial to the maintenance of the stationary waves, especially the nonlinear interaction between diabatic heating and orography. The main difference in the maintenance mechanisms between H1 and H2 is through the nonlinear interactions between different forcing components. Our results suggest that contributions of the response to diabatic heating tend to increase through its nonlinear interactions with orography and transients to some extent under a warmer climate.

B.6 DECOMPOSITION OF TRANSIENTS

As we have shown, transients play a dominant role in forcing stationary waves. To see which transient components contribute to this, we perform additional simulations. As shown in Fig. B.9, forcing the model with transient vorticity fluxes (Fig. B.9b) can generate identical anticyclonic centers with the model simulations with full forcings and the observations in Fig. B.5, rather than the transient divergence flux (Fig. B.9a). Our results are similar to heat waves over Europe and indicate that convective processes, driving divergent flows, contribute little to maintain anomalous stationary waves (Ma and Franzke, 2021). Moreover, the nonlinear effects of transient vorticity flux dominate the differences between H1 and H2 as well. This is consistent with Wang et al. (2017a) in which they demonstrated the important role of relative vorticity fluxes in representing the propagation of Rossby wave trains.

The spatial correlation for this separation suggests that the main changes between H1 and H2 are through transient vorticity fluxes (Fig. B.10a). All the correlations are significant. The contributions of transient divergence fluxes are almost the same for both periods, while the contributions of transient vorticity decrease clearly from H1 to H2. Our results show that there is no big difference between forcing the model merely using the transient vorticity flux and using the whole transients field (Fig. B.10a with Fig. B.6d).

We then investigate the observed transient vorticity fields for H1 and H2 in Fig. B.11. Note that transient vorticity fields are quite noisy, thus following Schubert et al. (2011) we smooth the observed fields by using an inverse Laplacian operator for display. Regions of negative values are associated with an anticyclonic system and positive values are controlled by cyclonic storms (Holton and Hakim, 2012b). For H2, there are two anticyclonic systems located in northeastern and southwestern inner East Asia and two cyclonic systems located in the diagonal direction (Fig. B.11b). The spatial pattern for H1 is different by being dominated by two cyclonic centers (Fig. B.11a). The difference between H1 and H2 bears a striking similarity to the pattern in H2 with strengthening and extending two anticyclonic systems (Fig. B.11c). Compared with the observed stationary waves in Fig. B.5, transient vorticity fluxes might have contributed to shape the direction of those observed anticyclonic systems and then maintain those systems through nonlinear effects as examined by NSWMM.

Following Ma and Franzke (2021), we filter transient vorticity flux into high- (less than 10 days) and low-frequency (from 10 to 30 days) eddies for different periods. The decomposed four nonlinear interaction components are calculated by:

$$TF_{vort} = -\nabla \cdot \overline{(\mathbf{v}'_L \zeta'_L)} - \nabla \cdot \overline{(\mathbf{v}'_L \zeta'_H)} - \nabla \cdot \overline{(\mathbf{v}'_H \zeta'_L)} - \nabla \cdot \overline{(\mathbf{v}'_H \zeta'_H)} \quad (\text{B.3})$$

where TF_{vort} is the transient vorticity flux, and the subscript L denotes low- and H high-pass filtered eddies. We then conduct experiments including

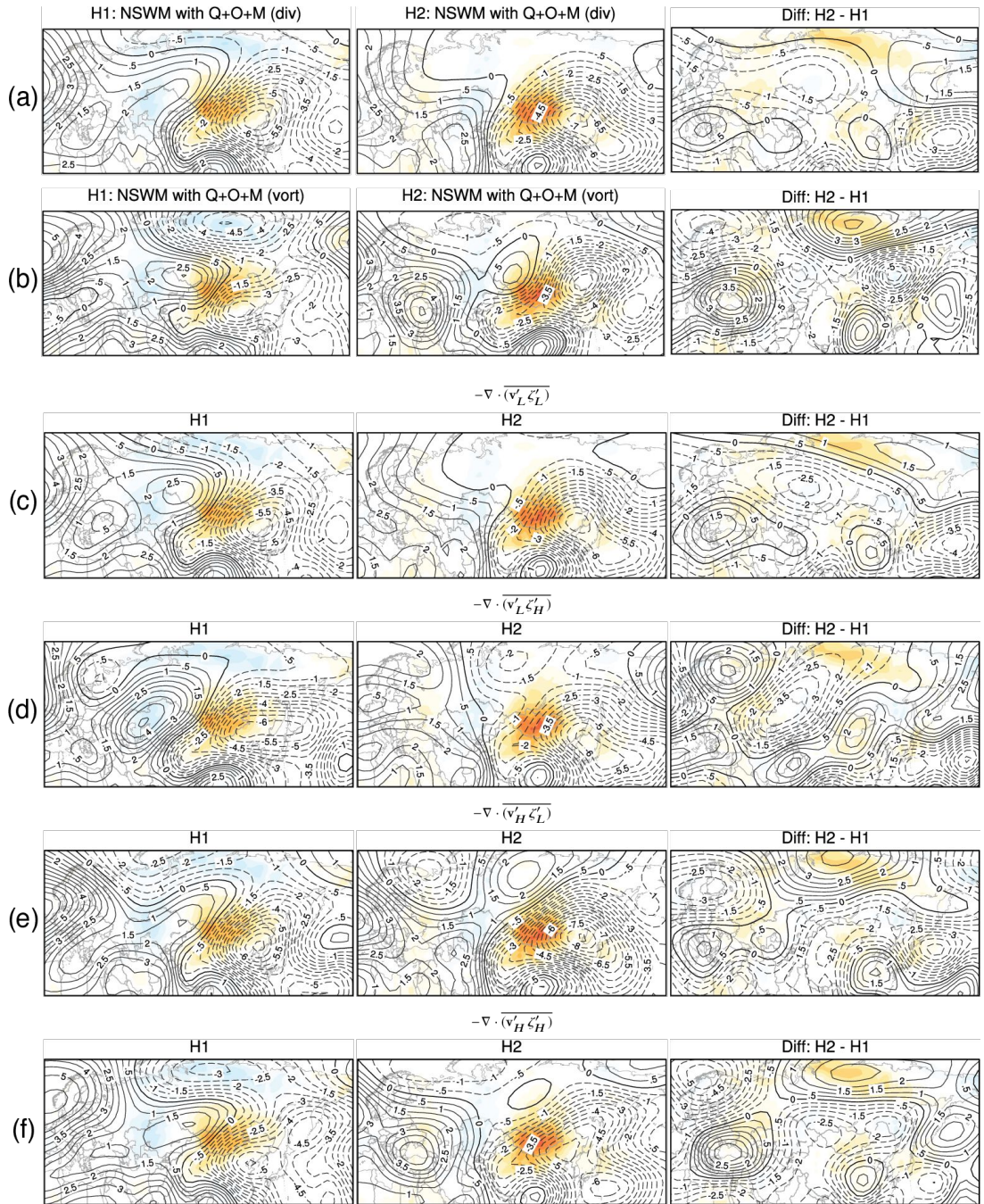


Figure B.9: Same as the right panel in Fig. B.5, results are the decomposition of transients. **a-b** The used transients is replaced by transient divergence (div, **a**) and vorticity (vor, **b**) fluxes. **c-f** The NSWM response to the decomposed transient vorticity flux: **(c)** $-\nabla \cdot (\mathbf{v}'_L \zeta'_L)$, **(d)** $-\nabla \cdot (\mathbf{v}'_L \zeta'_H)$, **(e)** $-\nabla \cdot (\mathbf{v}'_H \zeta'_L)$, and **(f)** $-\nabla \cdot (\mathbf{v}'_H \zeta'_H)$.

all the forcing terms but replacing the transient vorticity flux by each of the decomposed component in Eq. B.3 for different periods.

In general, the nonlinear effect of the high-frequency transient fluxes (Fig. B.9f) can generate similar spatial patterns over Eurasia (compare Fig. B.9b). However, contributions from the other three components cannot be neglected and vary or both periods. For H1, the low-frequency eddies (in Fig. B.9c) dominate the total response of the transient vorticity, and the other three terms contribute to extending the anticyclones. While for H2, the high-frequency wind anomalies dominated terms (Fig. B.9e and f) play important roles in maintaining the stationary waves rather than the low-frequency variabilities (Fig. B.9c and d). Moreover, concerning the differences between H2 and H1, responses to all the terms share a common feature, an anticyclonic system located in the southeastern inner East Asia as in Figs. B.9d and B.5h. Among these terms, the response to the nonlinear term $-\nabla \cdot (\mathbf{v}'_L \zeta'_H)$ (Fig. B.9d) can reproduce similar anticyclonic systems centered over inner East Asia, which is similar in the observed differences (Fig. B.5g). These results confirm that the changes in the maintenance mechanisms of the anomalous stationary waves could come partly from the nonlinear role of high-frequency vorticity variabilities under a warmer climate.

Again, results from the pattern correlation confirm the above reanalysis as shown in Fig. B.10b. All the correlations pass the significant test and the largest correlated values are all presented in the high-frequency eddies. Clear differences are also found between H1 and H2. The high-frequency wind anomalies dominated terms ($-\nabla \cdot (\mathbf{v}'_H \zeta'_L)$ and $-\nabla \cdot (\mathbf{v}'_H \zeta'_H)$) tend to weaken their contributions from H1 to H2, which supports the shifting anticyclonic centers in Figs. B.9e and f). Moreover, contributions from the response of NSWMM to the nonlinear term $-\nabla \cdot (\mathbf{v}'_L \zeta'_H)$ are increasing from H1 to H2. Therefore, our results indicate that contributions from high-frequency wind anomalies are decreased. This may be due to the weakening summer mid-latitude circulation resulting from Arctic amplification (Coumou et al., 2015).

B.7 DECOMPOSITION OF CONTRIBUTIONS FROM DIABATIC HEATING

B.7.1 *Spatial distribution of diabatic heating*

Figure B.12 presents the composites of the vertical averaged (900-150 hPa) diabatic heating anomalies. Significant diabatic cooling dominates over inner East Asia during heat waves for both periods, in agreement with previous studies (Ma and Franzke, 2021; Raveh-Rubin, 2017; Zschenderlein et al., 2019). Anticyclonic circulation controls the regional weather system during heat waves, leading to subsidence motion in the free atmosphere. This subsidence concurs with radiative cooling which causes diabatic cooling. Then, the upper-level anticyclonic system caused subsidence resulting in strong adiabatic warming. This warming compensates for diabatic cooling and enhances near-

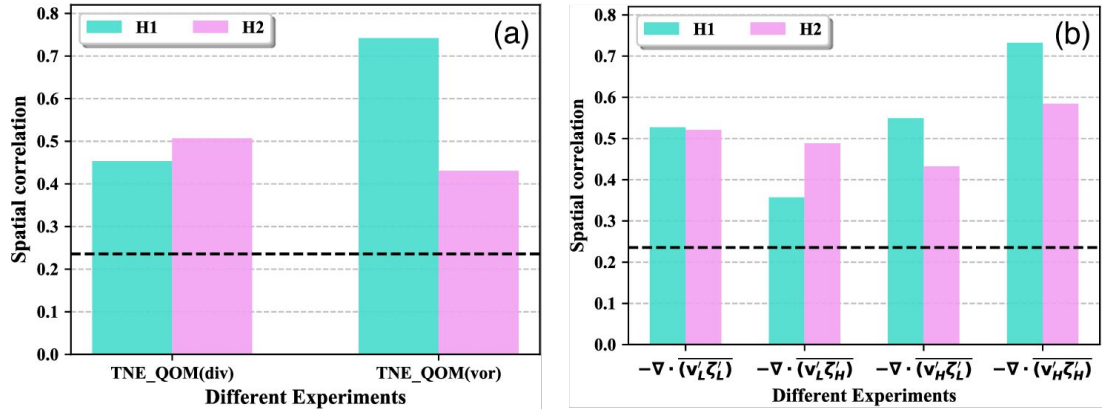


Figure B.10: Same as Fig. B.6d, but now the spatial correlations are based on the decomposition of transients. The experiments are: **a** separated transients into transient divergence (div) and vorticity (vor) fluxes, and **b** decomposed transient vorticity flux into four different parts based on different frequency ranges: $-\nabla \cdot (\mathbf{v}'_L \zeta'_L)$, $-\nabla \cdot (\mathbf{v}'_L \zeta'_H)$, $-\nabla \cdot (\mathbf{v}'_H \zeta'_L)$, and $-\nabla \cdot (\mathbf{v}'_H \zeta'_H)$.

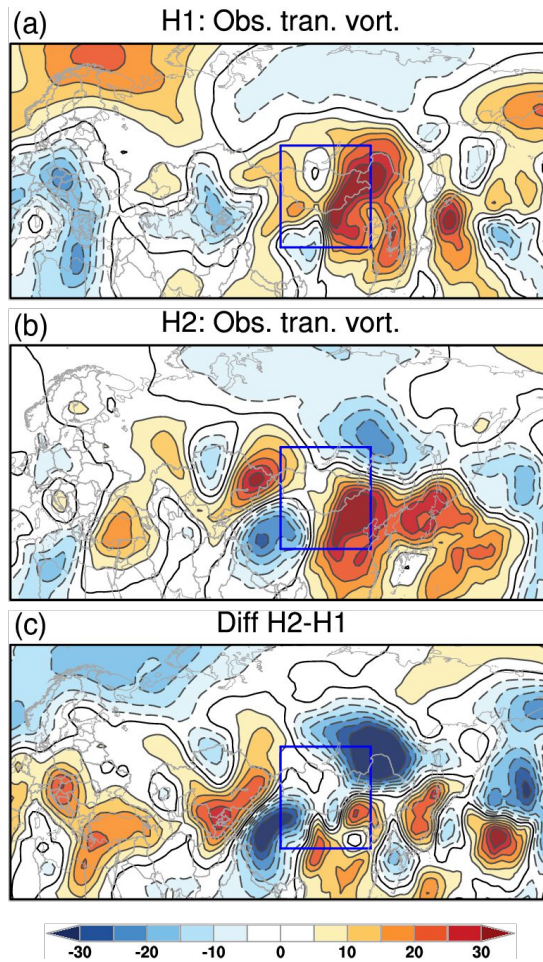


Figure B.11: The observed transient vorticity forcing fields at 200 hPa. The values are smoothed by applying the inverse Laplacian ($m^2 s^{-2}$).

surface warming. Moreover, the above analysis shows that the intensifying anticyclonic systems in H2 correspond to the significant decreasing diabatic heating over northern and northwestern inner East Asia (Figs. B.2b and c).

Other clear spatial patterns with significant heating anomalies tend to cluster over the ocean. The significant regions are more obvious over the tropical region: the Indian ocean, the Pacific, and the Atlantic. Meanwhile, there are evident differences between H1 and H2 (Fig. B.12c). These differences are quite similar with a strengthening spatial pattern for H2 over the ocean. For example, the South China Sea experiences an enhanced diabatic cooling, and enhanced tropical Atlantic diabatic heating is found. Our results suggest that those regions are important in exciting and maintaining large-scale circulations during heat waves. Thus, we will next investigate the contributions of the various heating sources to the observed circulation anomalies during heat waves for both periods.

Furthermore, the decomposition of the diabatic heating proves that the spatial patterns of latent heating anomalies (not shown) dominate in the spatial patterns in Fig. B.12. The predominant role of latent diabatic heating in driving large-scale circulation anomalies during summertime has also been shown (Baggett and Lee, 2019; Kim and Lee, 2021; Ting, 1994). However, to stay consistent, we still determine the total diabatic heating forcing for the regional contributions, although the latent heating anomalies are more dominant.

B.7.2 Contributions from regional diabatic heating

We now investigate the contributions from Pacific and Indian ocean heating anomalies. Five sub-regions are considered as shown in Fig. B.12: the tropical Pacific (TRPC), the Indian summer monsoon region (IDSM), the tropical western Pacific (TWPC), the tropical eastern Pacific (TEWPC), and the mid-latitude Pacific (MLPC). Following Ma and Franzke (2021), we perform NSWMM simulations to determine the regional contributions. Thus, the model responses are generated from the contributions of global orography, transients, and diabatic heating only over the considered region and also their nonlinear interactions.

Generally, the responses to the heating over the IDSM (Fig. B.13b), TWPC (Fig. B.13c), and MLPC (Fig. B.13e) regions excite anticyclonic systems over inner East Asia. However, the model responses are different for H1 and H2. The positive heating anomaly over MLPC (Fig. B.12a) could be mainly responsible for the generation of the zonally extended observed stationary waves for H1, while the significant cooling over MLPC (Fig. B.12b) generates the anticyclonic response for H2. Moreover, heating anomalies over TWPC and IDSM play different important roles for the two periods as well. Heating in IDSM produces an anticyclone centered over inner East Asia, and response to heating in TWPC enhances this anticyclone for H1; while for H2, both of

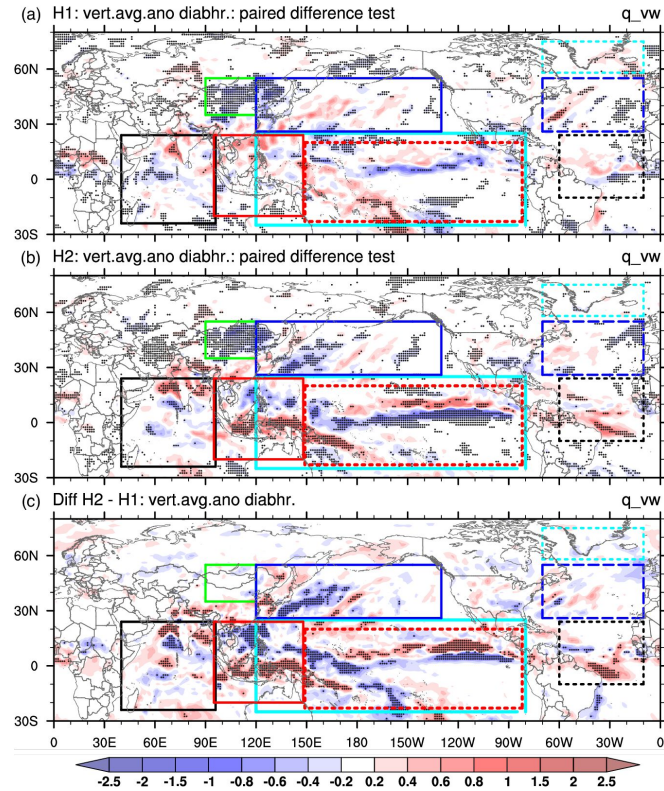


Figure B.12: Composites of vertically averaged diabatic heating anomalies from 900 hPa to 150 hPa during heat waves for **(a)** H₁, **(b)** H₂. The dots denote regions in which the anomalies are statistical significance at the 90% level based on the paired difference test (two-tailed *t*-test). **(c)** The differences of the heating anomalies between H₂ and H₁ period, and the dots indicate regions where the anomalies exceed 2 standard deviations of the differences. Green boxes denote the inner East Asia region, and other boxes represent the regional diabatic heating domains used for conducting the experiments: Tropical Pacific (TRPC, 25°S - 25°N, 120°E - 80°W; cyan-dashed), Tropical Indian Ocean (IDSM, 25°S - 25°N, 40°E - 95°E; black-soiled), West Tropical Pacific (TWPC, 25°S - 25°N, 95°E - 150°E; red-soiled), East Tropical Pacific (TEPC, 25°S - 25°N, 150°E - 80°W; red-dashed), Tropical North Atlantic (TRAT, 10°S - 25°N, 10°W - 60°W; black-dashed), Mid-latitude North Pacific (MLPC, 25°N - 55°N, 120°E - 130°W; blue-soiled), Mid-latitude North Atlantic (MLAT, 25°N - 55°N, 10°W - 70°W; blue-dashed), High-latitude North Atlantic (HLAT, 60°N - 75°N, 10°W - 70°W; cyan-dashed). Note that some latitude or longitude may be changed slightly for display purpose.

the responses to heating anomalies in IDSM and TWPC tend to strengthen the anticyclone produced by the response to heating in MLPC. Results indicate a different forcing mechanism between the two periods.

Considering the differences between H1 and H2, the response to the heating anomalies in MLPC is more important for the observed intensifying anticyclonic systems. As shown in Figs. B.12d, the role of MLPC could be determined due to the nonlinear effect of warming in the East China Sea and the Sea of Japan, and the cooling in the eastern North Pacific. Moreover, heating anomalies over IDSM and TWPC have also partly contributed to the intensifying anticyclonic systems.

We also consider three regional heating sources over the North Atlantic to conduct the simulations (Fig. B.12): the tropical (TRAT), the mid-latitude (MLAT), and the high-latitude North Atlantic (HLAT). The responses of NSWAM to the three regional heating anomalies are shown in Fig. B.14. In general, the amplitudes of the responses from the North Atlantic are smaller than those from the North Pacific. This indicates that heating anomalies over the North Atlantic play modest roles in maintaining stationary wave anomalies during heat waves for the two periods. For H1, the warming around HLAT leads to an anticyclonic response over inner East Asia. For H2, both contributions from the response to heating anomalies over TRAT and MLAT can generate an anticyclonic response extending to the inner East Asia region. For the differences between H2 and H1, results show that heating in TRAT and in MLAT tend to increase their contribution in strengthening the anticyclonic circulation over inner East Asia during heat waves.

B.8 ROLE OF MODES OF CLIMATE VARIABILITY

As mentioned in section B.3, a wave-train that resembles the Silk Road pattern is identified in Fig. B.5d, resulting in a clear barotropic anticyclonic anomaly over inner East Asia. Previous studies have connected the variations of this Silk Road Pattern with several modes of climate variability (Ding et al., 2011; Wang et al., 2017a), such as El Niño–Southern Oscillation (ENSO), the Pacific Decadal Oscillation (PDO), and the Atlantic Multidecadal Oscillation (AMO). Moreover, the Asian summer monsoon (Huang et al., 2021; Si and Ding, 2016) and Arctic warming (Coumou et al., 2015) contribute to the regional temperature anomalies as well.

To investigate the impacts on summertime (JJA) temperature anomalies for H1 and H2 we use the indices Arctic Oscillation (AO), the North Atlantic Oscillation (NAO), AMO, PDO, the ENSO index (NINO_{3.4}), and the Indian Dipole Mode Index (DMI). We obtained all the climate indices from (<https://climexp.knmi.nl/>). The monthly normalized South (SASMI) and East (EASMI) Asian Summer Monsoon indices (Li and Zeng, 2002) are used, which are archived at <http://ljp.gcess.cn/dct/page/65544>. We then compute the Pearson correlation between the monthly climate indices and monthly

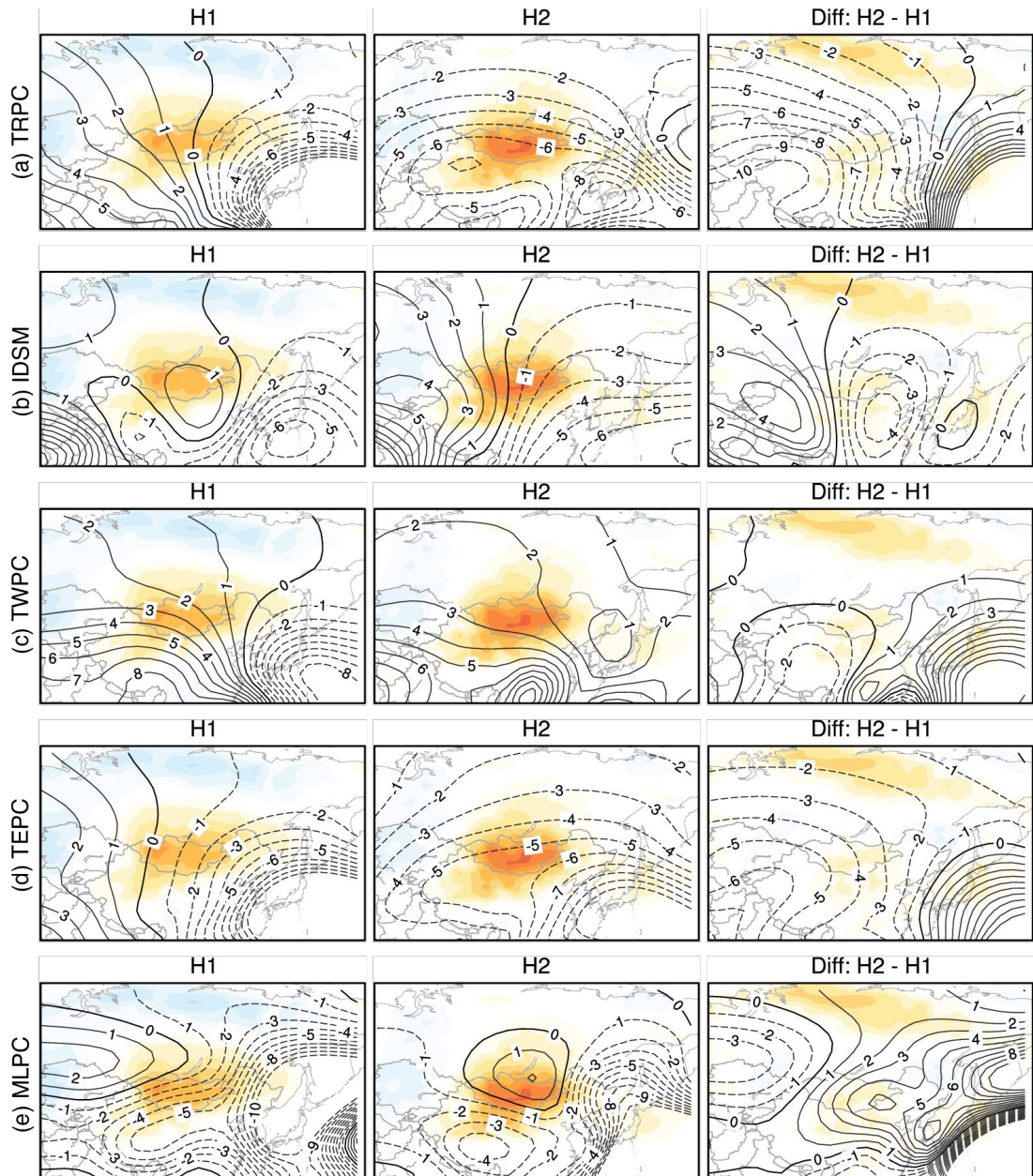


Figure B.13: NSWM responses to regional heating over the Pacific and Indian Ocean. Contour interval is $1.0 \times 10^5 m^2 s^{-1}$

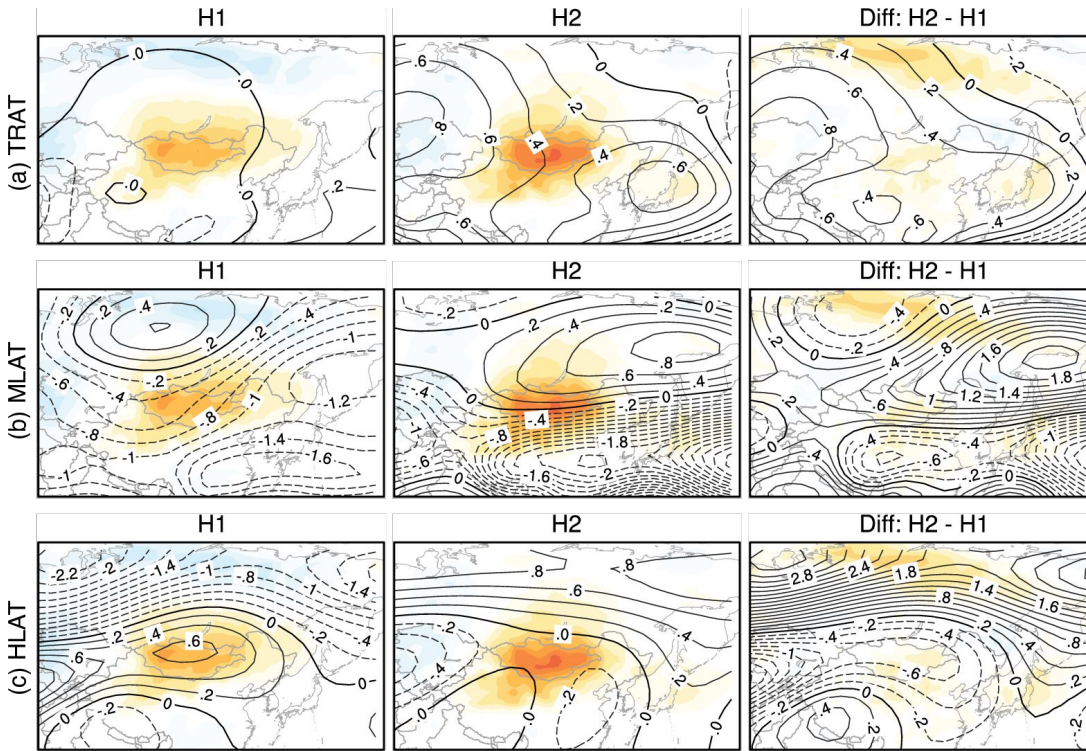


Figure B.14: NSWM responses to regional heating over the Atlantic. Contour interval is $0.2 \times 10^5 m^2 s^{-1}$

temperature anomalies for H1 and H2. As we focus on the differences between the two periods, the linear trends of the time series are not removed before calculating the correlations.

Obvious differences between the two periods can be found in the correlations with the AMO (Figs. B.15e and f), the PDO (Figs. B.15g and h), the DMI (Figs. B.15k and l), SASMI (Figs. B.15m and n), and EASMI (Figs. B.15o and p). The impacts of ENSO, NAO, and AO presents no clear change between the two periods. Results are consistent with Kosaka et al. (2012) to some degree. They pointed out that there are insignificant correlations between the Silk Road pattern and ENSO in both observational and model analysis.

Generally, our results imply that the temperature anomalies over inner East Asia tend to be linked to a certain SST pattern on decadal time scales and are modulated by the Asian summer monsoon and SST variabilities over the Indian Ocean on the inter-annual time scale. The prevailing negative correlation between DMI and temperature anomalies for H1 is changed to an overall significant positive correlation during H2. Similarly, the impacts of EASMI present a broadly significant positive correlation with temperature anomalies for H2 over inner East Asia as well. In contrast, the generally significant relationship between SASMI and temperature anomalies disappear from H1 to H2. Results are consistent with Ding and Wang (2005) and Wang et al. (2017a) that the Asian and Indian summer monsoon could affect the global teleconnection patterns by altering the atmospheric circulations. Hence,

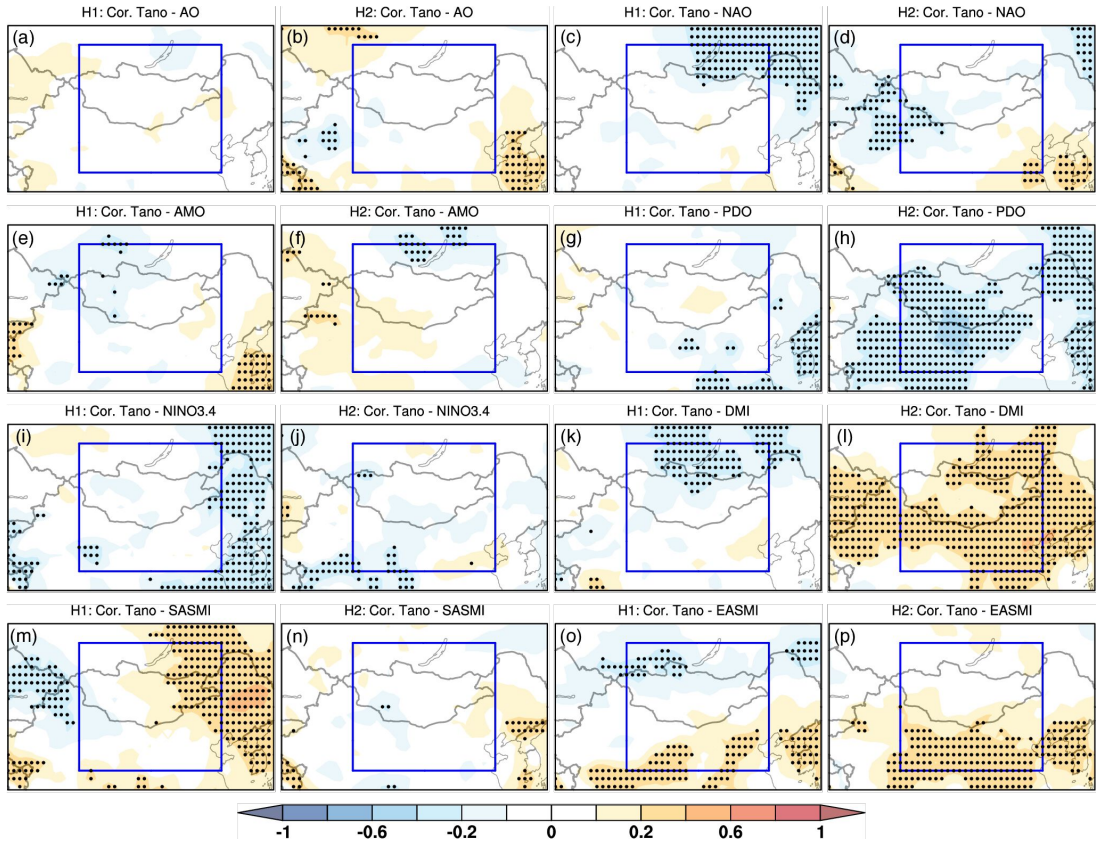


Figure B.15: Correlations between monthly climate indices and monthly temperature anomalies during summer (JJA) for H1 and H2 period. Dots denote the significance at the 95% confidence level based on the two-tailed student's t -test.

the correlation results confirm our analysis in section B.7, suggesting that heating anomalies over the North Pacific and tropical Indian regions play important roles in changing the observed stationary waves during heat waves.

B.9 SUMMARY

We have investigated whether the maintenance mechanisms of stationary waves have changed of inner East Asia heat waves in recent years, and examined which forcing mechanisms might have contributed to these changes. Based on the JRA-55 reanalysis dataset, we find a significant warming trend over inner East Asia from 1958 to 2019. A breakdown of the period into 1958–1988 (H1) and 1989–2019 (H2) shows that H2 is a significant warmer period with an intensified anticyclonic system over inner East Asia. This anticyclonic system is causing more frequent and longer-lasting heat waves over the last few decades. We then identify heat waves for H1 and H2, and composite large-scale circulation anomalies for each period during heat waves. The differences in the spatial patterns of the observed stationary waves for

H₁ and H₂ present a wavelike pattern, which resembles a strengthening Silk Road pattern over Eurasia (Ding and Wang, 2005). This Silk Road pattern has been shown to contribute frequent and longer-lasting heat waves over inner East Asia in Wang et al. (2017a) and Ding and Wang (2005).

We use the NSWMM to reproduce the observed anticyclonic system. When forced by orography, diabatic heating, and transients, the main features of the observed anticyclonic system over inner East Asia can be reproduced at 200 hPa, although with some discrepancies. The reproducibility of NSWMM is better for H₁ than that for H₂. This is likely due to the lack of land-atmospheric coupling process in NSWMM. In agreement with Zhang et al. (2020), they demonstrated that the stronger coupling of heat wave and drought exists after the 1990s, with significant drying in soil moisture over inner East Asia.

By using the factor separation method, we then investigate the maintenance mechanisms of the stationary waves during heat waves over inner East Asia and explore their changes under a warmer climate by comparing those mechanisms between H₁ and H₂. For both periods, transients are a dominant factor in reproducing the observed stationary waves, especially the high-frequency transient vorticity fluxes. The nonlinear interaction between different forcing terms is also important to the maintenance of the observed anomalous stationary waves for both periods. Further, our results suggest that the maintenance mechanisms have changed in a warmer climate, and these changes are mainly through the nonlinear interactions between different forcing terms. In particular, the nonlinear effects of diabatic heating become more dominant through its interaction with orography and transients (mainly the high-frequency vorticity momentum fluxes). Consistent with (Teng and Branstator, 2019), our results imply that the recent enhanced diabatic heating plays an important role in maintaining the anomalous stationary waves in a warmer climate.

Diabatic cooling due to radiative cooling dominates over inner East Asia, indicating the persistence of the anti-cyclonic system with strong descending motions, in line with Zschenderlein et al. (2019) and Ma and Franzke (2021). Further NSWMM simulations show that heating anomalies over the Indian Ocean and the Pacific are more important than the Atlantic in maintaining stationary waves during heat waves over inner East Asia. Under a warmer climate, the changes of the maintaining mechanisms between H₁ and H₂ are generally forced by the heating anomalies mainly over mid-latitude North Pacific and the tropical Indian Ocean as well. Furthermore, correlations between summer temperature anomalies and modes of climate variability for H₁ and H₂ confirm those key regions. Our results suggest the SST decadal oscillation over the Pacific, the East Asian summer monsoon, and the tropical Indian Ocean are strengthening their role in rising surface temperatures over inner East Asia. These results provide valuable insights into the improvement of climate models on heat wave forecasting.

Some previous studies have shown the changes in the large-scale circulations and their linkage with extremes under a warmer climate (Horton et al., 2015; Lee et al., 2017). Our study attempts to provide a feasible way to indicate that the warming climate has changed the maintenance mechanisms of large-scale circulation patterns, during heat waves at least. However, the impacts of enhanced land-atmosphere coupling and anthropogenic forcing are missing processes in the NSWCM (Held et al., 2002; Ma et al., 2021), which may affect our diagnostic results. The role of the missing processes in altering large-scale circulations and their maintaining mechanisms will be explored in the future by combining further observational data and fully climate models. Overall, our findings provide insights into improving climate models and building statistical methods in heat wave forecasting, to cope with the rising risk of livestock and range-land crisis under a hotter and drier climate (Zhang et al., 2020).

C

THE LORENZ ENERGY CYCLE: TRENDS AND THE IMPACT OF MODES OF CLIMATE VARIABILITY

Appendix C comprises a paper, which has been published in the journal of *Tellus A: Dynamic Meteorology and Oceanography* as:

Ma, Q., Lembo, V. & Franzke, C.L.E. (2021), "The Lorenz energy cycle: trends and the impact of modes of climate variability", *Tellus A: Dynamic Meteorology and Oceanography* 73:1, 1-15. doi: <https://doi.org/10.1080/16000870.2021.1900033> (last accessed on 30th of May 2021).

My and other's contributions to this paper are as follows:

I performed the calculations and the analysis, plotted figures, conceived the work, and wrote the manuscript. V.L. and C.F. contributed to conceive the work, review, and write the manuscript.

The Lorenz Energy Cycle: Trends and the Impact of Modes of Climate Variability

Qiyun Ma^{1,2}, Valerio Lembo³ and Christian L. E. Franzke^{4,5,6}

¹School of Integrated Climate System Science, University of Hamburg, Hamburg, Germany

²Meteorological Institute, University of Hamburg, Hamburg, Germany

³Institute of Atmospheric Sciences and Climate, National Research Council, Bologna, Italy

⁴School of Engineering and Science, Jacobs University, Bremen, Germany

⁵Institute of Oceanography, University of Hamburg, Hamburg, Germany

⁶Center for Climate Physics, Institute for Basic Science and Pusan National University, Busan, South Korea

ABSTRACT The atmospheric circulation is driven by heat transport from the tropics to the polar regions, embedding energy conversions between available potential and kinetic energy through various mechanisms. The processes of energy transformations related to the dynamics of the atmosphere can be quantitatively investigated through the Lorenz energy cycle formalism. Here we examine these variations and the impacts of modes of climate variability on the Lorenz energy cycle by using reanalysis data from the Japanese Meteorological Agency (JRA-55). We show that the atmospheric circulation is overall becoming more energetic and efficient. For instance, we find a statistically significant trend in the eddy available potential energy, especially in the transient eddy available potential energy in the Southern Hemisphere. We find significant trends in the conversion rates between zonal available potential and kinetic energy, consistent with an expansion of the Hadley cell, and in the conversion rates between eddy available potential and kinetic energy, suggesting an increase in mid-latitude baroclinic instability. We also show that planetary-scale waves dominate the stationary eddy energy, while synoptic-scale waves dominate the transient eddy energy with a significant increasing trend. Our results suggest that interannual variability of the Lorenz energy cycle is determined by modes of climate variability. We find that significant global and hemispheric energy fluctuations are caused by the El Niño-Southern Oscillation, the Arctic Oscillation, the Southern Annular Mode, and the meridional temperature gradient over the Southern Hemisphere.

C.1 INTRODUCTION

The inhomogeneous absorption of energy in the climate system is the primary fuel of atmospheric and oceanic dynamics. Energy is transformed within the system through several forms, following the motion of the atmosphere and the ocean, determining the mean state and variability of the climate system (Clément et al., 2017; Hu et al., 2004). The seminal work by Lorenz (1955) laid down a comprehensive picture of the various processes responsible for the conversion of available potential energy from inhomogeneous diabatic heating into kinetic energy and eventually (frictional) dissipation. This is commonly referred to as the "Lorenz energy cycle", describing the conversion of energies through different forms and treating the system as a thermodynamic cycle or, in our context, as a heat engine.

The atmospheric process of the Lorenz energy cycle can be described as follows: The zonal available potential energy is determined by the net heating of the atmosphere in low latitudes and the net cooling in high latitudes (Ulbrich and Speth, 1991). Then the energy cycle involved in the atmospheric general circulation experiences two main processes: baroclinic growth and barotropic decay (Lembo et al., 2019b; Ulbrich and Speth, 1991). The process of baroclinic growth occurs mainly due to the growth of mid-latitude baroclinic eddies at the synoptic scale, including the transformation of the zonal available potential energy into eddy available potential energy through horizontal and vertical transport of sensible heat, and the transformation of eddy available potential energy into eddy kinetic energy by rising warm air and sinking cold air. The energies undergo a process of barotropic decay, when a large part of eddy kinetic energy is dissipated by frictional heating and the remainder is converted back into zonal kinetic energy through horizontal and vertical transport of angular momentum by the eddies. This barotropic decay process ensures the maintenance of the extratropical jet streams and storm tracks (Lembo et al., 2019b; Li et al., 2007; Ulbrich and Speth, 1991), however, it is not the leading-order process for the subtropical jet which is mainly due to angular momentum conservation. Finally, the zonal mean meridional overturning circulation leads to the zonal available potential energy converted into zonal kinetic energy, which involves the combined actions of the Hadley and Ferrel cells (Hernández-Deckers and Storch, 2010; Kim and Kim, 2013).

The Lorenz energy cycle has been widely used to investigate atmospheric dynamics and the general circulation of the atmosphere by considering the physical processes involved in the energy transformation (Peixoto and Oort, 1974; Ulbrich and Speth, 1991, and references therein). By systematically identifying the path through which the atmosphere contributes to achieving a statistically non-equilibrium steady state of the climate system (Ambaum, 2010; Lucarini et al., 2011), the Lorenz energy cycle allows to conveniently describe the climate in the framework of macroscopic non-linear thermodynamics (Prigogine, 1962). In other words, once concepts borrowed from

classical thermodynamics, such as efficiency, irreversibility, mechanical work are adapted to the context of the Lorenz energy cycle, a set of metrics is readily available for systematically addressing the maintenance of the mean state and of the variability of the climate system (Lembo et al., 2019b).

The atmospheric Lorenz energy cycle has been evaluated in reanalysis datasets (Kim and Kim, 2013; Li et al., 2007; Pan et al., 2017), and has been used to assess climate model performance (Hernández-Deckers and Storch, 2010; Lembo et al., 2019b, 2011; Marques et al., 2009). Previous studies mainly focused on the mean state and the seasonal cycle of the Lorenz energy cycle. For instance, Hu et al. (2004) examined the Northern Hemisphere atmospheric energetics based on the Lorenz energy cycle framework, using reanalysis data. Marques et al. (2010) focused on the comparison of different reanalysis datasets in computing the Lorenz energy cycle from 1979-2001 while they did not analyze its trends. Pan et al. (2017) first explored the linear trends of various Lorenz energy cycle's components during the period 1979-2013 and compared two reanalysis datasets (ERA-Interim and NCEP-R2). However, trends and the variability of the Lorenz energy cycle as a whole have not been studied widely. A systematic characterization of these changes provides insight into the impact of anthropogenic global warming, not only in terms of how it affects the efficiency of energy conversions within the atmosphere, but also corresponding long-term trends of the atmospheric general circulation (Kim and Kim, 2013; Lembo et al., 2019b).

Here, we systematically examine the variability and trends in the Lorenz energy cycle components over the period 1979-2019. We believe that, for the first time, an extensive focus on long-term variations in Lorenz energy cycle components is provided here. The fluctuations of eddy activities have a major impact on synoptic-scale weather systems, e.g. cyclone and anticyclone systems in mid-latitudes (Pan et al., 2017). Therefore, we will investigate the variations of the Lorenz energy cycle by breaking down the contributions from the eddies into their stationary and transient components. Waves at different scales might contribute differently to the weather and climate variability by transferring heat and momentum fluxes (Chemke and Ming, 2020; Lembo et al., 2019a). We will thus separately examine the Lorenz energy cycle components for different zonal wavenumber regimes as well. We will then relate variations of the Lorenz energy cycle components to key modes of climate variability, investigating the physical processes lying behind such variability from the point of view of climate variability.

In section C.2 we describe the data and the Lorenz energy cycle methodology, in section C.3 we present our results with a focus on trends in global energies, energetics of stationary, transient eddies and wavenumber regimes and also the impact of modes of climate variability on energetics. In section C.4 we provide our conclusions.

C.2 DATA AND METHODOLOGY

We use reanalysis data provided by the Japan Meteorological Agency (JRA-55) (Kobayashi et al., 2015) to compute the Lorenz energy cycle during the period 1958-2019. The JRA-55 provides 6-hourly data for 37 pressure levels with a 1.25 degree horizontal resolution. The variables used in computing the Lorenz energy cycle include 3-dimensional fields of daily air temperature, zonal, meridional and vertical winds on pressure levels, and also 2-dimensional daily air temperature, zonal and meridional winds at 2 meters.

We employ the Thermodynamic Diagnostic Tool (TheDiaTo; Lembo et al. (2019b)) for diagnosing the variations of the Lorenz energy cycle (https://github.com/ValerioLembo/TheDiaTo_v1.0.git). The Lorenz energy cycle computations in TheDiaTo allow to systematically investigate the energy exchanges embedded in the general circulation of the atmosphere across different spatial scales of motion. This tool is ideal for our purpose to analyze the trends of various components in the Lorenz energy cycle. TheDiaTo subsets and calculates the integrated Lorenz energy cycle in the troposphere between the vertical levels of 900 and 100 hPa. Details of the equations that have been used can be found in Lembo et al. (2019b).

We calculate the following terms in the Lorenz energy cycle: zonal available potential energy P_M , eddy available potential energy P_E , zonal kinetic energy K_M , and eddy kinetic energy K_E . Then, we compute the conversion rates: between zonal and eddy available potential energies $C(P_M, P_E)$, between eddy available potential energy and kinetic energy $C(P_E, K_E)$, between eddy and mean kinetic energies $C(K_E, K_M)$, and between mean available potential energy and kinetic energy $C(P_M, K_M)$, the generation rate of zonal and eddy available potential energies $G(P_M)$ and $G(P_E)$ respectively, and the dissipation rate of zonal and eddy kinetic energies $D(K_M)$ and $D(K_E)$ respectively. Moreover, following Ulbrich and Speth (1991), we decompose the eddy energies in the Lorenz energy cycle into a stationary (subscript SE) and a transient (subscript TE) component. The stationary component is defined as the deviation from the zonal mean, while the transient component is defined as the deviation from the climatological time mean. In doing so, P_E is divided into stationary and transient eddy available potential energies P_{SE} and P_{TE} , and K_E is divided into stationary and transient eddy kinetic energy energies K_{SE} and K_{TE} , respectively. Similarly, we calculate the conversion rates $C(P_M, P_{SE})$, $C(P_M, P_{TE})$, $C(P_{TE}, K_{TE})$, $C(P_{SE}, K_{SE})$, $C(K_{TE}, K_M)$, $C(K_{SE}, K_M)$, two nonlinear conversion rates $C(P_{SE}, P_{TE})$ and $C(K_{TE}, K_{SE})$, the generation rates $G(P_{SE})$ and $G(P_{TE})$, and dissipation rates $D(K_{SE})$ and $D(K_{TE})$.

Then we decompose stationary and transient eddy energies into different zonal wave number groups: planetary-scale waves (PW, zonal wave-number 1-3), synoptic-scale waves (SW, wave-number 4-9), and meso-scale waves (MW, wave-number 10-21). This will help us to understand the contributions to the Lorenz energy cycle of different wave number groups representing different

weather regimes, from the planetary circulation to regional storms (e.g. Hu et al., 2004; Lembo et al., 2019a; Ruggieri et al., 2020). In this paper, we focus only on the decomposition of eddy available potential and eddy kinetic energies on global and hemispheric scales and do not consider the contribution of single wave numbers.

We use the non-parametric Mann-Kendall test to examine the trends for different components of the Lorenz energy cycle and Sen’s slope to estimate the magnitude of the trends (Franzke and Sentelles, 2020; Gocic and Trajkovic, 2013; Mann, 1945; Sen, 1968). The Mann-Kendall test and Sen’s slope are performed using the software MAKESENS (Salmi, 2002).

Three types of climate indices representing modes of climate variability are used in this study: atmospheric indices, oceanic indices, and temperature indices. The atmospheric indices include teleconnection patterns (Feldstein and Franzke, 2017; Hannachi et al., 2017) such as the Arctic Oscillation (AO), the North Atlantic Oscillation (NAO), the Pacific North American (PNA) pattern, the Southern Annular Mode (SAM), and the Quasi-biennial Oscillation (QBO) index. The oceanic indices consist of the El Niño-Southern Oscillation index (NINO_{3.4}), the Pacific Decadal Oscillation (PDO), and the Atlantic Multi-decadal Oscillation (AMO) index. Temperature indices are the monthly HadCRUT4 global mean surface temperature (GMST) anomaly and the weighted vertically average (900-100 hPa) meridional temperature difference from JRA-55 (ΔT) at hemispheric-scale. These monthly indices can be downloaded from the website <https://climexp.knmi.nl/>, except for ΔT . We define the ΔT by calculating the differences between the weighted vertical averaged temperature over the mid-latitudes (30° - 60° N/S) and the polar areas (60° - 90° N/S). Thus, ΔT_{NH} and ΔT_{SH} depict meridional temperature gradients in the troposphere over the Northern and Southern Hemispheres.

C.3 RESULTS

C.3.1 *How reliable is the pre-satellite period for atmospheric energetics?*

First we examine the climatological mean state of each component of the Lorenz energy cycle for the whole period (1958-2019) and the satellite period (1979-2019). From the viewpoint of the climatological mean state, no appreciable difference is found between the two time periods (not shown). However, there is a sudden jump before and after 1979 in the annual mean eddy available potential energy and eddy kinetic energy as shown in Fig. C.1. We also find similar sudden jumps in the zonal mean available potential and kinetic energy reservoirs, while the differences of the zonal mean before and after 1979 are slightly smaller than those of the eddy energies. These sudden jumps were also reported by Marques et al. (2009) for other reanalysis datasets as a result of the introduction of satellite data in 1979. A non-parametric test – the Mann-Whitney U test (Nachar, 2008) – is used for examining the statistical

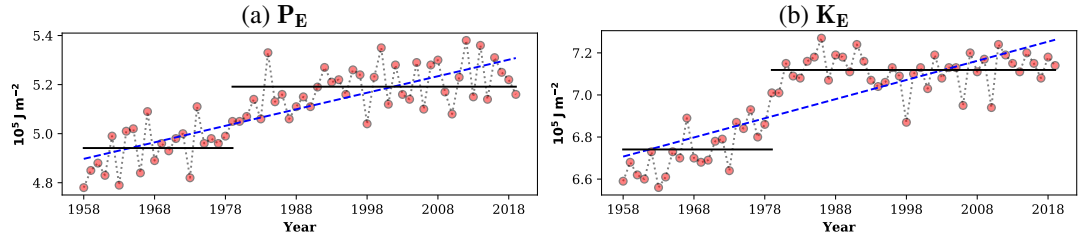


Figure C.1: Variations of eddy available potential energy (P_E) and eddy kinetic energy (K_E) for JRA-55 data. Solid black lines are averages over 1958–1979 and 1979–2019, respectively. Unit is 10^5 J m^{-2} .

difference between the two time periods. This test compares whether the distributions of the two samples of continuous observations belong to the same statistical population by determining if the medians are different or not (Ye and Ahammed, 2020). Results reveal that the differences are statistically significant at the 1% confidence level (2-tailed) among the zonal mean and eddy energies in the two time periods, except for P_M . This significant difference is also confirmed by using a two-sample t-test (Ye and Ahammed, 2020). Thus, we focus in the following on the Lorenz energy cycle during the satellite period 1979–2019.

c.3.2 Climatology of the Lorenz energy cycle

The climatological values of the global integrals of energies in the JRA-55 dataset are shown in Fig. C.2. The order of magnitude of the sum of the stationary P_{SE} and transient P_{TE} available potential energies is the same as the sum of the stationary K_{SE} and transient K_{TE} kinetic energies. The comparable order of magnitude between P_E and K_E is consistent with Li et al. (2007) and Lembo et al. (2019b). This is likely due to baroclinic instability which transforms available potential into kinetic energy instantaneously, mainly in mid-latitude weather systems, and which is driven by the meridional temperature gradient (Holton and Hakim, 2012a). By trying to reduce this meridional temperature gradient, the atmosphere acts by reducing the available potential energy.

The time-mean values for all the energy components are comparable with other reanalysis datasets (Li et al., 2007; Marques et al., 2010; Pan et al., 2017), although the time-mean values of zonal mean energy components in our study are generally larger than those calculated from other reanalysis datasets. The discrepancies could be due to different vertical levels and time periods used for the integration of the energies. We also find that the time-mean values of the zonal mean energy components in our study are generally lower than the results from the climate models (Boer and Lambert, 2008; Lembo et al., 2019b). However, our results are in agreement with Marques et al. (2009).

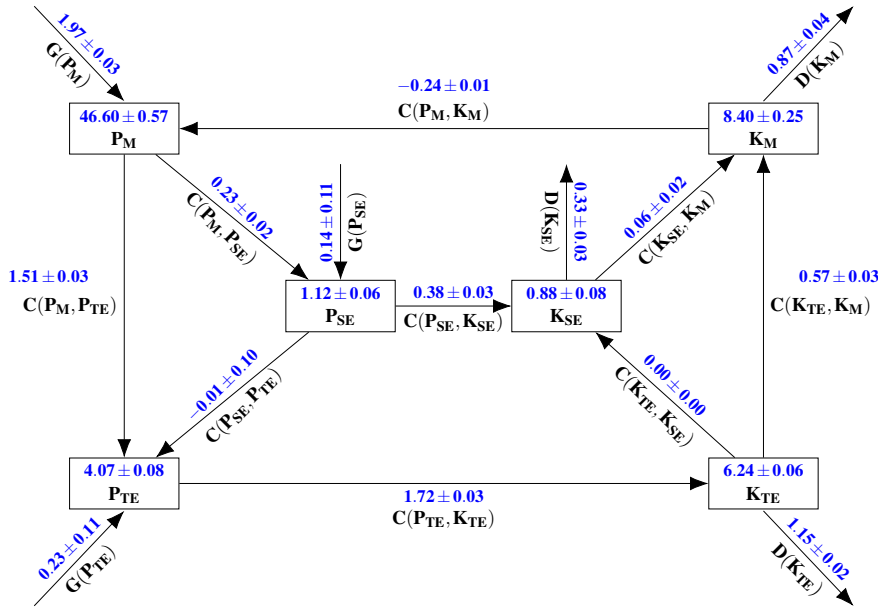


Figure C.2: The Lorenz energy cycle diagram from JRA-55 reanalysis dataset during 1979-2019. The uncertain range of the time-mean values stand for the standard deviations of the time series of the energy components. Units are $10^5 Jm^{-2}$ for energy and Wm^{-2} for the conversion rate, generation, and dissipation terms. The arrows indicate the direction that corresponds to positive values. Negative values imply the opposite direction.

C.3.3 Trends in global energies

Figure C.3 displays the time series of the globally averaged mechanical energies P_M , P_E , K_M , and K_E between 1979 and 2019. All mechanical energies display an increasing linear trend, suggesting a general intensification of the global Lorenz energy cycle. We examine the significance of these linear trends with the Mann-Kendall test (Tab. C.1). Among these energies, only P_E displays a significant upward trend of $390.48 Jm^{-2}$ per year.

The globally averaged conversion rates among the different mechanical energies are all increasing with time (Tab. C.1). The linear trend is significant for $C(P_E, K_E)$ and $C(P_M, K_M)$ with a rate of 1.18 and $0.32 \cdot 10^{-3} Wm^{-2}$ per year, respectively. The increasing trend of $C(P_E, K_E)$ (Fig. C.4) denotes a stronger mid-latitude baroclinic instability induced by the sinking of colder air and rising warmer air (Kim and Kim, 2013). The significant positive correlation between $C(P_E, K_E)$ and temperature differences between the mid-latitudes and the polar regions for both hemispheres (see Sec. C.3.7) suggests an increase in mid-latitude baroclinic instability. The trend of the $C(P_M, K_M)$ conversion rate links with the net effect of a number of processes occurring in the tropics and mid-latitudes, related to the activity of the Hadley ($C(P_M, K_M) > 0$) and Ferrel cells ($C(P_M, K_M) < 0$) (Li et al., 2007; Pan et al., 2017). As a significant trend exists, our results are consistent with an expansion of the Hadley cell

over the past few decades (Davis and Davis, 2018; Huang and McElroy, 2014; Kang and Lu, 2012; Seidel et al., 2008).

The variations of $C(P_M, P_E)$ are associated with baroclinic disturbances, related to the meridional temperature gradient and Arctic amplification (Li et al., 2007; Peixóto and Oort, 1974). The temporal variations of large-scale weather systems in the mid-latitudes can also contribute to the trend of $C(P_M, P_E)$ (Pan et al., 2017). As, unlike in previous work (Pan et al., 2017), there is no clear trend for $C(P_M, P_E)$, we argue that these effects are somehow compensating. This result is consistent with Dai and Song (2020), who show that Arctic amplification in recent decades has little influence on northern mid-latitude weather. $C(K_E, K_M)$ is related to temporal variations of the jet streams in the troposphere (Kim and Kim, 2013). The slightly increasing trend of $C(K_E, K_M)$ thus suggests an increased poleward displacement of the jet streams as a result of the transport of momentum by the motion of eddies.

Trends of the globally averaged generation and dissipation rates are examined and displayed in Tab. C.1. All the generation and dissipation rates for the zonal mean mechanical energies ($G(P_M)$ and $D(K_M)$) are increasing with time. In particular, the positive linear trends in the dissipation rate of $D(K_M)$ are statistically significant at the 95% level (Fig. C.5), which is mainly due to the increasing conversion rates related to transferring energies into K_M . Overall, the upward trend of the total dissipation rate of kinetic energies suggests an increasing efficiency of the global atmospheric thermal engine (Tab. C.1), in agreement with (Pan et al., 2017).

c.3.4 *Decomposition of global generation, dissipation, and conversion rates*

Stationary and transient eddies both play important roles in the global energy cycle of the atmosphere (Lembo et al., 2019b; Ulbrich and Speth, 1991). Here, we decompose the eddy energies into stationary and transient components. Fig. C.2 shows that the magnitude of mechanical energy of transient eddies (P_{TE} and K_{TE}) is larger than that of stationary eddies (P_{SE} and K_{SE}); however, they have the same order of magnitude.

We first investigate the partition of the globally averaged generation rates. Although the fluctuation exists (Figs. C.6a and C.6b), there are no statistically significant trends in $G(P_{SE})$ and $G(P_{TE})$. As for the decomposed globally averaged dissipation rates (Figs. C.6c and C.6d), there is a significant negative linear trend in the time series of $D(K_{SE})$, but no significant trend in $D(K_{TE})$.

For the decomposed conversion rates of zonal and eddy available potential energies, as shown in Tab. C.2, no significant trends are found for the conversion rates of $C(P_M, P_{SE})$ and $C(P_M, P_{TE})$, as well as $C(P_{SE}, P_{TE})$. However, in terms of the conversion rates between zonal and eddy kinetic energies, there is a significant upward linear trend in $C(K_{TE}, K_M)$, while $C(K_{SE}, K_M)$ and $C(K_{TE}, K_{SE})$ have no long-term trends (Tab. C.2). The significant increasing trend of $C(K_{TE}, K_M)$ has a slope of $0.94 \times 10^{-3} \text{Wm}^{-2}$ per year (Fig.

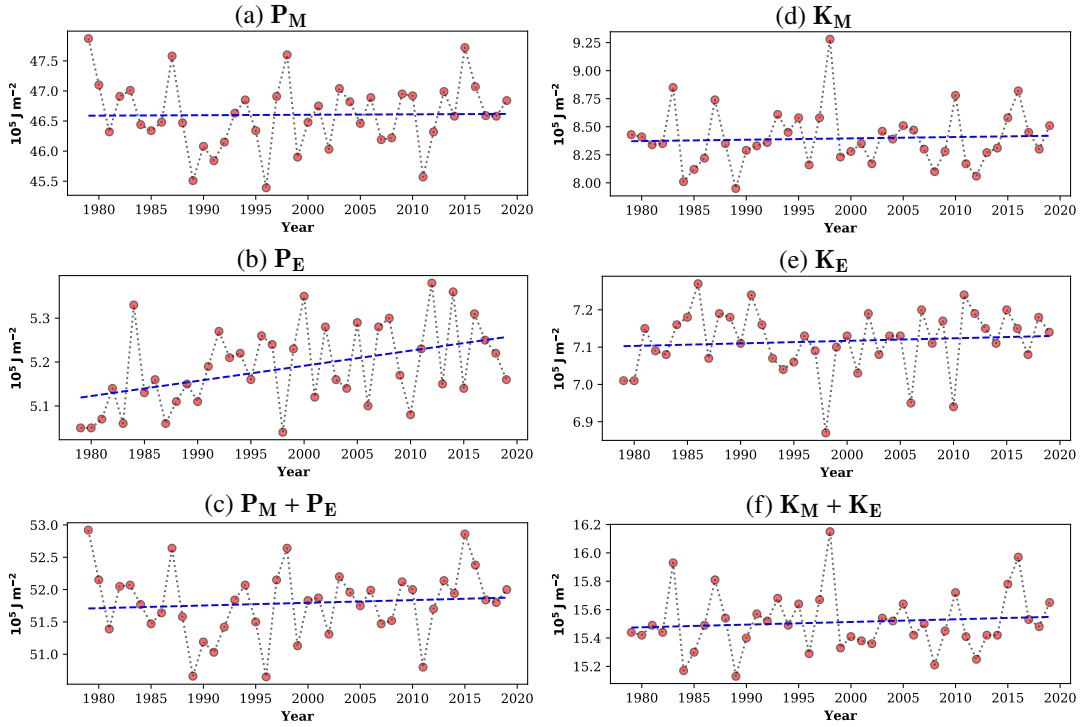


Figure C.3: Time series of the globally averaged atmospheric energies. (a) The mean available potential energy P_M . (b) The eddy available potential energy P_E . (c) The total available potential energy $P_M + P_E$. (d) The mean kinetic energy K_M . (e) The eddy kinetic energy K_E . (f) The total kinetic energy $K_M + K_E$.

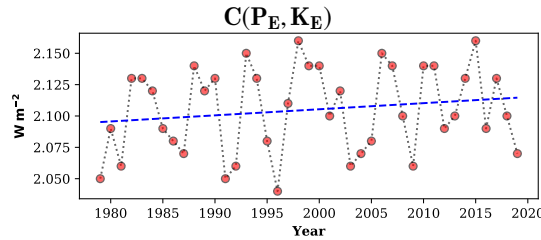


Figure C.4: Time series of the conversion rate between the eddy available potential energy and the eddy kinetic energy $C(P_E, K_E)$.

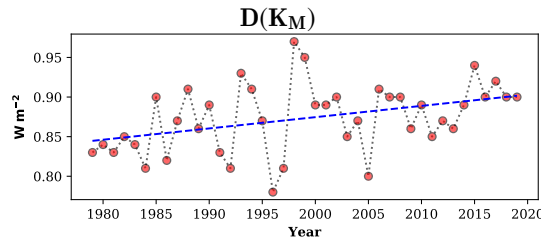


Figure C.5: The dissipation rate of the mean kinetic energy $D(K_M)$.

Table C.1: Trends in the global energies.

	Global		
	Trend	Sig.	Unit
P_M	344.09		Jm^{-2} per year
P_E	390.48	**	Jm^{-2} per year
$P_M + P_E$	543.75		Jm^{-2} per year
K_M	188.06		Jm^{-2} per year
K_E	121.06		Jm^{-2} per year
$K_M + K_E$	214.42		Jm^{-2} per year
$C(P_M, P_E)$	0.00		$10^{-3}Wm^{-2}$ per year
$C(P_E, K_E)$	1.08	*	$10^{-3}Wm^{-2}$ per year
$C(K_E, K_M)$	0.38		$10^{-3}Wm^{-2}$ per year
$C(P_M, K_M)$	-0.32	*	$10^{-3}Wm^{-2}$ per year
$G(P_M)$	0.53		$10^{-3}Wm^{-2}$ per year
$G(P_E)$	0.00		$10^{-3}Wm^{-2}$ per year
$D(K_M)$	1.45	*	$10^{-3}Wm^{-2}$ per year
$D(K_E)$	-0.44		$10^{-3}Wm^{-2}$ per year

+ at at 90% level.

* at 95% level.

** at 99% level.

*** at 99.9% level.

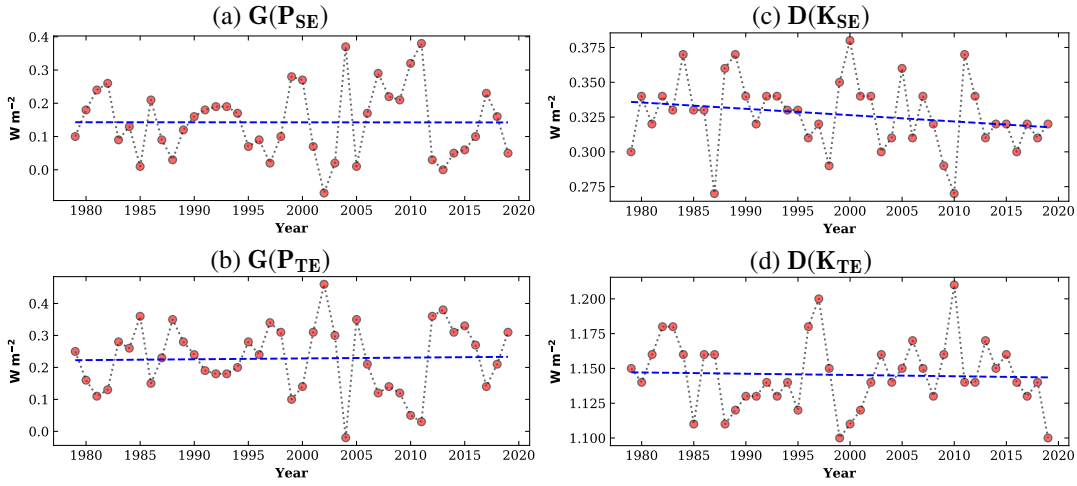


Figure C.6: Decomposed globally averaged generation and dissipation rates. **(a)** The generation rate of the stationary eddy available potential energy $G(P_{SE})$; **(b)** The generation rate of the transient eddy available potential energy $G(P_{TE})$; **(c)** The dissipation rate of the stationary eddy kinetic energy $D(K_{SE})$. **(d)** The dissipation rate of the transient eddy kinetic energy $D(K_{TE})$.

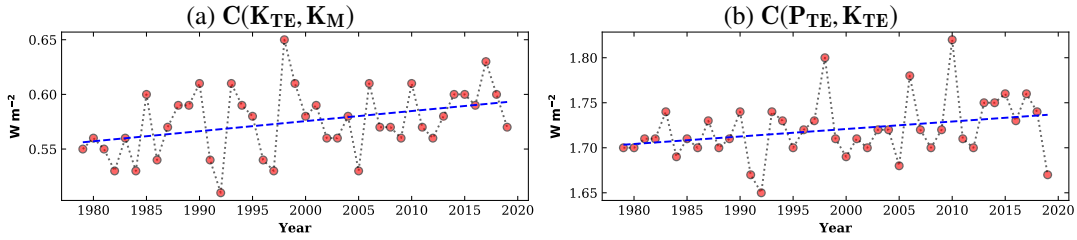


Figure C.7: Decomposed globally averaged conversion rates. **(a)** The conversion rate between the transient eddy kinetic energy and mean kinetic energy $C(K_{TE}, K_M)$; **(b)** The conversion rate between the transient eddy kinetic energy and transient eddy kinetic energy $C(P_{TE}, K_{TE})$.

C.7a). The trends of $C(K_{TE}, K_M)$ are likely linked to the increasing trend of $C(K_E, K_M)$ in Tab. C.1. This indicates the strengthening of horizontal transport of momentum and energy from eddies to the zonal mean flow (K_M).

In addition to that, as denoted in Tab. C.1, the conversion rate of $C(P_E, K_E)$ presents a significantly increasing trend. Here, we mainly attribute this increasing trend to the significant trend of $C(P_{TE}, K_{TE})$ (Fig. C.7b and Tab. C.2), as $C(P_{SE}, K_{SE})$ displays insignificantly negative trend. Our results suggest that baroclinic instability is becoming stronger, leading to more unstable weather systems mainly in the mid-latitudes through transient eddies.

Table C.2: Decomposition of global energies into eddies.

	Global		
	Trend	Sig.	Unit
$G(P_{SE})$	-0.32		$10^{-3} \mathbf{Wm}^{-2}$ per year
$G(P_{TE})$	0.48		$10^{-3} \mathbf{Wm}^{-2}$ per year
$D(K_{SE})$	-0.45		$10^{-3} \mathbf{Wm}^{-2}$ per year
$D(K_{TE})$	0.00		$10^{-3} \mathbf{Wm}^{-2}$ per year
$C(P_M, P_{SE})$	0.00		$10^{-3} \mathbf{Wm}^{-2}$ per year
$C(P_M, P_{TE})$	0.00		$10^{-3} \mathbf{Wm}^{-2}$ per year
$C(P_{SE}, P_{TE})$	0.00		$10^{-3} \mathbf{Wm}^{-2}$ per year
$C(K_{TE}, K_M)$	0.94	*	$10^{-3} \mathbf{Wm}^{-2}$ per year
$C(K_{SE}, K_M)$	0.00		$10^{-3} \mathbf{Wm}^{-2}$ per year
$C(K_{TE}, K_{SE})$	0.00		$10^{-3} \mathbf{Wm}^{-2}$ per year
$C(P_{TE}, K_{TE})$	0.73	+	$10^{-3} \mathbf{Wm}^{-2}$ per year
$C(P_{SE}, K_{SE})$	-0.35		$10^{-3} \mathbf{Wm}^{-2}$ per year

c.3.5 Hemispheric differences in eddy potential and kinetic energies

We consider the averaged eddy available potential and kinetic energies separately in the Northern and Southern hemispheres (Fig. C.8). As shown in Figs. C.8a and C.8b, all the components of P_E are larger in the Northern Hemisphere than in the Southern Hemisphere. Concerning the trends, components of P_E experience an increasing trend, except for P_{SE} in the Southern Hemisphere (Tab. C.3). Our results suggest that the globally increasing trend of P_E (Tab. C.1) is mainly due to the significantly increasing trend in P_{TE} in the Southern Hemisphere. The conversion of available potential energy from the zonal mean to transients involves the meridional transport of heat (Ulbrich and Speth, 1991). In this respect, our results suggest an increase of the meridional temperature perturbation at the troposphere in the Southern Hemisphere, which is in agreement with Pan et al. (2017). Indeed, we find that the vertically averaged meridional temperature gradient in the troposphere over the Southern Hemisphere ΔT_{SH} has a statistically significant increasing trend (not shown).

As for trends of the components decomposed from the eddy kinetic energy, the results of the linear trends shown in Fig. C.8c and Fig. C.8d are well in agreement with Tab. C.3. An upward trend is found in K_{TE} mainly over the Southern Hemisphere, responsible for the overall increasing trend of K_E (Tab. C.1). K_{SE} has a slightly negative trend at the global scale, however, it has positive trends in both hemispheres. The strong interannual variations

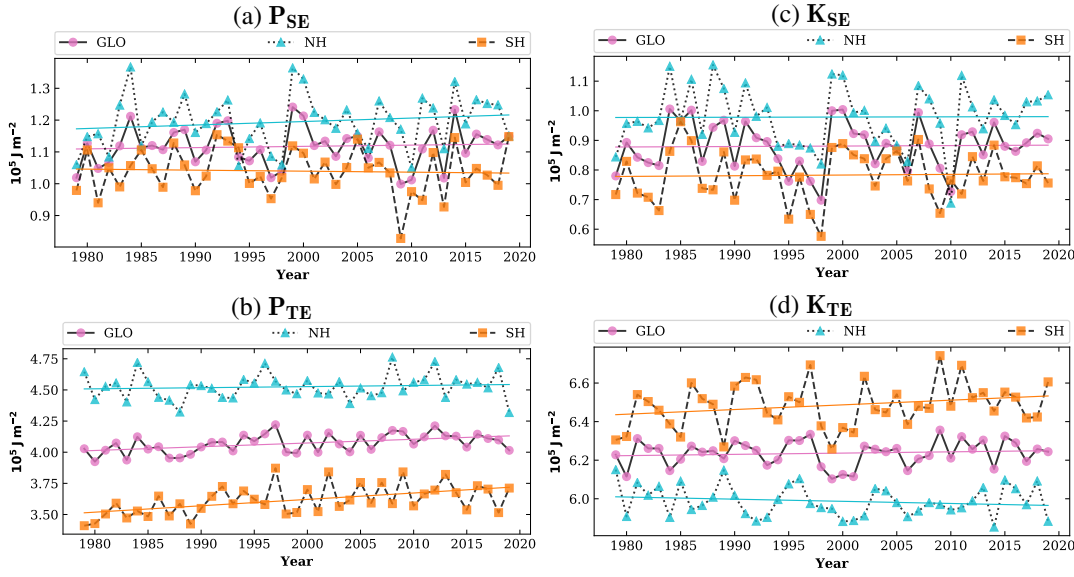


Figure C.8: Decomposed the globally averaged eddy available potential energy and kinetic energy. **(a)** The stationary eddy available potential energy P_{SE} ; **(b)** The transient eddy available potential energy P_{TE} ; **(c)** The stationary eddy kinetic energy K_{TE} ; **(d)** The transient eddy kinetic energy K_{TE} .

Table C.3: Decomposition of potential and kinetic energy (Jm^{-2} per year).

		Global		NH		SH	
		Trend	Sig.	Trend	Sig.	Trend	Sig.
P_E	P_{TE}	315.14	**	132.24		539.17	***
	P_{SE}	61.90		100.00		-20.00	
K_E	K_{TE}	54.77		-106.11		242.58	
	K_{SE}	-1.35		83.33		37.72	

in K_{SE} on the hemispheric scale could explain the slightly negative trend on the global scale, as the global K_{SE} is calculated by averaging the K_{SE} from the two hemispheric scales. These results indicate that the storm tracks altogether may be intensifying along with poleward shifts of the jet streams (Li et al., 2007), especially in the Southern Hemisphere.

c.3.6 Wave number decomposition of the global eddy energies

c.3.6.1 The climatological mean state

As expected, planetary-scale waves dominate P_{SE} on global and hemispheric scales. The sum of the energies in the three wave number groups represents around 83% of P_{SE} over the globe, 74% in the Northern Hemisphere, and 92% in the Southern Hemisphere (Tab. C.4 and Fig. C.2). As for P_{TE} , the

contribution of planetary-scale waves is comparable, though slightly smaller than the one from synoptic-scale waves at the global and the Northern Hemispheric scales, and more than 2 times smaller over the Southern Hemisphere. In general, the energy of meso-scale waves only makes a modest contribution.

Similar to those related to P_E , the energy of planetary-scale waves also dominate K_{SE} on a global and a hemispheric scale, followed by synoptic-scale waves and meso-scale waves. The percentage of the sum of the three wave-number groups of K_{SE} accounts for around 81% of K_{SE} at a global scale. As expected, the synoptic-scale waves generally make the most substantial contributions in K_{TE} , which is 3 - 4 times bigger than planetary-scale waves and meso-scale waves at the global and Southern Hemispheric scales.

Overall, the percentage of the sum of the three wave-number groups for the transient eddy energies is smaller than those for stationary eddy energy, except for the energies over the Northern Hemisphere. This indicates that besides the meso-scale waves, small-scale waves (wave-numbers larger than 21) are also playing an important role in carrying and transforming transient eddy energies, especially over the Northern Hemisphere.

c.3.6.2 Trends of eddy energies

We focus now on the trends of the wave number groups (Fig. C.9 and Tab. C.5). For P_{SE} , the energies embedded in planetary-scale waves show a negative trend in the Southern Hemisphere (Fig. C.9a), and the negative trend exists in the energies associated with the synoptic-scale waves in the Northern Hemisphere as well. These decreased trends lead to a negative trend of P_{SE} for the sum of energies of those three wave-number groups (Tab. C.5). In contrast, an insignificant positive trend of P_{SE} is identified (Tab. C.3). This contradictory result can be inferred from the contributions from small-scale waves in P_{SE} .

In terms of P_{TE} , the energy carried by synoptic-scale waves exhibits a clear positive trend (Fig. C.9b and Tab. C.5). These positive trends are all significant at the 95% level, especially for the Southern Hemispheric and global scales with the significance level at 99.9%. The energies of meso-scale waves exhibit a significant increasing trend as well, except in the Northern Hemisphere. These significant positive trends suggest an increase in baroclinic disturbances in the mid- and high-latitudes over both hemispheres, in agreement with Hu et al. (2004). Furthermore, the increasing trends in the energies of the three wave number groups explain the positive trend of P_{TE} (Tab. C.5).

Although all the components related to K_E present insignificant trends in Tab. C.3, the decomposition of those components into different wave-number groups provide valuable information. The negative trend of K_{SE} can likely be attributed to the global decline in the energies within all three wave-number groups (Tab. C.5), especially the significant negative trend of energies with meso-scale waves. Although energies within planetary-scale waves are

Table C.4: The climatological eddy available potential and kinetic energy on different wave-number domain during 1979-2019 (Jm^{-2} per year).

	Group	GLO	NH	SH		Group	GLO	NH	SH
P_{SE}	PW	0.66	0.63	0.69	K_{SE}	PW	0.47	0.46	0.49
	SW	0.25	0.24	0.25		SW	0.23	0.28	0.18
	MW	0.02	0.02	0.02		MW	0.02	0.02	0.02
	SUM	0.92	0.89	0.96		SUM	0.71	0.75	0.68
	Percent	82.57%	74.11%	92.24%		Percent	81.11%	76.40%	86.93%
P_{TE}	PW	1.04	1.28	0.80	K_{TE}	PW	0.92	1.02	0.82
	SW	1.86	1.87	1.84		SW	3.38	2.98	3.79
	MW	0.26	0.29	0.24		MW	0.72	0.75	0.69
	SUM	3.16	3.44	2.88		SUM	5.02	4.75	5.29
	Percent	77.59%	75.96%	79.63%		Percent	80.50%	79.26%	81.64%

dominant in the climatological K_{SE} , the trends of this energy component are not statistically significant (Fig. C.9c). As for the globally increasing trend of K_{TE} in Tab. C.3, it stems mainly from the significant upward trend of energies provided by synoptic-scale waves, especially over the Southern Hemisphere (Fig. C.9d), although the trend for K_{TE} within planetary-scale waves is significantly negative at the global scale. Our results implicitly suggest a poleward shift of the tropospheric jets and intensifying storm tracks, mainly occurring over the Southern Hemisphere (Kim and Kim, 2013; Li et al., 2007).

c.3.7 The impact of modes of climate variability on the Lorenz Energy Cycle

c.3.7.1 Analysis of the correlations

We calculate the Pearson correlation between detrended Lorenz energy cycle components and climate indices as mentioned in section C.2 (Tabs. C.6 and C.7). The significance of the correlation is tested based on the two-tailed student's t-test. As shown in Tab. C.6, P_M presents a close relationship with most climate indices, except NAO, QBO, AMO, and ΔT_{NH} . The total available potential energy ($P_M + P_E$) is dominated by P_M and therefore shares nearly the same correlation with P_M . As for P_E , it seems unrelated to most of the indices, except for AMO, GMST, and ΔT_{SH} , and it tends to have correlations of the opposite sign compared with P_M . The significant correlation with ΔT_{SH} is consistent with Li et al. (2007), where they found that variation of P_E is associated with the land-sea temperature contrast mainly over the Southern Hemisphere. By decomposing P_E (Tab. C.7), we find that P_{SE} and P_{TE} contribute differently to the variations of P_E in different hemispheres.

Table C.5: Decomposition of mechanical energy into wave number domain (Jm^{-2} per year).

		Global		NH		SH	
		Trend	Sig.	Trend	Sig.	Trend	Sig.
P_{SE}	PW	-3.57		57.19		-51.92	
	SW	-23.75		-44.10	+	8.01	
	MW	-0.00	*	0.00		-5.00	***
	SUM	-32.29		-55.14		-53.49	
P_{TE}	PW	88.23		10.43		177.37	+
	SW	176.47	***	146.86	*	225.66	***
	MW	12.50	*	1.35		16.67	*
	SUM	279.40	***	78.24		448.81	***
K_{SE}	PW	-6.93		24.17		-40.00	
	SW	-0.00		-50.81		33.81	
	MW	-2.94	***	0.00	+	-3.28	**
	SUM	-50.55		-67.42		-14.64	
K_{TE}	PW	-100.00	+	-120.61		-62.35	
	SW	210.17	**	93.52		276.03	**
	MW	-0.00		-29.86		26.79	
	SUM	103.85		-34.72		252.66	+

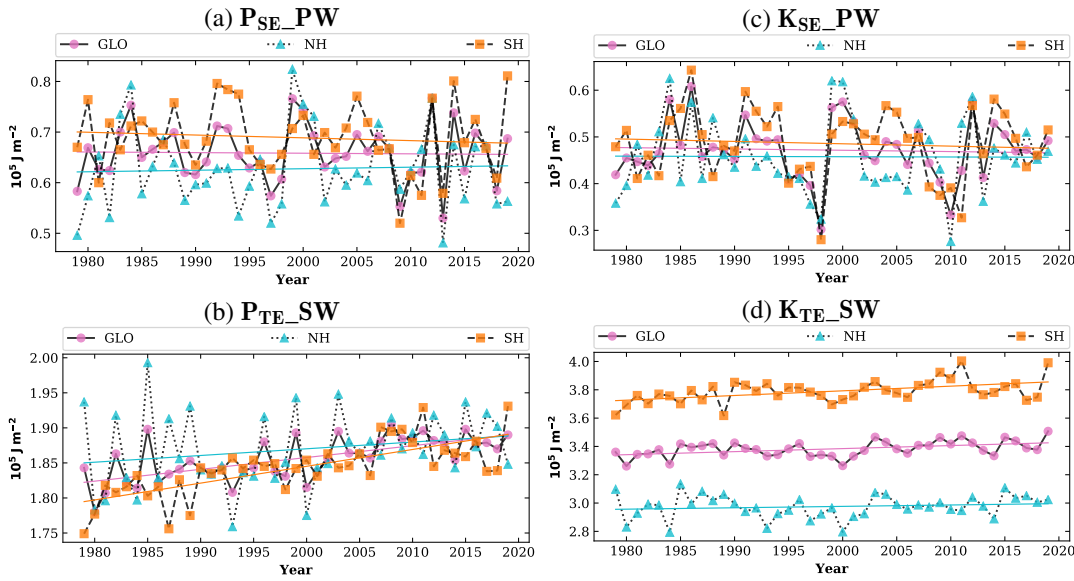


Figure C.9: Decomposed the stationary and transient eddy energies into wave-number domain. **(a)** Energies in Planetary-scale Waves group for the stationary eddy available potential energy P_{SE_PW} ; **(b)** Energies in Synoptic-scale Waves group for the transient eddy available potential energy P_{TE_SW} ; **(c)** Energies in Planetary-scale Waves group for the stationary eddy kinetic energy K_{SE_PW} ; **(d)** Energies in Synoptic-scale Waves group for the transient eddy kinetic energy K_{TE_SW} .

P_{SE} has stronger correlations with atmospheric indices over the Northern Hemisphere, while P_{SE} is responsible for the significant negative correlation between P_E and ΔT_{SH} occurring over the Southern Hemisphere. This is suggestive of the peculiar role of orographically forced stationary Rossby waves in the Southern Hemisphere, adding details on the importance of the land-sea contrast described in Li et al. (2007).

K_M experiences a strong relationship with all climate indices, except QBO and ΔT_{NH} . The total kinetic energy ($K_M + K_E$) shares the same correlations as K_M (Tab. C.6). As for K_E , it is affected mainly by atmospheric and temperature indices and tends to represent the opposite correlations compared with K_M for most indices. Our results show that the modes of climate variability more strongly affect the eddy kinetic energy than the available potential energy, in particular, the impacts of long-lived oceanic variability (PDO and AMO). As shown in Tab. C.7, we find that correlations for K_E with climate indices in Tab. C.6 are dominated by K_{SE} , especially over the Northern Hemisphere.

Concerning the correlations in conversion rates (Tab. C.6), $C(P_M, P_E)$ has a significant positive correlation with PNA, SAM, PDO, and ΔT_{SH} . As $C(P_M, P_E)$ is related to mid-latitude cyclones and anticyclones (Li et al., 2007), these correlations indicate that its variations link with the fluctuations in the jet stream over the PNA and associate with the meridional heat transport mainly over the Southern Hemisphere. $C(P_E, K_E)$ has significant correlations with the AO,

SAM, ΔT_{NH} , and ΔT_{SH} , which suggests that its variations are connected with heat-driven rising and sinking motions through strengthening temperature perturbations in the troposphere over mid-latitudes (Li et al., 2007; Pan et al., 2017). $C(K_E, K_M)$ is associated with the changes in the positions of the jet streams in the troposphere (Li et al., 2007), and it has a significant positive correlation with the QBO, SAM and ΔT_{SH} . Our results illustrate that the variations of $C(K_E, K_M)$ occur mainly over the Southern Hemisphere and are affected by the zonal wind variations in the tropical lower stratosphere. As for $C(P_M, K_M)$, it presents no significant correlation with climate indices. Our results suggest that the selected climate indices do not play a role in converting changes in the energy conversions mediated by the zonal mean flow and changes in the strength of the zonal mean mass circulation itself at the global scale. However, we should be cautious in interpreting these correlation results as a cause-effect relationship. What our results show is that the respective climate variability modes develop in line with the conversions rates they correlate with. The cause-effect relationships cannot be inferred with correlations.

c.3.7.2 *The mechanisms behind the correlations*

Results from the correlations illustrate that the indices of NINO_{3.4}, AO, and SAM contribute the most to the variation of the Lorenz energy cycle. In terms of the zonal mean energetics, the NAO, PDO, and AMO play an important role as well, especially for the zonal mean kinetic energy. ENSO has indeed a well known strong impact on global mean temperatures, so it is not surprising that ENSO affects the Lorenz energy cycle, particularly during El Niño and La Niña years (Li et al., 2011; Trenberth and Fasullo, 2013). ENSO causes enhanced tropical heating as well, which in turn excites both quasi-stationary and poleward propagating Rossby waves (Feldstein and Franzke, 2017; Franzke et al., 2011; Sardeshmukh and Hoskins, 1988). We speculate that these Rossby waves, triggering NAO events (Cassou, 2008; Franzke et al., 2019), explain the role of the NAO in the variation of eddy energies. The PNA also has strong impacts on the zonal mean flow (e.g. Feldstein and Franzke, 2017) and, thus, affects zonal mean energetics (Castanheira and Marques, 2019; Martineau et al., 2020).

As mentioned, the PDO contributes to the variations of zonal mean energetics, while the AMO is more important for eddy kinetic energies. Being the most dominant SST variability mode in the Pacific Ocean on low-frequency timescales (Sohn et al., 2013), the PDO can modulate the interannual variations of ENSO and is associated with the Walker Circulation (Seidel et al., 2008), thus having an impact on the variations of the Lorenz energy cycle consistent with Veiga et al. (2013). On the contrary, variations of the AMO are connected with the meridional sea surface temperature anomalies, which likely influence the atmospheric circulation (Frajka-Williams et al., 2017) and therefore are

associated with the variations of P_E and as a consequence, possibly with K_E and K_M .

The meridional temperature gradients are driving the meridional circulations and their related energy transformations (Makarieva et al., 2017). As sharp topographic and thermal contrasts exist, the Antarctic and subantarctic regions are characterized by the very energetic nature of synoptic activity (Simmonds et al., 2003). Thus, it is not surprising that the variations of the Lorenz energy cycle tend to have significant correlations with ΔT_{SH} over the Southern Hemisphere for most of the Lorenz energy cycle components, especially for the eddy available potential and kinetic energies.

C.4 CONCLUSION

Here we investigate the atmospheric Lorenz energy cycle and its spatio-temporal variability using the JRA-55 reanalysis. We first calculate the Lorenz energy cycle from 1958 to 2019 and find that a clear sudden jump exists in the zonal mean and eddy energies around 1979, likely due to the introduction of satellite data in that year, introducing an inhomogeneity into components of the Lorenz energy cycle. Thus, we decided to focus on the trends and variability of the Lorenz energy cycle between 1979 and 2019. Our main results can be summarized as follows:

- The total mechanic energy in the troposphere did not significantly change during the period 1979–2019. However, the eddy available potential energy exhibits significant positive trends, especially the transient eddy available potential energy in the Southern Hemisphere. This is consistent with an increase in storm track strength in the Southern Hemisphere (Franzke and Harnik, submitted).
- The conversion rates between eddy available potential and eddy kinetic energy, and between zonal mean available potential and zonal mean kinetic energy have significantly increased. The significant trend of the former is mainly through transient eddies, and indicates the strengthening of baroclinic eddy activity in the climate system; the latter suggests a role played in the expansion of the Hadley cell over the last few recent decades.
- A decomposition of the eddy energies into different wave-number groups shows that the energies of planetary-scale waves dominate the stationary eddy energies; the energy carried by synoptic-scale waves dominates the transient eddy energies with a significant increasing trend. Results confirm recent findings on the intensification of eddy activity (Pan et al., 2017) and synoptic-scale waves (Chemke and Ming, 2020).
- Correlations between the Lorenz energy cycle and climate indices reveal the tight relation between the temporal variations of most Lorenz energy

Table C.6: Correlations between climate indices and different global Lorenz energy cycle components.

	$P_M + P_E$	$K_M + K_E$	P_M	P_E	K_M	K_E	$C(P_M, P_E)$
AO	-0.31*	-0.21	-0.32*	0.16	-0.29+	0.35*	0.01
NAO	-0.19	-0.19	-0.21	0.22	-0.31+	0.46**	-0.07
NINO3.4	0.54***	0.47**	0.53***	-0.20	0.41**	-0.04	0.05
PNA	0.30+	0.61***	0.30+	-0.17	0.56***	-0.15	0.26+
SAM	0.26+	0.24	0.27+	-0.19	0.33*	-0.38*	0.31*
QBO	-0.08	0.09	-0.04	-0.23	0.06	0.07	0.17
PDO	0.44**	0.56***	0.43**	-0.10	0.47**	-0.03	0.26+
AMO	0.20	0.29*	0.23	-0.28+	0.38*	-0.43**	0.13
GMST	0.47**	0.68***	0.52***	-0.49**	0.69***	-0.39*	0.18
ΔT_{NH}	-0.07	-0.01	-0.07	0.01	-0.04	0.09	0.18
ΔT_{SH}	0.32*	0.21	0.36*	-0.39*	0.35*	-0.52***	0.46**
	$C(P_E, K_E)$	$C(K_E, K_M)$	$C(P_M, K_M)$	G_{PM}	G_{PE}	D_{KM}	D_{KE}
AO	0.35*	0.19	0.00	0.01	0.49**	0.17	0.21
NAO	0.13	0.04	0.02	-0.08	0.27+	0.03	0.12
NINO3.4	-0.17	-0.13	0.02	0.04	-0.30+	-0.12	-0.05
PNA	0.07	0.08	0.09	0.20	-0.16	0.05	-0.02
SAM	0.35*	0.41**	-0.22	0.38*	0.19	0.41**	-0.09
QBO	0.09	0.26+	-0.09	0.19	-0.04	0.25	-0.24
PDO	-0.08	-0.05	0.13	0.18	-0.37*	-0.08	-0.03
AMO	0.05	0.13	0.00	0.12	-0.06	0.11	-0.10
GMST	0.07	0.21	-0.10	0.21	-0.08	0.21	-0.20
ΔT_{NH}	0.39*	0.26	0.10	0.12	0.38*	0.20	0.17
ΔT_{SH}	0.4*	0.46**	-0.03	0.43**	0.11	0.41**	-0.10

Table C-7: Correlations between climate indices and different eddies Lorenz energy cycle components at different scales

	Global						NH			SH		
	P_{SE}	P_{TE}	K_{SE}	K_{TE}	P_{SE}	P_{TE}	K_{SE}	K_{TE}	P_{SE}	P_{TE}	K_{SE}	K_{TE}
	AO	0.20	0.03	0.27+	0.13	0.23	-0.00	0.40**	0.10	0.08	0.04	0.02
NAO	0.31*	0.00	0.42**	0.09	0.40**	0.01	0.47**	0.20	0.08	-0.01	0.22	-0.03
NINO3.4	-0.29+	-0.00	-0.36*	0.39*	-0.33*	-0.22	-0.33*	-0.00	-0.12	0.22	-0.27+	0.46**
PNA	0.09	-0.31*	-0.12	-0.04	0.08	-0.41**	-0.05	-0.20	0.06	0.01	-0.17	0.10
SAM	-0.11	-0.15	-0.26+	-0.18	-0.09	0.23	-0.28+	0.28+	-0.09	-0.43**	-0.16	-0.40**
QBO	-0.07	-0.21	-0.05	0.16	-0.07	-0.44**	0.07	-0.04	-0.04	0.17	-0.17	0.21
PDO	0.06	-0.19	-0.17	0.18	0.01	-0.25	-0.17	0.08	0.08	0.01	-0.12	0.15
AMO	-0.17	-0.21	-0.35*	-0.12	-0.17	-0.11	-0.33*	0.04	-0.10	-0.16	-0.27+	-0.17
GMST	-0.33*	-0.34*	-0.50***	0.12	-0.32*	-0.35*	-0.39*	0.09	-0.21	-0.09	-0.46**	0.08
ΔT_{NH}	0.00	0.01	0.01	0.12	0.00	-0.05	0.16	0.01	0.00	0.07	-0.16	0.13
ΔT_{SH}	-0.20	-0.33*	-0.32*	-0.28+	-0.10	0.18	-0.36*	0.18	-0.23	-0.60***	-0.17	-0.45**

cycle components and atmospheric and oceanic indices. Among those indices, NINO_{3.4}, AO, SAM, and PDO contribute most to the interannual variability of the Lorenz energy cycle. The correlations with vertical averaged temperature differences indicate that the variations of Lorenz energy cycle are more related to the meridional heat transport over the Southern Hemisphere. While most correlations with modes of climate variability have modest correlation values, these modes nevertheless have a significant impact on the Lorenz energy cycle.

The physical relevance of trends depends closely on the length of the time series. Here we were able to use the period 1979-2019. The pre-satellite period 1958-1978 was not usable because of a significant jump in between these two periods. This calls for an improvement of satellite data assimilation in reanalysis data sets. Results suggest that eddy energetics are underestimated, before the satellite revolution, but to clarify this, further research is needed.

The Lorenz energetics are integrated from a quasi-hydrostatic dry atmosphere. Since anthropogenic global warming will potentially lead to more water vapor in the atmosphere, it would be beneficial to also include the effects of moisture and latent heat in the energy cycle. Current attempts focus mainly on the moist static energy (Barpanda and Shaw, 2017; Neelin and Held, 1987; Shaw et al., 2018). These studies also focus either on the tropics or on mid-latitude storm tracks. A global picture of how increasing moisture in the atmosphere will affect the energetics and the circulation is still missing and hinders the attempt to better understand and predict the effects of global warming.

The results presented in this paper show that the variations of the energetics can be used to help to evaluate atmospheric general circulation models and to diagnose the intensification of the eddy activity in the climate system. As part of our future research, results will be used to systematically evaluate and constrain the latest generation of Earth System Models of the Coupled Model Intercomparison Project phase 6 (CMIP6). The scope of our current research is limited to the global and hemispheric annual time-series as well. Future research on the temporal and spatial variation of energetics at a shorter- and finer-scale will further improve our understanding of the climate system.

BIBLIOGRAPHY

BIBLIOGRAPHY

- Al-Ghussain, Loiy (2019). "Global warming: review on driving forces and mitigation." In: *Environmental Progress & Sustainable Energy* 38.1, pp. 13–21.
- Alexander, Lisa Victoria, Xuebin Zhang, Tom C Peterson, John Caesar, B Gleason, AMG Klein Tank, Malcolm Haylock, Dean Collins, Blair Trewin, Fatemah Rahimzadeh, et al. (2006). "Global observed changes in daily climate extremes of temperature and precipitation." In: *Journal of Geophysical Research: Atmospheres* 111.D5.
- Alexander, Lisa (2011). "Climate science: Extreme heat rooted in dry soils." In: *Nature Geoscience* 4.1, p. 12.
- Ambaum, Maarten HP (2010). *Thermal physics of the atmosphere*. Wiley Online Library.
- Anderson, G Brooke and Michelle L Bell (2011). "Heat waves in the United States: mortality risk during heat waves and effect modification by heat wave characteristics in 43 US communities." In: *Environmental health perspectives* 119.2, pp. 210–218.
- Arblaster, Julie M and Lisa V Alexander (2012). "The impact of the El Niño–Southern Oscillation on maximum temperature extremes." In: *Geophysical Research Letters* 39.20.
- Bader, Jürgen and Mojib Latif (2005). "North Atlantic Oscillation response to anomalous Indian Ocean SST in a coupled GCM." In: *Journal of climate* 18.24, pp. 5382–5389.
- Baggett, Cory and Sukyoung Lee (2019). "Summertime midlatitude weather and climate extremes induced by moisture intrusions to the west of Greenland." In: *Quarterly Journal of the Royal Meteorological Society* 145.724, pp. 3148–3160.
- Baldwin, Jane Wilson, Jay Benjamin Dessy, Gabriel A Vecchi, and Michael Oppenheimer (2019). "Temporally compound heat wave events and global warming: An emerging hazard." In: *Earth's Future* 7.4, pp. 411–427.
- Barnes, Elizabeth A and James A Screen (2015). "The impact of Arctic warming on the midlatitude jet-stream: Can it? Has it? Will it?" In: *Wiley Interdisciplinary Reviews: Climate Change* 6.3, pp. 277–286.
- Barnes, Elizabeth A, Etienne Dunn-Sigouin, Giacomo Masato, and Tim Woollings (2014). "Exploring recent trends in Northern Hemisphere blocking." In: *Geophysical Research Letters* 41.2, pp. 638–644.
- Barpanda, Pragallva and Tiffany Shaw (2017). "Using the moist static energy budget to understand storm-track shifts across a range of time scales." In: *J. Atmos. Sci* 74.8, pp. 2427–2446.

- Barriopedro, David, Erich M Fischer, Jürg Luterbacher, Ricardo M Trigo, and Ricardo García-Herrera (2011). "The hot summer of 2010: redrawing the temperature record map of Europe." In: *Science* 332.6026, pp. 220–224.
- Behera, Swadhin, Jayanthi V Ratnam, Yukio Masumoto, and Toshio Yamagata (2013). "Origin of extreme summers in Europe: the Indo-Pacific connection." In: *Climate dynamics* 41.3-4, pp. 663–676.
- Benjamini, Yoav and Yosef Hochberg (1995). "Controlling the false discovery rate: a practical and powerful approach to multiple testing." In: *Journal of the Royal statistical society: series B (Methodological)* 57.1, pp. 289–300.
- Berner, Judith, Hannah M Christensen, and Prashant D Sardeshmukh (2020). "Does ENSO regularity increase in a warming climate?" In: *Journal of Climate* 33.4, pp. 1247–1259.
- Binder, Hanin, Maxi Boettcher, Christian M Grams, Hanna Joos, Stephan Pfahl, and Heini Wernli (2017). "Exceptional air mass transport and dynamical drivers of an extreme wintertime Arctic warm event." In: *Geophysical Research Letters* 44.23, pp. 12–028.
- Black, Emily, Mike Blackburn, Giles Harrison, Brian Hoskins, and John Methven (2004). "Factors contributing to the summer 2003 European heat wave." In: *Weather* 59.8, pp. 217–223.
- Boer, George J and S Lambert (2008). "The energy cycle in atmospheric models." In: *Climate dynamics* 30.4, pp. 371–390.
- Boos, William R and John V Hurley (2013). "Thermodynamic bias in the multimodel mean boreal summer monsoon." In: *Journal of climate* 26.7, pp. 2279–2287.
- Boschat, Ghyslaine, Ian Simmonds, Ariaan Purich, Tim Cowan, and Alexandre Bernardes Pezza (2016). "On the use of composite analyses to form physical hypotheses: An example from heat wave–SST associations." In: *Scientific reports* 6.1, pp. 1–10.
- Branstator, Grant (2014). "Long-lived response of the midlatitude circulation and storm tracks to pulses of tropical heating." In: *Journal of Climate* 27.23, pp. 8809–8826.
- Campbell, Sharon, Tomas A Remenyi, Christopher J White, and Fay H Johnston (2018). "Heatwave and health impact research: A global review." In: *Health & place* 53, pp. 210–218.
- Carril, Andrea F, Silvio Gualdi, Annalisa Cherchi, and Antonio Navarra (2008). "Heatwaves in Europe: areas of homogeneous variability and links with the regional to large-scale atmospheric and SSTs anomalies." In: *Climate Dynamics* 30.1, pp. 77–98.
- Cassou, Christophe (2008). "Intraseasonal interaction between the Madden–Julian Oscillation and the North Atlantic Oscillation." In: *Nature* 455.7212, pp. 523–527.
- Cassou, Christophe, Laurent Terray, and Adam S Phillips (2005). "Tropical Atlantic influence on European heat waves." In: *Journal of climate* 18.15, pp. 2805–2811.

- Castanheira, José M and Carlos AF Marques (2019). "The energy cascade associated with daily variability of the North Atlantic Oscillation." In: *Quarterly Journal of the Royal Meteorological Society* 145.718, pp. 197–210.
- Casty, Carlo, Heinz Wanner, Jürg Luterbacher, Jan Esper, and Reinhard Böhm (2005). "Temperature and precipitation variability in the European Alps since 1500." In: *International Journal of Climatology: A Journal of the Royal Meteorological Society* 25.14, pp. 1855–1880.
- Change, Intergovernmental Panel On Climate (2007). "Climate change 2007: the physical science basis: summary for policymakers." In: *Geneva: IPCC*, pp. 104–116.
- Charney, Jule G and John G DeVore (1979). "Multiple flow equilibria in the atmosphere and blocking." In: *Journal of Atmospheric Sciences* 36.7, pp. 1205–1216.
- Chemke, R and Y Ming (2020). "Large Atmospheric Waves Will Get Stronger, While Small Waves Will Get Weaker by the End of the 21st Century." In: *Geophysical Research Letters* 47.22, e2020GL090441.
- Chen, Ruidan and Riyu Lu (2015). "Comparisons of the circulation anomalies associated with extreme heat in different regions of eastern China." In: *Journal of Climate* 28.14, pp. 5830–5844.
- Chowdary, Jasti S, Kaiming Hu, G Srinivas, Yu Kosaka, Lin Wang, and K Koteswara Rao (2019). "The Eurasian jet streams as conduits for East Asian monsoon variability." In: *Current Climate Change Reports* 5.3, pp. 233–244.
- Clément, Marilyns, Oumarou Nikiéma, and René Laprise (2017). "Limited-area atmospheric energetics: illustration on a simulation of the CRCM5 over eastern North America for December 2004." In: *Climate Dynamics* 48.9-10, pp. 2797–2818.
- Cleveland, Judah L, Jeffrey A Smith, and James P Collins (2020). "Factor Effects in Numerical Simulations." In: *Journal of the Atmospheric Sciences* 77.7, pp. 2439–2451.
- Cogato, Alessia, Franco Meggio, Massimiliano De Antoni Migliorati, and Francesco Marinello (2019). "Extreme weather events in agriculture: A systematic review." In: *Sustainability* 11.9, p. 2547.
- Coumou, Dim and Alexander Robinson (2013). "Historic and future increase in the global land area affected by monthly heat extremes." In: *Environmental Research Letters* 8.3, p. 034018.
- Coumou, Dim, Vladimir Petoukhov, Stefan Rahmstorf, Stefan Petri, and Hans Joachim Schellnhuber (2014). "Quasi-resonant circulation regimes and hemispheric synchronization of extreme weather in boreal summer." In: *Proceedings of the National Academy of Sciences* 111.34, pp. 12331–12336.
- Coumou, Dim, Jascha Lehmann, and Johanna Beckmann (2015). "The weakening summer circulation in the Northern Hemisphere mid-latitudes." In: *Science* 348.6232, pp. 324–327.

- Coumou, Dim, Giorgia Di Capua, Steve Vavrus, Lei Wang, and Simon Wang (2018). "The influence of Arctic amplification on mid-latitude summer circulation." In: *Nature communications* 9.1, p. 2959.
- Dai, Aiguo (2013). "Increasing drought under global warming in observations and models." In: *Nature climate change* 3.1, pp. 52–58.
- Dai, Aiguo and Mirong Song (2020). "Little influence of Arctic amplification on mid-latitude climate." In: *Nature Climate Change* 10.3, pp. 231–237.
- Dashkhuu, Dulamsuren, Jong Pil Kim, Jong Ahn Chun, and Woo-Seop Lee (2015). "Long-term trends in daily temperature extremes over Mongolia." In: *Weather and Climate Extremes* 8, pp. 26–33.
- Davis, NA and Sean M Davis (2018). "Reconciling Hadley cell expansion trend estimates in reanalyses." In: *Geophysical Research Letters* 45.20, pp. 11–439.
- Davis, Robert E, Glenn R McGregor, and Kyle B Enfield (2016). "Humidity: A review and primer on atmospheric moisture and human health." In: *Environmental research* 144, pp. 106–116.
- De Viron, O, JO Dickey, and M Ghil (2013). "Global modes of climate variability." In: *Geophysical Research Letters* 40.9, pp. 1832–1837.
- Della-Marta, Paul M, Jürg Luterbacher, Hans von Weissenfluh, Elena Xoplaki, Manola Brunet, and Heinz Wanner (2007). "Summer heat waves over western Europe 1880–2003, their relationship to large-scale forcings and predictability." In: *Climate Dynamics* 29.2-3, pp. 251–275.
- Deng, Kaiqiang, Song Yang, Mingfang Ting, Ailan Lin, and Ziqian Wang (2018a). "An intensified mode of variability modulating the summer heat waves in eastern Europe and northern China." In: *Geophysical Research Letters* 45.20, pp. 11–361.
- Deng, Kaiqiang, Mingfang Ting, Song Yang, and Yaheng Tan (2018b). "Increased frequency of summer extreme heat waves over texas area tied to the amplification of pacific zonal SST gradient." In: *Journal of Climate* 31.14, pp. 5629–5647.
- Ding, Qinghua and Bin Wang (2005). "Circumglobal teleconnection in the Northern Hemisphere summer." In: *Journal of Climate* 18.17, pp. 3483–3505.
- Ding, Qinghua, Bin Wang, John M Wallace, and Grant Branstator (2011). "Tropical–extratropical teleconnections in boreal summer: Observed interannual variability." In: *Journal of Climate* 24.7, pp. 1878–1896.
- Ding, Qinghua, John M Wallace, David S Battisti, Eric J Steig, Ailie JE Gallant, Hyung-Jin Kim, and Lei Geng (2014). "Tropical forcing of the recent rapid Arctic warming in northeastern Canada and Greenland." In: *Nature* 509.7499, pp. 209–212.
- Dirmeyer, Paul A, Benjamin A Cash, James L Kinter III, Cristiana Stan, Thomas Jung, Lawrence Marx, Peter Towers, Nils Wedi, Jennifer M Adams, Eric L Altshuler, et al. (2012). "Evidence for enhanced land–atmosphere feedback in a warming climate." In: *Journal of Hydrometeorology* 13.3, pp. 981–995.
- Dole, Randall, Martin Hoerling, Judith Perlwitz, Jon Eischeid, Philip Pegion, Tao Zhang, Xiao-Wei Quan, Taiyi Xu, and Donald Murray (2011). "Was there

- a basis for anticipating the 2010 Russian heat wave?" In: *Geophysical Research Letters* 38.6.
- Donat, MG, LV Alexander, H Yang, I Durre, R Vose, RJH Dunn, KM Willett, E Aguilar, M Brunet, J Caesar, et al. (2013). "Updated analyses of temperature and precipitation extreme indices since the beginning of the twentieth century: The HadEX2 dataset." In: *Journal of Geophysical Research: Atmospheres* 118.5, pp. 2098–2118.
- Dong, Buwen, Rowan T Sutton, Tim Woollings, and Kevin Hodges (2013). "Variability of the North Atlantic summer storm track: Mechanisms and impacts on European climate." In: *Environmental Research Letters* 8.3, p. 034037.
- Duan, AM and GX Wu (2005). "Role of the Tibetan Plateau thermal forcing in the summer climate patterns over subtropical Asia." In: *Climate dynamics* 24.7, pp. 793–807.
- Erdenebat, Enkhbat and Tomonori Sato (2016). "Recent increase in heat wave frequency around Mongolia: role of atmospheric forcing and possible influence of soil moisture deficit." In: *Atmospheric science letters* 17.2, pp. 135–140.
- Feldstein, Steven B. and C. L. E. Franzke (2017). "Atmospheric Teleconnection Patterns." In: *Nonlinear and Stochastic Climate Dynamics*. Ed. by C. L. E. Franzke and T. O'Kane. Cambridge University Press, pp. 54–104.
- Fischer, Erich M and Christoph Schär (2010). "Consistent geographical patterns of changes in high-impact European heatwaves." In: *Nature geoscience* 3.6, pp. 398–403.
- Fischer, Erich M, Sonia I Seneviratne, Pier Luigi Vidale, Daniel Lüthi, and Christoph Schär (2007). "Soil moisture–atmosphere interactions during the 2003 European summer heat wave." In: *Journal of Climate* 20.20, pp. 5081–5099.
- Folland, Chris K, Jeff Knight, Hans W Linderholm, David Fereday, Sarah Ineson, and James W Hurrell (2009). "The summer North Atlantic Oscillation: past, present, and future." In: *Journal of Climate* 22.5, pp. 1082–1103.
- Fragkoulidis, G, V Wirth, P Bossmann, and AH Fink (2018). "Linking Northern Hemisphere temperature extremes to Rossby wave packets." In: *Quarterly Journal of the Royal Meteorological Society* 144.711, pp. 553–566.
- Frajka-Williams, Eleanor, Claudie Beaulieu, and Aurelie Duchez (2017). "Emerging negative Atlantic Multidecadal Oscillation index in spite of warm subtropics." In: *Scientific Reports* 7.1, pp. 1–8.
- Francis, Jennifer A and Stephen J Vavrus (2012). "Evidence linking Arctic amplification to extreme weather in mid-latitudes." In: *Geophysical research letters* 39.6.
- Franzke, Christian L E and Marcin Czupryna (2020). "Probabilistic assessment and projections of US weather and climate risks and economic damages." In: *Clim. Change* 158, pp. 503–515.

- Franzke, Christian L. E. and Steven B Feldstein (2005). "The continuum and dynamics of Northern Hemisphere teleconnection patterns." In: *J. Atmos. Sci.* 62.9, pp. 3250–3267.
- Franzke, Christian L E and Herminia Torelló i Sentelles (2020). "Mortality Risks and Modes of Climate Variability." In: *Clim. Change* 162, pp. 141–157.
- Franzke, Christian L. E., Steven B Feldstein, and Sukyoung Lee (2011). "Synoptic analysis of the Pacific–North American teleconnection pattern." In: *Q. J. R. Meteorol. Soc.* 137.655, pp. 329–346.
- Franzke, Christian L E, Damjan Jelic, Sukyoung Lee, and Steven B Feldstein (2019). "Systematic decomposition of the MJO and its Northern Hemispheric extratropical response into Rossby and inertio-gravity components." In: *Q. J. Roy. Meteorol. Soc.* 145.720, pp. 1147–1164.
- Franzke, Christian, Sukyoung Lee, and Steven B Feldstein (2004). "Is the North Atlantic Oscillation a breaking wave?" In: *Journal of the atmospheric sciences* 61.2, pp. 145–160.
- Galfi, Verena Melinda (2018). "Mathematics of extreme events in atmospheric models." PhD thesis. Universität Hamburg Hamburg.
- Gettelman, Andrew, William D Collins, Eric J Fetzer, Annmarie Eldering, Fredrick W Irion, Phillip B Duffy, and Govindasamy Bala (2006). "Climatology of upper-tropospheric relative humidity from the Atmospheric Infrared Sounder and implications for climate." In: *Journal of climate* 19.23, pp. 6104–6121.
- Ghosh, Rohit, Wolfgang A Müller, Johanna Baehr, and Jürgen Bader (2017). "Impact of observed North Atlantic multidecadal variations to European summer climate: A linear baroclinic response to surface heating." In: *Climate Dynamics* 48.11-12, pp. 3547–3563.
- Ghosh, Rohit, Wolfgang A Müller, Astrid Eichhorn, Johanna Baehr, and Jürgen Bader (2019). "Atmospheric pathway between Atlantic multidecadal variability and European summer temperature in the atmospheric general circulation model ECHAM6." In: *Climate dynamics* 53.1-2, pp. 209–224.
- Gocic, Milan and Slavisa Trajkovic (2013). "Analysis of changes in meteorological variables using Mann-Kendall and Sen's slope estimator statistical tests in Serbia." In: *Global and Planetary Change* 100, pp. 172–182.
- Guo, Yuming, Antonio Gasparrini, Ben G Armstrong, Benjawan Tawatsupa, Aurelio Tobias, Eric Lavigne, Micheline de Sousa Zanotti Stagliorio Coelho, Xiaochuan Pan, Ho Kim, Masahiro Hashizume, et al. (2017). "Heat wave and mortality: a multicountry, multicomunity study." In: *Environmental health perspectives* 125.8, p. 087006.
- Hannachi, Abdel, Ian T Jolliffe, and David B Stephenson (2007). "Empirical orthogonal functions and related techniques in atmospheric science: A review." In: *International Journal of Climatology: A Journal of the Royal Meteorological Society* 27.9, pp. 1119–1152.
- Hannachi, Abdel, David M Straus, Christian LE Franzke, Susanna Corti, and Tim Woollings (2017). "Low-frequency nonlinearity and regime behavior

- in the Northern Hemisphere extratropical atmosphere." In: *Reviews of Geophysics* 55.1, pp. 199–234.
- Held, Isaac M, Mingfang Ting, and Hailan Wang (2002). "Northern winter stationary waves: Theory and modeling." In: *Journal of climate* 15.16, pp. 2125–2144.
- Hernández-Deckers, Daniel and Jin-Song von Storch (2010). "Energetics responses to increases in greenhouse gas concentration." In: *Journal of Climate* 23.14, pp. 3874–3887.
- Hernández, Armand, Celia Martin-Puertas, Paola Moffa-Sánchez, Eduardo Moreno-Chamarro, Pablo Ortega, Simon Blockley, Kim M Cobb, Laia Comas-Bru, Santiago Giralt, Hugues Goosse, et al. (2020). "Modes of climate variability: Synthesis and review of proxy-based reconstructions through the Holocene." In: *Earth-Science Reviews*, p. 103286.
- Hessl, Amy E, Kevin J Anchukaitis, Casey Jelsema, Benjamin Cook, Oyunsanaa Byambasuren, Caroline Leland, Baatarbileg Nachin, Neil Pederson, Hanqin Tian, and Laia Andreu Hayles (2018). "Past and future drought in Mongolia." In: *Science advances* 4.3, e1701832.
- Holton, James R and Gregory J Hakim (2012a). *An Introduction to Dynamic Meteorology*. Vol. 88. Academic Press.
- (2012b). *An Introduction to Dynamic Meteorology*. Vol. 88. Academic Press.
- Horton, Daniel E, Nathaniel C Johnson, Deepti Singh, Daniel L Swain, Bala Rajaratnam, and Noah S Diffenbaugh (2015). "Contribution of changes in atmospheric circulation patterns to extreme temperature trends." In: *Nature* 522.7557, pp. 465–469.
- Horton, Radley M, Justin S Mankin, Corey Lesk, Ethan Coffel, and Colin Raymond (2016). "A review of recent advances in research on extreme heat events." In: *Current Climate Change Reports* 2.4, pp. 242–259.
- Hoskins, Brian and Tim Woollings (2015). "Persistent extratropical regimes and climate extremes." In: *Current Climate Change Reports* 1.3, pp. 115–124.
- Hu, Qi, Y Tawaye, and S Feng (2004). "Variations of the Northern Hemisphere atmospheric energetics: 1948–2000." In: *Journal of Climate* 17.10, pp. 1975–1986.
- Huang, Junling (2014). "A climate-friendly energy future: prospects for wind." PhD thesis.
- Huang, Junling and Michael B McElroy (2014). "Contributions of the Hadley and Ferrel Circulations to the Energetics of the Atmosphere over the Past 32 Years." In: *Journal of Climate* 27.7, pp. 2656–2666.
- Huang, Weizhi, Yunting Qiao, and Maoqiu Jian (2021). "Surface temperature-related variations in the East Asian summer monsoon during three warming stages." In: *International Journal of Climatology*. DOI: <https://doi.org/10.1002/joc.7153>.
- Iles, Carley E, Robert Vautard, Jane Strachan, Sylvie Jousaume, Bernd R Eggen, and Chris D Hewitt (2019). "The benefits of increasing resolution in

- global and regional climate simulations for European climate extremes." In: *Geoscientific Model Development Discussions*, pp. 1–39.
- Kang, Sarah M and Jian Lu (2012). "Expansion of the Hadley cell under global warming: Winter versus summer." In: *Journal of Climate* 25.24, pp. 8387–8393.
- Kendall, Maurice George (1948). "Rank correlation methods." In:
- Kenyon, Jesse and Gabriele C Hegerl (2008). "Influence of modes of climate variability on global temperature extremes." In: *Journal of Climate* 21.15, pp. 3872–3889.
- (2010). "Influence of modes of climate variability on global precipitation extremes." In: *Journal of Climate* 23.23, pp. 6248–6262.
- Kim, Dong Wan and Sukyoung Lee (2021). "Relationship between Boreal Summer Circulation Trend and Destructive Stationary–Transient Wave Interference in the Western Hemisphere." In: *Journal of Climate* 34.12, pp. 4989–4999.
- Kim, WonMoo and Yong-Sang Choi (2017). "Long-term change of the atmospheric energy cycles and weather disturbances." In: *Climate Dynamics* 49.9, pp. 3605–3617.
- Kim, Yeon-Hee and Maeng-Ki Kim (2013). "Examination of the global lorenz energy cycle using MERRA and NCEP-reanalysis 2." In: *Climate Dynamics* 40.5-6, pp. 1499–1513.
- Kobayashi, Shinya, Yukinari Ota, Yayoi Harada, Ayataka Ebita, Masami Moriya, Hirokatsu Onoda, Kazutoshi Onogi, Hirotaka Kamahori, Chiaki Kobayashi, Hirokazu Endo, et al. (2015). "The JRA-55 reanalysis: General specifications and basic characteristics." In: *Journal of the Meteorological Society of Japan. Ser. II* 93.1, pp. 5–48.
- Kornhuber, K, V Petoukhov, D Karoly, S Petri, S Rahmstorf, and D Coumou (2017). "Summertime planetary wave resonance in the Northern and Southern Hemispheres." In: *Journal of Climate* 30.16, pp. 6133–6150.
- Kornhuber, Kai, Scott Osprey, Dim Coumou, Stefan Petri, Vladimir Petoukhov, Stefan Rahmstorf, and Lesley Gray (2019). "Extreme weather events in early summer 2018 connected by a recurrent hemispheric wave-7 pattern." In: *Environmental Research Letters* 14.5, p. 054002.
- Kosaka, Yu, JS Chowdary, Shang-Ping Xie, Young-Mi Min, and June-Yi Lee (2012). "Limitations of seasonal predictability for summer climate over East Asia and the northwestern Pacific." In: *Journal of Climate* 25.21, pp. 7574–7589.
- Krueger, Arthur F, Jay S Winston, and Donald A Haines (1965). "Computations of atmospheric energy and its transformation for the Northern Hemisphere for a recent five-year period." In: *Monthly Weather Review* 93.4, pp. 227–238.
- Lee, Min-Hee, Sukyoung Lee, Hyo-Jong Song, and Chang-Hoi Ho (2017). "The recent increase in the occurrence of a boreal summer teleconnection and its relationship with temperature extremes." In: *Journal of Climate* 30.18, pp. 7493–7504.

- Lehmann, Jascha and Dim Coumou (2015). "The influence of mid-latitude storm tracks on hot, cold, dry and wet extremes." In: *Scientific reports* 5.1, pp. 1–9.
- Lehmann, Jascha, Dim Coumou, Katja Frieler, Alexey V Eliseev, and Anders Levermann (2014). "Future changes in extratropical storm tracks and baroclinicity under climate change." In: *Environmental Research Letters* 9.8, p. 084002.
- Lembo, Valerio, Gabriele Messori, Rune Graversen, and Valerio Lucarini (2019a). "Spectral decomposition and extremes of atmospheric meridional energy transport in the Northern Hemisphere midlatitudes." In: *Geophysical Research Letters* 46.13, pp. 7602–7613.
- Lembo, Valerio, Frank Lunkeit, and Valerio Lucarini (2019b). "TheDiaTo (v1.0)—a new diagnostic tool for water, energy and entropy budgets in climate models." In: *Geoscientific Model Development* 12.8, pp. 3805–3834.
- Li, Jianping and Qingcun Zeng (2002). "A unified monsoon index." In: *Geophysical Research Letters* 29.8, pp. 115–1.
- Li, Liming, Andrew P Ingersoll, Xun Jiang, Daniel Feldman, and Yuk L Yung (2007). "Lorenz energy cycle of the global atmosphere based on reanalysis datasets." In: *Geophysical Research Letters* 34.16.
- Li, Liming, Xun Jiang, Moustafa T Chahine, Jingqian Wang, and Yuk L Yung (2011). "The mechanical energies of the global atmosphere in El Niño and La Niña years." In: *Journal of the atmospheric sciences* 68.12, pp. 3072–3078.
- Li, Muyuan, Yao Yao, Ian H Simmonds, Dehai Luo, Linhao Zhong, and Xiaodan Chen (2020). "Collaborative impact of the NAO and atmospheric blocking on European heatwaves, with a focus on the hot summer of 2018." In: *Environmental Research Letters*.
- Liu, Alan Z, Mingfang Ting, and Hailan Wang (1998). "Maintenance of circulation anomalies during the 1988 drought and 1993 floods over the United States." In: *Journal of the atmospheric sciences* 55.17, pp. 2810–2832.
- Lorenz, Edward N (1955). "Available potential energy and the maintenance of the general circulation." In: *Tellus* 7.2, pp. 157–167.
- Lucarini, Valerio (2009). "Thermodynamic efficiency and entropy production in the climate system." In: *Physical Review E* 80.2, p. 021118.
- Lucarini, Valerio, Klaus Fraedrich, and Francesco Ragone (2011). "New results on the thermodynamic properties of the climate system." In: *Journal of the Atmospheric Sciences* 68.10, pp. 2438–2458.
- Lucarini, Valerio, Richard Blender, Corentin Herbert, Francesco Ragone, Salvatore Pascale, and Jeroen Wouters (2014). "Mathematical and physical ideas for climate science." In: *Reviews of Geophysics* 52.4, pp. 809–859.
- Luo, Dehai, Anthony R Lupo, and Han Wan (2007). "Dynamics of eddy-driven low-frequency dipole modes. Part I: A simple model of North Atlantic Oscillations." In: *Journal of the atmospheric sciences* 64.1, pp. 3–28.
- Luo, Qunying (2011). "Temperature thresholds and crop production: a review." In: *Climatic Change* 109.3, pp. 583–598.

- Ma, Chun-Sen, Lin Wang, Wei Zhang, and Volker HW Rudolf (2018a). "Resolving biological impacts of multiple heat waves: interaction of hot and recovery days." In: *Oikos* 127.4, pp. 622–633.
- Ma, Ding, William Boos, and Zhiming Kuang (2014). "Effects of orography and surface heat fluxes on the South Asian summer monsoon." In: *Journal of Climate* 27.17, pp. 6647–6659.
- Ma, Qiyun and Christian LE Franzke (2021). "The role of transient eddies and diabatic heating in the maintenance of European heat waves: a nonlinear quasi-stationary wave perspective." In: *Climate Dynamics*, pp. 1–20.
- Ma, Qiyun, Jiquan Zhang, Caiyun Sun, Feng Zhang, Rina Wu, and Lan Wu (2018b). "Drought characteristics and prediction during pasture growing season in Xilingol grassland, northern China." In: *Theoretical and Applied Climatology* 133.1, pp. 165–178.
- Ma, Qiyun, Valerio Lembo, and Christian LE Franzke (2021). "The Lorenz energy cycle: trends and the impact of modes of climate variability." In: *Tellus A: Dynamic Meteorology and Oceanography* 73.1, pp. 1–15.
- Makarieva, AM, VG Gorshkov, AV Nefiodov, D Sheil, AD Nobre, PL Shearman, and B-L Li (2017). "Kinetic energy generation in heat engines and heat pumps: the relationship between surface pressure, temperature and circulation cell size." In: *Tellus A: Dynamic Meteorology and Oceanography* 69.1, p. 1272752.
- Mann, Henry B (1945). "Nonparametric tests against trend." In: *Econometrica: Journal of the econometric society*, pp. 245–259.
- Mann, Michael E, Stefan Rahmstorf, Kai Kornhuber, Byron A Steinman, Sonya K Miller, and Dim Coumou (2017). "Influence of anthropogenic climate change on planetary wave resonance and extreme weather events." In: *Scientific reports* 7.1, pp. 1–12.
- Marques, CAF, A Rocha, and J Corte-Real (2010). "Comparative energetics of ERA-40, JRA-25 and NCEP-R2 reanalysis, in the wave number domain." In: *Dynamics of atmospheres and oceans* 50.3, pp. 375–399.
- Marques, Carlos AF, Alfredo Rocha, João Corte-Real, José M Castanheira, Juan Ferreira, and Paulo Melo-Gonçalves (2009). "Global atmospheric energetics from NCEP–Reanalysis 2 and ECMWF–ERA40 Reanalysis." In: *International Journal of Climatology: A Journal of the Royal Meteorological Society* 29.2, pp. 159–174.
- Marques, Carlos Alberto Fernandes (2011). "Global atmospheric energetics under present and future climate conditions." PhD thesis. Universidade de Aveiro (Portugal).
- Marshall, AG, Debra Hudson, MC Wheeler, O Alves, HH Hendon, MJ Pook, and JS Risbey (2014). "Intra-seasonal drivers of extreme heat over Australia in observations and POAMA-2." In: *Climate dynamics* 43.7-8, pp. 1915–1937.
- Martineau, Patrick, Hisashi Nakamura, Yu Kosaka, and Ayako Yamamoto (2020). "Importance of a vertically tilting structure for energizing the North Atlantic Oscillation." In: *Scientific reports* 10.1, pp. 1–10.

- Miralles, Diego G, Adriaan J Teuling, Chiel C Van Heerwaarden, and Jordi Vilà-Guerau De Arellano (2014). "Mega-heatwave temperatures due to combined soil desiccation and atmospheric heat accumulation." In: *Nature geoscience* 7.5, p. 345.
- Nachar, Nadim et al. (2008). "The Mann-Whitney U: A test for assessing whether two independent samples come from the same distribution." In: *Tutorials in quantitative Methods for Psychology* 4.1, pp. 13–20.
- Nakamura, Noboru and Clare SY Huang (2018). "Atmospheric blocking as a traffic jam in the jet stream." In: *Science* 361.6397, pp. 42–47.
- Neelin, J David and Isaac M Held (1987). "Modeling tropical convergence based on the moist static energy budget." In: *Mon. Wea. Rev.* 115.1, pp. 3–12.
- Newson, Roger L (1973). "Response of a general circulation model of the atmosphere to removal of the Arctic ice-cap." In: *Nature* 241.5384, pp. 39–40.
- Notz, Dirk and Julienne Stroeve (2016). "Observed Arctic sea-ice loss directly follows anthropogenic CO₂ emission." In: *Science* 354.6313, pp. 747–750.
- Oort, Abraham H (1964). "On estimates of the atmospheric energy cycle." In: *Monthly Weather Review* 92.11, pp. 483–493.
- (1983). *Global atmospheric circulation statistics, 1958-1973*. 14. US Department of Commerce, National Oceanic and Atmospheric Administration.
- Oort, Abraham H and José P Peixóto (1974). "The annual cycle of the energetics of the atmosphere on a planetary scale." In: *Journal of Geophysical Research* 79.18, pp. 2705–2719.
- Pan, Yefeng, Liming Li, Xun Jiang, Gan Li, Wentao Zhang, Xinyue Wang, and Andrew P Ingersoll (2017). "Earth's changing global atmospheric energy cycle in response to climate change." In: *Nature communications* 8.1, pp. 1–8.
- Park, Mingyu and Sukyoung Lee (2019). "Relationship between Tropical and Extratropical Diabatic Heating and their Impact on Stationary-transient Wave Interference." In: *Journal of the Atmospheric Sciences* 76, pp. 2617–2633.
- Peixóto, José P and Abraham H Oort (1974). "The annual distribution of atmospheric energy on a planetary scale." In: *Journal of Geophysical Research* 79.15, pp. 2149–2159.
- Perkins-Kirkpatrick, SE and PB Gibson (2017). "Changes in regional heatwave characteristics as a function of increasing global temperature." In: *Scientific Reports* 7.1, pp. 1–12.
- Perkins-Kirkpatrick, SE and SC Lewis (2020). "Increasing trends in regional heatwaves." In: *Nature communications* 11.1, pp. 1–8.
- Perkins, SE, LV Alexander, and JR Nairn (2012). "Increasing frequency, intensity and duration of observed global heatwaves and warm spells." In: *Geophysical Research Letters* 39.20.
- Perkins, Sarah E (2015). "A review on the scientific understanding of heatwaves—Their measurement, driving mechanisms, and changes at the global scale." In: *Atmospheric Research* 164, pp. 242–267.
- Perkins, Sarah E and Lisa V Alexander (2013). "On the measurement of heat waves." In: *Journal of Climate* 26.13, pp. 4500–4517.

- Peterson, Thomas C, Richard R Heim Jr, Robert Hirsch, Dale P Kaiser, Harold Brooks, Noah S Diffenbaugh, Randall M Dole, Jason P Giovannetone, Kristen Guirguis, Thomas R Karl, et al. (2013). "Monitoring and understanding changes in heat waves, cold waves, floods, and droughts in the United States: State of knowledge." In: *Bulletin of the American Meteorological Society* 94.6, pp. 821–834.
- Petoukhov, Vladimir, Stefan Rahmstorf, Stefan Petri, and Hans Joachim Schellnhuber (2013). "Quasiresonant amplification of planetary waves and recent Northern Hemisphere weather extremes." In: *Proceedings of the National Academy of Sciences* 110.14, pp. 5336–5341.
- Petoukhov, Vladimir, Stefan Petri, Stefan Rahmstorf, Dim Coumou, Kai Kornhuber, and Hans Joachim Schellnhuber (2016). "Role of quasiresonant planetary wave dynamics in recent boreal spring-to-autumn extreme events." In: *Proceedings of the National Academy of Sciences* 113.25, pp. 6862–6867.
- Pfahl, Stephan, Cornelia Schwierz, Mischa Croci-Maspoli, Christian M Grams, and Heini Wernli (2015). "Importance of latent heat release in ascending air streams for atmospheric blocking." In: *Nature Geoscience* 8.8, pp. 610–614.
- Po-Chedley, Stephen, Mark D Zelinka, Nadir Jeevanjee, Tyler J Thorsen, and Benjamin D Santer (2019). "Climatology explains intermodel spread in tropical upper tropospheric cloud and relative humidity response to greenhouse warming." In: *Geophysical Research Letters* 46.22, pp. 13399–13409.
- Praveen, Bushra, Swapan Talukdar, Susanta Mahato, Jayanta Mondal, Priyee Sharma, Abu Reza Md Towfiqul Islam, Atiqur Rahman, et al. (2020). "Analyzing trend and forecasting of rainfall changes in India using non-parametrical and machine learning approaches." In: *Scientific reports* 10.1, pp. 1–21.
- Prigogine, Ilya (1962). *Non-equilibrium statistical mechanics*. New York: Wiley, p. 336.
- Quesada, Benjamin, Robert Vautard, Pascal Yiou, Martin Hirschi, and Sonia I Seneviratne (2012). "Asymmetric European summer heat predictability from wet and dry southern winters and springs." In: *Nature Climate Change* 2.10, pp. 736–741.
- Raveh-Rubin, Shira (2017). "Dry intrusions: Lagrangian climatology and dynamical impact on the planetary boundary layer." In: *Journal of Climate* 30.17, pp. 6661–6682.
- Risbey, James S, Terence J O'Kane, Didier P Monselesan, Christian LE Franzke, and Illia Horenko (2018). "On the dynamics of austral heat waves." In: *Journal of Geophysical Research: Atmospheres* 123.1, pp. 38–57.
- Robinson, Peter J (2001). "On the definition of a heat wave." In: *Journal of Applied Meteorology and Climatology* 40.4, pp. 762–775.
- Ruggieri, Paolo, M Carmen Alvarez-Castro, Panos Athanasiadis, Alessio Bellucci, Stefano Materia, and Silvio Gualdi (2020). "North Atlantic circulation regimes and heat transport by synoptic eddies." In: *Journal of Climate* 33.11, pp. 4769–4785.

- Russo, Simone, Alessandro Dosio, Rune G Graversen, Jana Sillmann, Hugo Carrao, Martha B Dunbar, Andrew Singleton, Paolo Montagna, Paulo Barbola, and Jürgen V Vogt (2014). "Magnitude of extreme heat waves in present climate and their projection in a warming world." In: *Journal of Geophysical Research: Atmospheres* 119.22, pp. 12–500.
- Russo, Simone, Jana Sillmann, and Erich M Fischer (2015). "Top ten European heatwaves since 1950 and their occurrence in the coming decades." In: *Environmental Research Letters* 10.12, p. 124003.
- Russo, Simone, Jana Sillmann, and Andreas Sterl (2017). "Humid heat waves at different warming levels." In: *Scientific reports* 7.1, pp. 1–7.
- Salmi, Timo (2002). *Detecting trends of annual values of atmospheric pollutants by the Mann-Kendall test and Sen's slope estimates-the Excel template application MAKESENS*. Ilmatieteen laitos.
- Saltsman, Barry (1957). "Equations governing the energetics of the larger scales of atmospheric turbulence in the domain of wave number." In: *Journal of Meteorology* 14.6, pp. 513–523.
- Sardeshmukh, Prashant D and Brian J Hoskins (1988). "The generation of global rotational flow by steady idealized tropical divergence." In: *J. Atmos. Sci.* 45.7, pp. 1228–1251.
- Schär, Christoph, Pier Luigi Vidale, Daniel Lüthi, Christoph Frei, Christian Häberli, Mark A Liniger, and Christof Appenzeller (2004). "The role of increasing temperature variability in European summer heatwaves." In: *Nature* 427.6972, p. 332.
- Schneiderreit, Andrea, Silke Schubert, Pavel Vargin, Frank Lunkeit, Xiuhua Zhu, Dieter HW Peters, and Klaus Fraedrich (2012). "Large-scale flow and the long-lasting blocking high over Russia: summer 2010." In: *Mon. Wea. Rev.* Pp. 2967–2981.
- Schoetter, Robert, Julien Cattiaux, and Hervé Douville (2015). "Changes of western European heat wave characteristics projected by the CMIP5 ensemble." In: *Climate dynamics* 45.5, pp. 1601–1616.
- Schubert, Siegfried D, Hailan Wang, Randal D Koster, Max J Suarez, and Pavel Ya Groisman (2014). "Northern Eurasian heat waves and droughts." In: *Journal of Climate* 27.9, pp. 3169–3207.
- Schubert, Siegfried, Hailan Wang, and Max Suarez (2011). "Warm season subseasonal variability and climate extremes in the Northern Hemisphere: The role of stationary Rossby waves." In: *Journal of Climate* 24.18, pp. 4773–4792.
- Schumacher, Dominik L, Jessica Keune, Chiel C Van Heerwaarden, Jordi Vilà-Guerau de Arellano, Adriaan J Teuling, and Diego G Miralles (2019). "Amplification of mega-heatwaves through heat torrents fuelled by upwind drought." In: *Nature Geoscience* 12.9, pp. 712–717.
- Screen, James A and Ian Simmonds (2013). "Exploring links between Arctic amplification and mid-latitude weather." In: *Geophysical Research Letters* 40.5, pp. 959–964.

- Screen, James A and Ian Simmonds (2014). "Amplified mid-latitude planetary waves favour particular regional weather extremes." In: *Nature Climate Change* 4.8, pp. 704–709.
- Seager, Richard, Naomi Naik, and Gabriel A Vecchi (2010). "Thermodynamic and dynamic mechanisms for large-scale changes in the hydrological cycle in response to global warming." In: *Journal of Climate* 23.17, pp. 4651–4668.
- Seidel, Dian J, Qiang Fu, William J Randel, and Thomas J Reichler (2008). "Widening of the tropical belt in a changing climate." In: *Nature geoscience* 1.1, pp. 21–24.
- Sellevold, Raymond, Stefan Sobolowski, and Camille Li (2016). "Investigating possible Arctic-midlatitude teleconnections in a linear framework." In: *Journal of Climate* 29.20, pp. 7329–7343.
- Sen, Pranab Kumar (1968). "Estimates of the regression coefficient based on Kendall's tau." In: *J. Amer. Stat. Assoc.* 63.324, pp. 1379–1389.
- Seneviratne, Sonia I, Thierry Corti, Edouard L Davin, Martin Hirschi, Eric B Jaeger, Irene Lehner, Boris Orlowsky, and Adriaan J Teuling (2010). "Investigating soil moisture–climate interactions in a changing climate: A review." In: *Earth-Science Reviews* 99.3-4, pp. 125–161.
- Shaw, Tiffany A, Pragallva Barpanda, and Aaron Donohoe (2018). "A Moist Static Energy Framework for Zonal-Mean Storm-Track Intensity." In: *J. Atmos. Sci* 75.6, pp. 1979–1994.
- Shi, Ning, Pinyu Tian, Yicheng Wang, and Xiaoqiong Wang (2020). "Contrasting Relationship between Wintertime Blocking Highs over Europe–Siberia and Temperature Anomalies in the Yangtze River Basin." In: *Monthly Weather Review* 148.7, pp. 2953–2970.
- Si, Dong and Yihui Ding (2016). "Oceanic forcings of the interdecadal variability in East Asian summer rainfall." In: *Journal of Climate* 29.21, pp. 7633–7649.
- Silverman, Bernard W (1986). *Density estimation for statistics and data analysis*. Vol. 26. CRC press.
- Simmonds, Ian, Kevin Keay, and Eun-Pa Lim (2003). "Synoptic activity in the seas around Antarctica." In: *Monthly Weather Review* 131.2, pp. 272–288.
- Simpson, Isla R, Richard Seager, Mingfang Ting, and Tiffany A Shaw (2016). "Causes of change in Northern Hemisphere winter meridional winds and regional hydroclimate." In: *Nature Climate Change* 6.1, p. 65.
- Sobolowski, Stefan, Gavin Gong, and Mingfang Ting (2011). "Investigating the linear and nonlinear stationary wave response to anomalous North American snow cover." In: *Journal of the Atmospheric Sciences* 68.4, pp. 904–917.
- Sohn, BJ, Sang-Wook Yeh, Johannes Schmetz, and Hwan-Jin Song (2013). "Observational evidences of Walker circulation change over the last 30 years contrasting with GCM results." In: *Climate Dynamics* 40.7-8, pp. 1721–1732.

- Stefanon, Marc, Fabio D'Andrea, and Philippe Drobinski (2012). "Heatwave classification over Europe and the Mediterranean region." In: *Environmental Research Letters* 7.1, p. 014023.
- Stein, U and PINHAS Alpert (1993). "Factor separation in numerical simulations." In: *Journal of the Atmospheric Sciences* 50.14, pp. 2107–2115.
- Stephenson, DB, A Hannachi, and AQJR O'Neill (2004). "On the existence of multiple climate regimes." In: *Quarterly Journal of the Royal Meteorological Society: A journal of the atmospheric sciences, applied meteorology and physical oceanography* 130.597, pp. 583–605.
- Storch, Jin-Song von, Carsten Eden, Irina Fast, Helmuth Haak, Daniel Hernández-Deckers, Ernst Maier-Reimer, Jochem Marotzke, and Detlef Stammer (2012). "An estimate of the Lorenz energy cycle for the world ocean based on the STORM/NCEP simulation." In: *Journal of physical oceanography* 42.12, pp. 2185–2205.
- Tao, Shengli, Jingyun Fang, Xia Zhao, Shuqing Zhao, Haihua Shen, Huifeng Hu, Zhiyao Tang, Zhiheng Wang, and Qinghua Guo (2015). "Rapid loss of lakes on the Mongolian Plateau." In: *Proceedings of the National Academy of Sciences* 112.7, pp. 2281–2286.
- Teng, Haiyan and Grant Branstator (2019). "Amplification of waveguide teleconnections in the boreal summer." In: *Current Climate Change Reports* 5.4, pp. 421–432.
- Teng, Haiyan, Grant Branstator, Hailan Wang, Gerald A Meehl, and Warren M Washington (2013). "Probability of US heat waves affected by a subseasonal planetary wave pattern." In: *Nature Geoscience* 6.12, pp. 1056–1061.
- Ting, Mingfang (1994). "Maintenance of northern summer stationary waves in a GCM." In: *Journal of Atmospheric Sciences* 51.22, pp. 3286–3308.
- Ting, Mingfang and Linhai Yu (1998). "Steady response to tropical heating in wavy linear and nonlinear baroclinic models." In: *Journal of the atmospheric sciences* 55.24, pp. 3565–3582.
- Ting, Mingfang, Hailan Wang, and Linhai Yu (2001). "Nonlinear stationary wave maintenance and seasonal cycle in the GFDL R30 GCM." In: *Journal of the atmospheric sciences* 58.16, pp. 2331–2354.
- Trenberth, Kevin E and John T Fasullo (2012). "Climate extremes and climate change: The Russian heat wave and other climate extremes of 2010." In: *Journal of Geophysical Research: Atmospheres* 117.D17.
- Trenberth, Kevin E. and John T. Fasullo (2013). "An apparent hiatus in global warming?" In: *Earth's Future* 1.1, pp. 19–32. DOI: <https://doi.org/10.1002/2013EF000165>. eprint: <https://agupubs.onlinelibrary.wiley.com/doi/pdf/10.1002/2013EF000165>. URL: <https://agupubs.onlinelibrary.wiley.com/doi/abs/10.1002/2013EF000165>.
- Ulbrich, U and P Speth (1991). "The global energy cycle of stationary and transient atmospheric waves: Results from ECMWF analyses." In: *Meteorology and Atmospheric Physics* 45.3-4, pp. 125–138.

- Vautard, Robert, Andreas Gobiet, Daniela Jacob, Michal Belda, Augustin Colette, Michel Déqué, Jesús Fernández, Markel García-Díez, Klaus Goergen, Ivan Güttler, et al. (2013). "The simulation of European heat waves from an ensemble of regional climate models within the EURO-CORDEX project." In: *Climate Dynamics* 41.9-10, pp. 2555–2575.
- Vavrus, Stephen J (2018). "The influence of Arctic amplification on mid-latitude weather and climate." In: *Current Climate Change Reports* 4.3, pp. 238–249.
- Veiga, José Augusto P, Alexandre B Pezza, Tercio Ambrizzi, V Brahmananda Rao, Sergio H Franchito, and Marcos C Yoshida (2013). "The energy cycle associated to the Pacific Walker circulation and its relationship to ENSO." In: *Atmospheric and Climate Sciences* 2013.
- Vogel, Johannes, Eva Paton, Valentin Aich, and Axel Bronstert (2021). "Increasing compound warm spells and droughts in the Mediterranean Basin." In: *Weather and Climate Extremes* 32, p. 100312.
- Vose, Russell S, Scott Applequist, Mark A Bourassa, Sara C Pryor, Rebecca J Barthelmie, Brian Blanton, Peter D Bromirski, Harold E Brooks, Arthur T DeGaetano, Randall M Dole, et al. (2014). "Monitoring and understanding changes in extremes: Extratropical storms, winds, and waves." In: *Bulletin of the American Meteorological Society* 95.3, pp. 377–386.
- Walsh, DA (2008). "Simple rule of thumb for statistically significant correlation." In: *Middle Tennessee State University*. Available from Internet: < <http://frank.mtsu.edu/~dwalsh/436/CORRSIG.pdf>.
- Walsh, John E, Thomas J Ballinger, Eugénie S Euskirchen, Edward Hanna, Johanna Mård, James E Overland, Helge Tangen, and Timo Vihma (2020). "Extreme weather and climate events in northern areas: A review." In: *Earth-Science Reviews*, p. 103324.
- Wang, Hailan and Mingfang Ting (1999). "Seasonal cycle of the climatological stationary waves in the NCEP–NCAR reanalysis." In: *Journal of the atmospheric sciences* 56.22, pp. 3892–3919.
- Wang, Lei (2010). *Stationary Waves in the Stratosphere-Troposphere Circulation*. University of Toronto.
- Wang, Lin, Peiqiang Xu, Wen Chen, and Yong Liu (2017a). "Interdecadal variations of the Silk Road pattern." In: *Journal of Climate* 30.24, pp. 9915–9932.
- Wang, Pinya, Jianping Tang, Shuyu Wang, Xinning Dong, and Juan Fang (2018). "Regional heatwaves in china: a cluster analysis." In: *Climate dynamics* 50.5, pp. 1901–1917.
- Wang, Shih-Yu, Robert E Davies, and Robert R Gillies (2013). "Identification of extreme precipitation threat across midlatitude regions based on short-wave circulations." In: *Journal of Geophysical Research: Atmospheres* 118.19, pp. 11–059.
- Wang, Xiaofan, Jianping Li, Cheng Sun, and Ting Liu (2017b). "NAO and its relationship with the Northern Hemisphere mean surface temperature in

- CMIP5 simulations." In: *Journal of Geophysical Research: Atmospheres* 122.8, pp. 4202–4227.
- Warshaw, M and RR Rapp (1973). "An experiment on the sensitivity of a global circulation model." In: *Journal of Applied Meteorology and Climatology* 12.1, pp. 43–49.
- Wilks, Daniel S (2016). "'The stippling shows statistically significant grid points': How research results are routinely overstated and overinterpreted, and what to do about it." In: *Bulletin of the American Meteorological Society* 97.12, pp. 2263–2273.
- Wills, Robert CJ, Rachel H White, and Xavier J Levine (2019). "Northern hemisphere stationary waves in a changing climate." In: *Current climate change reports* 5.4, pp. 372–389.
- Wolf, Gabriel, David J Brayshaw, Nicholas P Klingaman, and Arnaud Czaja (2018). "Quasi-stationary waves and their impact on European weather and extreme events." In: *Quarterly Journal of the Royal Meteorological Society* 144.717, pp. 2431–2448.
- Woollings, Tim, David Barriopedro, John Methven, Seok-Woo Son, Olivia Martius, Ben Harvey, Jana Sillmann, Anthony R Lupo, and Sonia Seneviratne (2018). "Blocking and its response to climate change." In: *Current climate change reports* 4.3, pp. 287–300.
- Xu, Zhiwei, Perry E Sheffield, Hong Su, Xiaoyu Wang, Yan Bi, and Shilu Tong (2014). "The impact of heat waves on children's health: a systematic review." In: *International journal of biometeorology* 58.2, pp. 239–247.
- Yamagami, Akio and Tanaka HL (2016). "Characteristics of the JRA-55 and ERA-Interim Datasets by Using the Three-Dimensional Normal Mode Energetics." In: *SOLA* 12, pp. 27–31.
- Yang, Xiaoye, Gang Zeng, Shiyue Zhang, Zhixin Hao, and Vedaste Iyakaremye (2021). "Relationship between two types of heat waves in northern East Asia and temperature anomalies in Eastern Europe." In: *Environmental Research Letters* 16.2, p. 024048.
- Ye, Qianping and Faisal Ahammed (2020). "Quantification of relationship between annual daily maximum temperature and annual daily maximum rainfall in South Australia." In: *Atmospheric and Oceanic Science Letters*, pp. 1–8.
- Yeh, T-C (1957). "The wind structure and heat balance in the lower troposphere over the Tibetan Plateau and its surroundings." In: *Acta. Meteor. Sinica* 28, pp. 108–121.
- Yue, Sheng and Chun Yuan Wang (2002). "Applicability of prewhitening to eliminate the influence of serial correlation on the Mann-Kendall test." In: *Water resources research* 38.6, pp. 4–1.
- Zampieri, M, A Toreti, A Schindler, Enrico Scoccimarro, and Silvio Gualdi (2017). "Atlantic multi-decadal oscillation influence on weather regimes over Europe and the Mediterranean in spring and summer." In: *Global and Planetary Change* 151, pp. 92–100.

- Zhang, Kai, William J Randel, and Rong Fu (2017). "Relationships between outgoing longwave radiation and diabatic heating in reanalyses." In: *Climate Dynamics* 49.7-8, pp. 2911–2929.
- Zhang, Peng, Jee-Hoon Jeong, Jin-Ho Yoon, Hyungjun Kim, S-Y Simon Wang, Hans W Linderholm, Keyan Fang, Xiuchen Wu, and Deliang Chen (2020). "Abrupt shift to hotter and drier climate over inner East Asia beyond the tipping point." In: *Science* 370.6520, pp. 1095–1099.
- Zhang, Xuebin, Gabriele Hegerl, Sonia Seneviratne, Ronald Stewart, Francis Zwiers, and Lisa Alexander (2014). *WCRP grand challenge: Understanding and predicting weather and climate extremes*. Tech. rep. Tech. rep., World Climate Research Program, <http://www.wcrp-climate.org> . . .
- Zschenderlein, Philipp, Andreas H Fink, Stephan Pfahl, and Heini Wernli (2019). "Processes determining heat waves across different European climates." In: *Quarterly Journal of the Royal Meteorological Society* 145.724, pp. 2973–2989.

ACKNOWLEDGMENTS

Foremost, I would like to express my sincere gratitude to my advisors Christian Franzke and Johanna Baehr for their continuous supports of my Ph.D. study and research. I must thank Christian for his kind guidance during my Ph.D. research, encouragement, great advice, and patience. He provides me great opportunities to help me build my international research network. He motivates me when I feel very frustrated and self-doubt. I also must thank Johanna for her patience, encouragement, and support during the whole Ph.D. She also teaches me to enjoy my research and life. I am also thankful for my advisory panel chair Stefan Bühler for taking care that everything is going well and supporting me during panel meetings.

I am grateful to the *China Scholarship Council (CSC)* for the financial support. I am also sincerely grateful to the MIN Graduate School (MINGS), for planning to support my travel to Columbia University. In this regard, I must thank the *School of Integrated Climate System Sciences (SICSS)*. My sincere thanks go to Ingo Harms, Berit Hachfeld, and Sebastian Zubrzycki, for being always supportive and caring about our Ph.D. progresses and future career. Then, I have to thank SICSS and the International Max Planck Research School on Earth System Modelling (IMPRS-ESM) for providing all the valuable courses and enjoyable activities.

Special thanks go to the colleagues in *Atmospheric Dynamics* (formerly *Theoretical Meteorology*) group. I would like to thank Nedjeljka Žagar, Richard Blender, Frank Lunkeit, and Frank Sielmann for taking the time to answer both scientific and technical questions and always being supportive in every way. I would like to thank all my colleagues and friends for their support during these years and especially during this pandemic period. I will remember all the cheerful lunch and coffee breaks, jokes and laughs, and all the amazing times we spent together. I am grateful to Valerio Lembo for answering my dumb questions and providing any kind of help when we collaborate on the LEC paper. I would also like to thank Guannan Hu for his support, caring, and sharing during these years. I thank Vera Melinda Galfi for her encouragement and comfort words all the time. I also thank Denny Gohlke for his support in German abstract and for bringing a lot of laughs to me. I would like to much thank Elliot McKinnon-Gray for being a great officemate in 4012 and helping me a lot with English grammar check through this thesis and other documents. I would like to also thank Iana Strigunova for being supportive and sharing all the problems and worries. I thank Lichao Yang, Wenlin Xiao, Federica Gugole, Heena Patel, Alexia Karwat, Sergiy Vasylkevych, Valentino Neduhai, Gözde Özden for their support and great company.

ACKNOWLEDGMENTS

I am indebted to Yumeng Chen for particularly his support, taking plenty of time to answer my more or less naive questions, giving me a lot of help in many aspects, and being always there when I need help. Special thanks goes to Ge Cheng, Song Li, Yifan Li, Chuangchuang Zhou, Jue Li, and particularly goes to Yongfei Liu. I wish to thank all old and new friends for being the shoulder I can always rely on. I can not list every name here, but I will cherish all of you in my life.

My sincere thanks go to Mingfang Ting for providing me the invitation letter to visit the Lamont-Doherty Earth Observatory. Although the trip didn't work out in the end due to the COVID-19 pandemic, she still provides great advice for my work. I would like to thank my master supervisor Jiquan Zhang and Chuantao Song for being my CSC guarantors and providing continuous support after I graduated.

I am extremely grateful to my parents and my sister and her families. Thank you for the everlasting moral and emotional support, for your love and care. Sorry for not being around you for the past few years and possibly in the next few years. Love all of you!

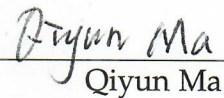
In the end, I would say some words to thank the COVID pandemic. I have never thought it will happen during my study abroad or in my life. Although it leads to some impacts on my Ph.D. research and life, I do learn a lot through this ongoing pandemic.

This thesis is dedicated to you all!

VERSICHERUNG AN EIDES STATT – AFFIRMATION ON
OATH

Hiermit versichere ich an Eides statt, dass ich die vorliegende Dissertation mit dem Titel: „Extreme events: maintenance mechanisms and energetics“ selbstständig verfasst und keine anderen als die angegebenen Hilfsmittel – insbesondere keine im Quellenverzeichnis nicht benannten Internet-Quellen – benutzt habe. Alle Stellen, die wörtlich oder sinngemäß aus Veröffentlichungen entnommen wurden, sind als solche kenntlich gemacht. Ich versichere weiterhin, dass ich die Dissertation oder Teile davon vorher weder im In- noch im Ausland in einem anderen Prüfungsverfahren eingereicht habe und die eingereichte schriftliche Fassung der auf dem elektronischen Speichermedium entspricht.

Hamburg, June 2021


Qiyun Ma
